The cell adhesion molecule BT-IgSF is essential for a functional blood-testis barrier and male fertility in mice

Inaugural-Dissertation
to obtain the academic degree
Doctor rerum naturalium (Dr. rer. nat.)

submitted to the Department of Biology, Chemistry and Pharmacy
of Freie Universität Berlin

by

LAURA PELZ

from Karlsruhe

Berlin, 2017

Diese Arbeit wurde in der Zeit zwischen dem 01.10.2014 und dem 21.12.2017
unter der Leitung von Professor Fritz G. Rathjen
am Max-Delbrück-Centrum für Molekulare Medizin Berlin angefertigt.

1. Gutachter: Professor Fritz G. Rathjen

2. Gutachter: Professor Oliver Daumke

Disputation am 02.03.2018

INDEX

1. LIST OF ABBREVIATIONS

- aES apical ectoplasmic specialization
- ASCM artificial Sertoli cell medium
- bES basal ectoplasmic specialization
- BT-IgSF brain and testis-specific immunoglobulin superfamily protein
- CAM cell adhesion molecule
- CAR coxsackie and adenovirus receptor
- CLMP CAR-like membrane protein
- CTA cancer-testis antigen
- CTX cortical thymocyte marker in *Xenopus*
- DNA deoxyribonucleic acid
- E embryonic day
- ES ectoplasmic specialization
- ESAM endothelial cell-selective adhesion molecule
- FSH follicle stimulating hormone
- GnRH gonadotropin-releasing hormone
- IgCAMs immunoglobulin cell adhesion molecules
- IgSF immunoglobulin superfamily
- JAM-C Junctional adhesion molecule C
- kb Kilobase
- kDa Kilodalton
- LH luteinizing hormone
- LNX-1 ligand-of-Numb protein-X 1
- Mab monoclonal antibody
- P postnatal day
- PNA peanut agglutinin
- qRT-PCR real-time quantitative reverse transcription PCR
- SDS sodium dodecyl sulfate
- SSC spermatogonial stem cell
- UV ultraviolet
- ZO-1 Zonula occludens protein 1

2. LIST OF FIGURES

3. ABSTRACT

Infertility is a major problem worldwide, with around 1% of the male population suffering from azoospermia. This disease can be caused by different influences such as environmental pollution, genetic and epigenetic factors and hormonal disorders.

The cell adhesion molecule BT-IgSF is known to be expressed mainly in brain and testis of mice and humans. One study explored the function of BT-IgSF in the brain. However, the role of BT-IgSF in the testis remains to be established. To analyze the function of BT-IgSF in the murine testis, the expression pattern was analyzed, and genetic mouse models were investigated.

The results of this work show that BT-IgSF is essential for fertility of male mice. In the absence of BT-IgSF, mice are unable to produce sperm, have a smaller testis size and a disturbed testis morphology. Azoospermia of BT-IgSF knockout animals is caused by a disturbed blood-testis barrier (BTB). The expression of BTB proteins such as Cx43 and ZO-1 are increased and the localization of these proteins is shifted from an expression at the basal site in the wildtype to a diffuse expression in case of Cx43 and a disorganized expression of ZO-1. Functional assessment of the BTB with a BTB impermeable tracer revealed an impaired BTB in BT-IgSF mice.

Due to the strong expression of BT-IgSF in Sertoli cells, a Sertoli-cell specific knockout of BT-IgSF was generated to further support the findings. Interestingly, the Sertoli cell-specific knockout mice showed the same phenotype as the global BT-IgSF knockout, indicating that the expression of BT-IgSF in Sertoli cells is essential for male fertility.

In another conditional knockout of BT-IgSF, which was induced by tamoxifen administration to adult mice, similar effects were seen as in the global and Sertoli cell-specific knockout, such as a reduced testis size, reduced sperm count and Cx43 mislocalization. This demonstrated that BT-IgSF is also crucial in adult mice to maintain proper spermatogenesis and male fertility.

Taken together, this study shows that BT-IgSF is essential for male fertility in mice. The absence of BT-IgSF results in an impaired BTB and in mislocalization of BTB proteins. These findings might help to further understand spermatogenesis and might be applied to elucidate human infertility.

4. ZUSAMMENFASSUNG

Infertilität ist weltweit ein bedeutendes Problem. Ungefähr 1% der männlichen Bevölkerung leidet an Azoospermie. Diese Krankheit kann durch verschiedene Einflüsse wie Umweltverschmutzung, genetische und epigenetische Faktoren oder hormonelle Störungen verursacht werden.

Es ist bekannt, dass das Zelladhäsionsmolekül BT-IgSF vor allem im Gehirn und im Hoden von Mäusen und Menschen exprimiert wird. Es gibt bereits Studien, die die Funktion von BT-IgSF im Gehirn untersucht haben. Die Funktion von BT-IgSF im Hoden ist allerdings noch nicht erforscht worden. Um die Funktion von BT-IgSF zu analysieren wurde das Expressionsmuster im Hoden charakterisiert und genetische Mausmodelle von BT-IgSF untersucht.

Die Ergebnisse dieser Arbeit zeigen, dass BT-IgSF essentiell für die Fertilität männlicher Mäuse ist. In Abwesenheit von BT-IgSF können Mäuse keine Spermien bilden, haben kleinere Hoden und eine gestörte Hoden-Morphologie. Weitere Untersuchungen zeigten, dass der Grund der Azoospermie der BT-IgSF Knockout-Mäuse in einer gestörten Blut-Hoden-Schranke liegt. Die Expression von wichtigen Blut-Hoden-Schranken Proteinen wie Cx43 und ZO-1 ist erhöht und die Lokalisierung dieser Proteine ist im Falle von Cx43 diffus und nicht mehr auf den basalen Bereich beschränkt und im Falle von ZO-1 unorganisiert. Die funktionale Analyse der Blut-Hoden-Schranke mit einem Blut-Hoden-Schranken impermeablen Tracer ergab, dass die Blut-Hoden-Schranke defekt ist.

Die starke Expression von BT-IgSF in Sertoli Zellen legte nahe, eine Sertoli Zell-spezifische BT-IgSF Knockout-Maus zu generieren, um die bisherigen Ergebnisse zu überprüfen. Interessanter Weise zeigte der Sertoli Zell-spezifische Knockout den gleichen Phänotyp wie der globale Knockout. Dies beweist, dass die Expression von BT-IgSF in Sertoli Zellen essentiell für die Fertilität ist.

In einem konditionellen Knockout von BT-IgSF, der durch die Gabe von Tamoxifen in adulten Mäusen induziert wird, wurden ebenfalls kleinere Hoden, eine Reduktion der Spermienzahl sowie die Fehllokalisation von Cx43 beobachtet. Diese Befunde zeigen, dass BT-IgSF auch in adulten Mäusen entscheidend für die Aufrechthaltung der Spermatogenese und männlicher Fertilität ist.

Diese Arbeit zeigt, dass BT-IgSF notwendig für die männliche Fertilität in Mäusen ist. Die Abwesenheit führt zu einer defekten Blut-Hoden-Schranke und zur Fehllokalisierung von Blut-Hoden-Schranken Proteinen. Diese Ergebnisse führen zu einem besseren Verständnis über die Abläufe der Spermatogenese und dieses Wissen kann dazu genutzt werden, menschliche Infertilität besser zu verstehen.

5. INTRODUCTION

5.1. Testis

The mammalian testis is a paired organ in males responsible to ensure reproduction. The development of the testis starts at E10.5 in mice (Koopman et al., 1991). Primordial germ cells migrate from the hindgut into the genital ridge between E10.5 to E11.5 in mice (Ginsburg et al., 1990). The fate of the primordial germ cells is determined by their environment, more precisely by the presence or absence of Sertoli cells. From then on, the testis is composed of seminiferi tubuli and the interstitial cells, surrounded by the tunica albuginea. The interstitium contains blood and lymphatic vessels, nerves and Leydig cells. The seminiferi tubuli consist mainly of two cell types: the differentiating germ cells and the Sertoli cells. The seminiferi tubuli are surrounded by contractile peritubular myoid cells (Figure 1).

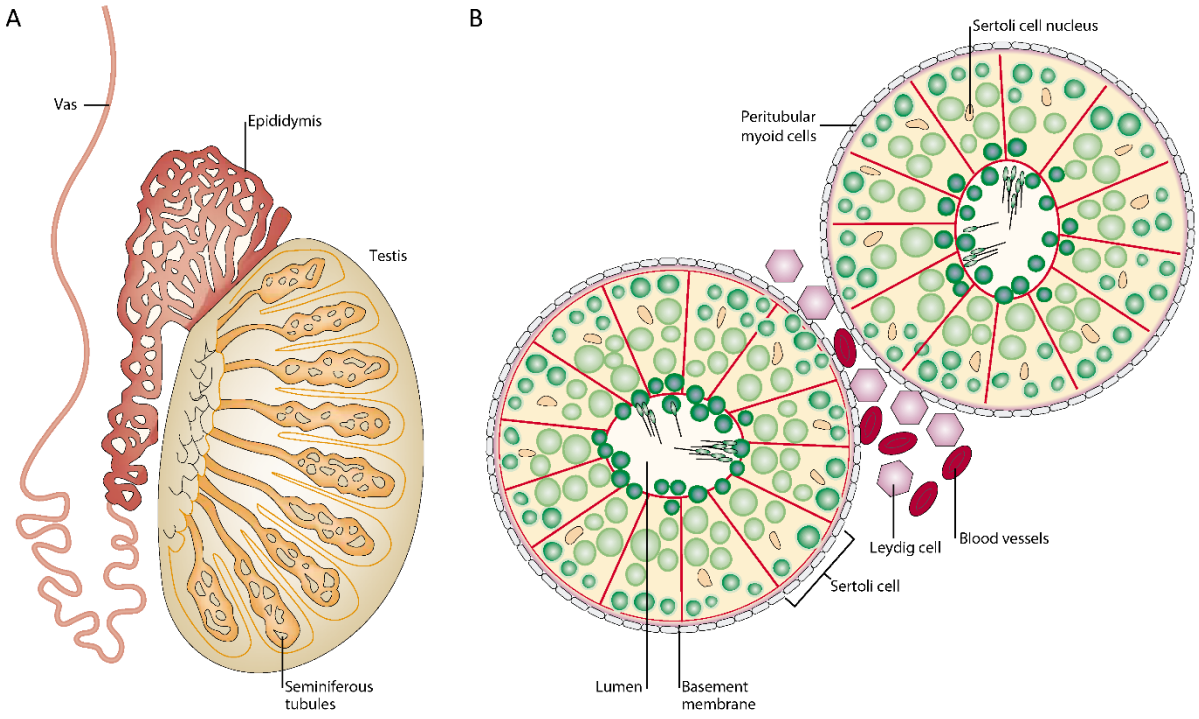

Figure 1: Organization of the testis
(A) Cross section of a testis with a schematic illustration of the seminiferi tubuli and the adjacent epididymis, which terminates in the vas. (B) Cross section through a seminiferous tubule with developing germ cells in different stages (green) embedded in Sertoli cells (outlined in red). Each tubule is surrounded by peritubular myoid cells and a basement membrane. In the interstitium the testosterone producing Leydig cells and the blood vessels are located. Modified after Cooke and Saunders, 2002.

5.2. Spermatogenesis and the cycle of the seminiferous epithelium

Inside the seminiferi tubuli, spermatogenesis takes place to produce sperm. In this process, germ cells migrate from the outer basal site towards the adluminal site and differentiate from spermatogonial stem cells into spermatozoa (sperm) (Figure 2 A). At the beginning, spermatogonia undergo mitosis to

become primary spermatocytes which then enter meiosis I to become secondary spermatocytes. The secondary spermatocytes enter meiosis II to become spermatids.

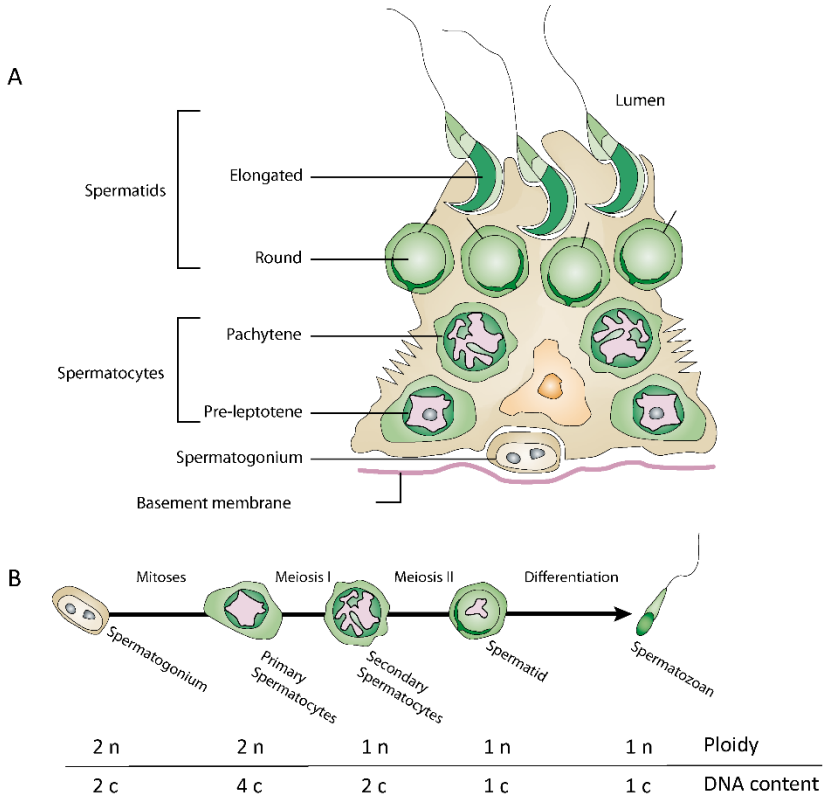

Figure 2: The seminiferous epithelium and the process of spermatogenesis
(A) The seminiferous epithelium is composed of nursing Sertoli cells and developing germ cells. The epithelium is polarized in a basal and an adluminal compartment. Spermatogonial stem cells are located at the basal side and migrate towards the lumen during their differentiation. This compartmentalization is established by Sertoli cells through cell junctions (indicated with zigzag lines). Pre-meiotic germ cells are located in the basal compartment, whereas meiotic and post-meiotic germ cells are located at the adluminal side. (B) Stages of the spermatogenesis. Spermatogonial stem cells first divide mitotically to produce high cell numbers needed for sperm output. The resulting primary spermatocytes enter meiosis I and become secondary spermatocytes. They then enter meiosis II and develop into spermatids. These spermatids are structurally remodeled to generate mature sperms (spermatozoa). DNA content and ploidy of the single developmental stages are depicted under each step. c: DNA/chromatid content, n: number of sets of chromosomes (ploidy). Modified after Cooke and Saunders, 2002.

During spermatogenesis the chromosome and chromatid content are changing (Figure 2 B). In the first mitotic division from spermatogonia to primary spermatocytes the number of chromosomes (n) and the chromatid number or DNA copies (c) remains the same (2n, 2c). Before meiosis I, the primary spermatocytes enter S-phase, where the chromatids are copied, resulting in 2n, 4c. In the following meiosis I, the homologous chromosomes are separated and secondary spermatocytes with 1n, 2c are generated. During meiosis II, the sister chromatids are separated, resulting in spermatids with 1n, 1c. Spermatids then differentiate into spermatozoa in a process called spermiogenesis. During this phase, the DNA is condensed, the histones are exchanged for protamines and the acrosome is formed. The spermatozoa are then released into the lumen in a process called spermiation and are transported to

the epididymis where the maturation is completed, and the sperm are stored until they are released. The first meiotic divisions start between P8 and P10 in mice and the development to a mature sperm takes 35 days. (Nebel et al., 1961; Cooke and Saunders, 2002).

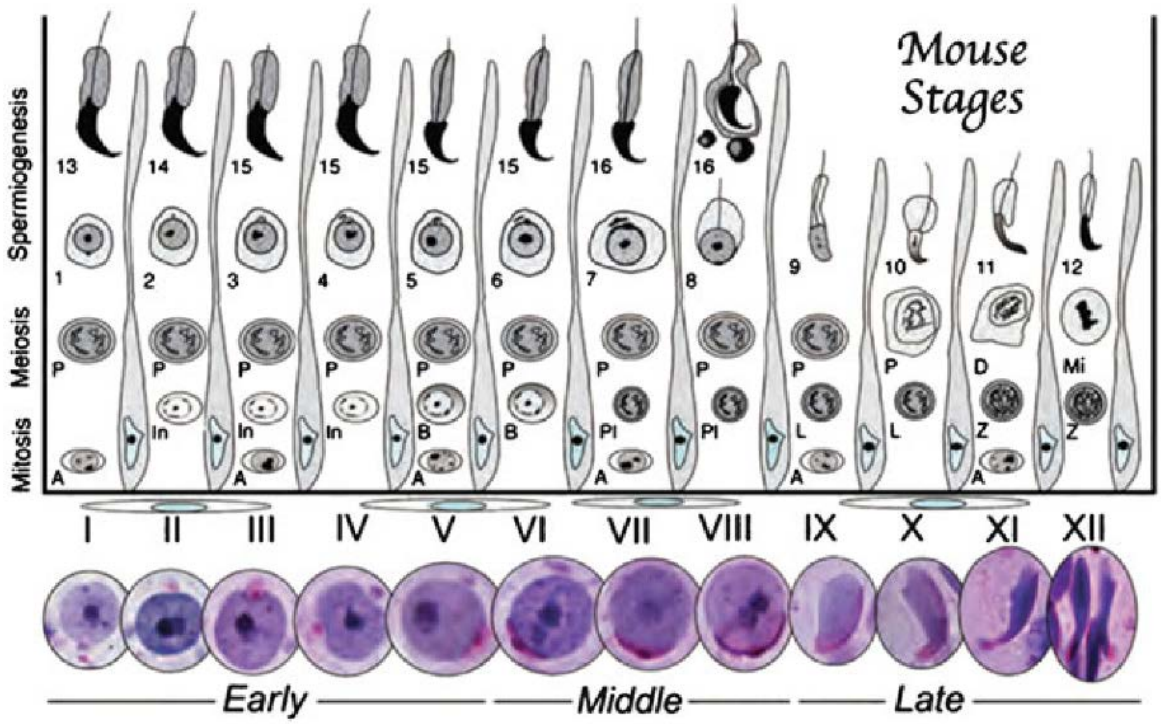

Figure 3: Staging map of different stages of the seminiferous epithelium in mice
Twelve different stages of spermatids can be distinguished due to Golgi staining visualized with PAS staining and the nucleus visualized by hematoxylin (bottom). Each germ cell passes 4.5 times the whole cycle in its development until a mature sperm is developed. Spermatogonia (A, In, B); spermatocytes (Pl: preleptotene, L: leptotene, Z: zygotene, P: pachytene, D: diakinesis, Mi: meiotic division); round spermatids (1-8); elongated spermatids (9-16). Modified after Hess and De Franca, 2008.

The different germ cell stages are located in a defined organization in the seminiferous epithelium: Less differentiated cells localize at the basal side, more mature germ cells are found at the luminal side. The subset of different germ cell layers at a given time point is well defined and is called a stage, however, this is purely an artificial definition (Leblond and Clermont, 1952). There are twelve stages in mice with different subsets defining the so called seminiferous cycle (Oakberg, 1956a). The twelve stages are organized in a wave-like manner, always repeating the consecutive sequence from I to XII (Figure 3). The twelve stages in mice are defined after the twelve different maturation stages (I-XII) of spermatids in the testis, according to histological differences. In the rat 14 and in humans 6 distinct stages exist. The complete seminiferous cycle takes 8.6 days in mice (Oakberg, 1956b). The different stages can be distinguished by morphological differences of the Golgi region and the nucleus, as determined by PAS staining (Hess and De Franca, 2008). In one cross-section of the seminiferous tubule, only one stage is found in the mouse, whereas several stages are found in parallel in humans. It is difficult to determine exactly one specific stage because spermatogenesis is a continuous process

resulting in a transition between two stages in an observed area. Therefore, it is easier to group stages in early (stage I-V), middle (VI-VIII) and late (IX-XII) stages.

5.3. The Sertoli cell

5.3.1. Role of Sertoli cells for germ cell differentiation

Enrico Sertoli discovered a new cell type in 1865 and described those cells as irregular in shape, having nucleolated nuclei and homogeneous cytoplasm containing fine fat droplets (Sertoli, 1987). These nursing cells, which later became known as Sertoli cells, have a very special morphological shape with a big nucleus and very thin cytoplasmic protrusions (França et al., 2016) (Figure 4). The nucleus resides near the basement membrane of a seminiferous tubule and has three distinct parts with the nucleolus and two satellite chromocenters (Kushida et al., 1993). The very thin cytoplasmic arms, often less than 50 nm in width (Hess and Vogl, 2015), surround the germ cells to attach and nurture them throughout their maturation. Each Sertoli cell interacts with 30-50 developing germ cells (Wong and Russell, 1983).

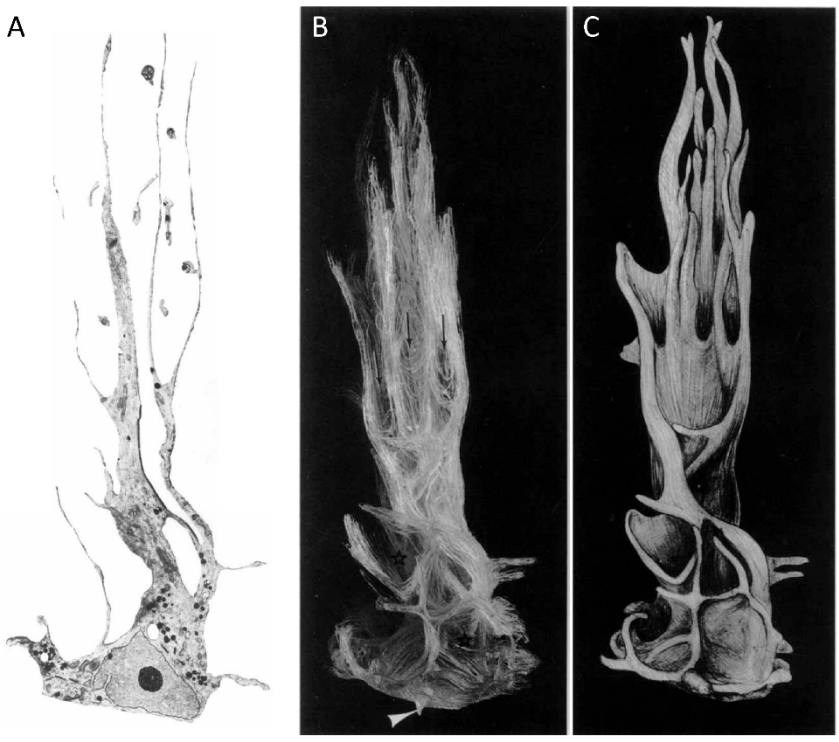

Figure 4: Three-dimensional reconstruction of a stage V Sertoli cell
(A) The reconstructed Sertoli cell is shown isolated from its surroundings. Several processes of the upper half penetrate elongated spermatids. (B) and (C) Anteriolateral part of a Sertoli cell, above the basal part cup-like and sheet-like processes, hollow parts are occupied by round spermatids (black stars), in the cylindrical openings three elongated spermatids are accommodated (arrow). Arrowhead: emanating canonical process from the lateral surface. Modified after Wong and Russell, 1983.

They support the developing germ cells with micronutrients such as Fe^{3+} and Cu^{2+} via the control of the exit and entry of ions but also with lactate and acetate, which serve as fuel to the developing germ cells (Boussouar and Benahmed, 2004). Furthermore, they take care of the waste produced by germ

cells and phagocytose spermatid cytoplasm and degenerating germ cells (Rex A. Hess and Luiz R. França, 2015).

5.3.2. The spermatogonial stem cell niche

Sertoli cells create the spermatogonial stem cell (SSC) niche. For the self-renewal and differentiating properties of stem cells, special environments are necessary. SSCs reside at the very basal site of the seminiferous tubule and are in direct contact with Sertoli cells. The special environment for the SSC niche is created by interstitial cells, the basement membrane, paracrine factors from the vascular system and the Sertoli cells. A very important niche factor is GDNF which is produced by Sertoli cells and is essential for SSC maintenance and self-renewal (Meng et al., 2000). Other growth factors such as FGF2 and EGF are also critical to maintain long-term stem cell properties (Chen and Liu, 2015; França et al., 2016). FSH (follicle stimulating hormone) acts on Sertoli cells and enhances GDNF as well as FGF2 production and thereby the stem cell character of SSCs (Tadokoro et al., 2002; Mullaney and Skinner, 1992).

5.3.3. Hormonal regulation

Hormones are not only important for the maintenance of the stem cell character of SSCs, but play crucial roles for the whole spermatogenesis. The hypothalamic-pituitary-gonadal axis controls the production of sex hormones which regulate spermatogenesis (Figure 5). The hypothalamus produces

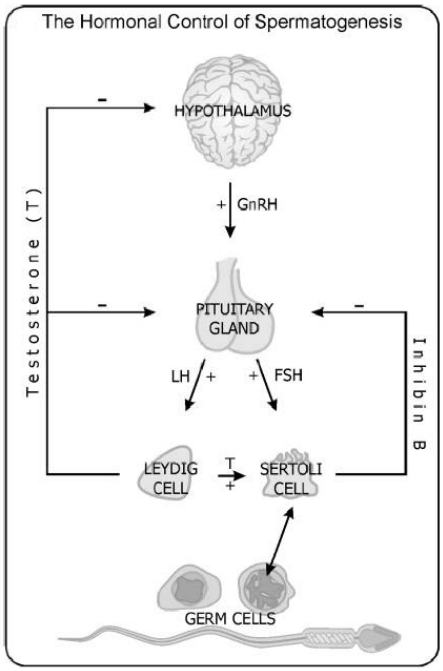

Figure 5: The hypothalamic-pituitary-gonadal axis
Spermatogenesis is hormonally controlled. Gonadotropin-releasing hormone (GnRH) from the hypothalamus stimulates the pituitary gland to produce (FSH) and luteinizing hormone (LH). LH acts on Leydig cells and induce the production of testosterone which in turn acts together with FSH on Sertoli cells to activate germ cell development. FSH secretion is inhibited by the production of inhibin b by Sertoli cells and the production of testosterone is negatively regulated by testosterone itself. Adapted from Borg et al., 2010.

GnRH (gonadotropin-releasing hormone) which acts on the pituitary gland, which in turn secrets the paracrine hormones LH (luteinizing hormone) and FSH. LH acts on Leydig cells in the testis and causes the production of testosterone. Testosterone binds to androgen receptors on the surface of Sertoli cells. The expression of androgen receptors is crucial for testosterone signaling and the expression is cycle dependent with the strongest expression occurring in stage VII in rats (Kerr et al., 1993). FSH acts on Sertoli cells and causes the production of ABP (androgen-binding protein). This protein is important for the binding of testosterone in the testis and the transport to germ cells or the epididymis (Griswold, 1988). FSH secretions is regulated by inhibin and activin which are both secreted by Sertoli cells.

5.3.4. The blood-testis barrier

The blood-testis barrier (BTB), also called Sertoli cell barrier, is a physical barrier formed by Sertoli cells. It develops during puberty, in mice around P17, in humans around 11 to 13 years of age (Hosoi et al., 2002; de Kretser et al., 2016). The BTB is built by tight junctions, gap junctions, ectoplasmic specializations and desmosomes (Mruk and Cheng, 2015) (Figure 6). Desmosomes create stable

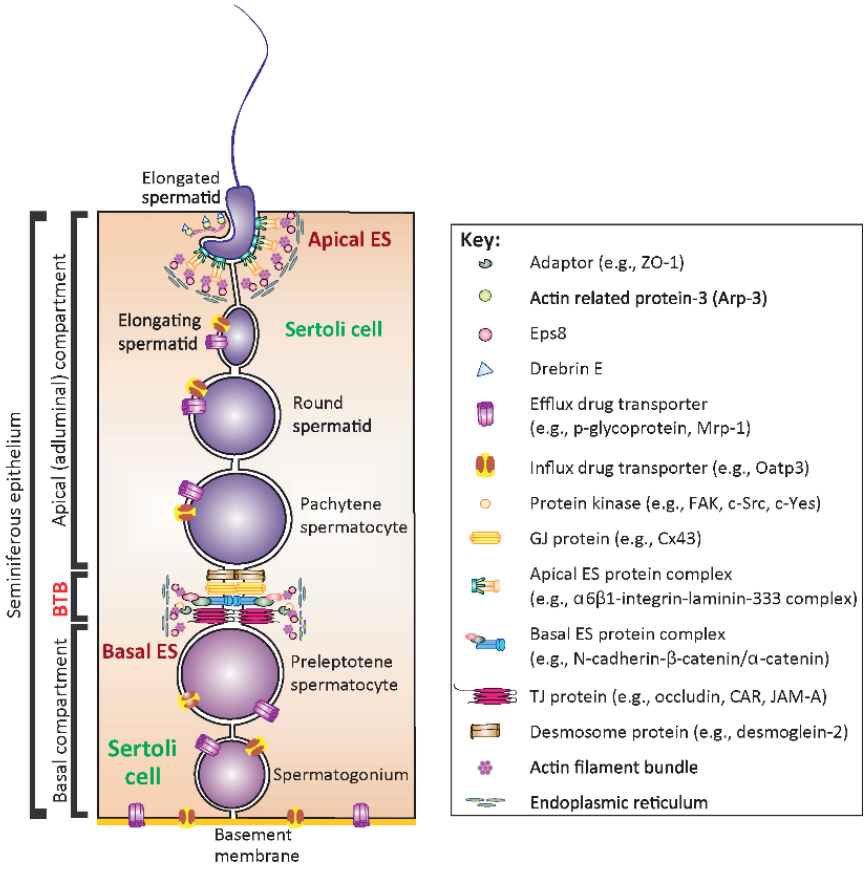

Figure 6: Relative Location of the BTB, the bES and the aES inside the seminiferous epithelium
The BTB, located near the basement membrane (BM), divides the epithelium in a basal and apical (adluminal) compartment. The BTB is composed of tight junctions (TJs), gap junctions (GJs), desmosomes and basal ectoplasmic specializations. Tightly packed actin bundles are sandwich-like positioned between endoplasmic reticulum and the Sertoli cell membrane. bES and aES share similar structural features, but the tightly packed actin bundles are only present in Sertoli cells and are not seen in elongating/elongated spermatids. The aES is the only anchoring mechanism for elongating/elongated spermatids in the epithelium until they are released into the lumen. Modified after Wan et al., 2013.

adhesions which attach to the intermediate filament vimentin. The tight junctions form a barrier which restricts water, solutes and large molecules as well as lipids and proteins from the paracellular space. The most important tight junction proteins for the BTB in mice are Occludin, Claudin-3, Claudin-11, ZO-1 and ZO-2 (Morrow et al., 2010). Gap junctions allow the diffusion of molecules smaller than 1 kDa such as second messengers and ions. The most abundant gap junction protein in the testis is Cx43 but also other Connexins are expressed in the testis such as Cx33, which is only present in the testis of rodents, Cx26 and Cx50 (Pointis and Segretain, 2005). The ectoplasmic specializations (ES) are testis-specific adherens junctions, which consist of hexagonally arranged filamentous actin microfilaments positioned between the plasma membrane and a cistern of endoplasmic reticulum. The ES consists of the Cadherin-Catenin multifunctional complex. ES between Sertoli-Sertoli cells are called basal ES (bES) and ES between Sertoli cells and elongating/elongated spermatids are termed apical ES (aES) (Mruk and Cheng, 2015).

The BTB creates two distinct compartments in the seminiferous epithelium. The basal compartment contains the SSCs, the Sertoli cell nucleus and all premeiotic germ cells. In the apical (adluminal) compartment, meiotic and post-meiotic cells are located separated from blood supply. Sertoli cells control the passage of molecules through the barrier via the expression of transporters and junctions. This barrier also protects the advanced germ cells from antibodies and immune cells, thereby creating an immunoprivileged microenvironment for the developing germ cells (França et al., 2016). The immunoprivilege is not only based on the BTB itself. Sertoli cells modulate the immune response by secreting yet unknown immunoregulatory factors which modify the immune response and create a local tolerogenic environment. Together with the peritubular myoid cells, immune cells are restricted to the interstitial space (Mital et al., 2010).

During the differentiation, germ cells must migrate from the basal to the apical side of the epithelium and must pass the BTB. Therefore, a highly regulated BTB disassembly and reassembly is necessary. Preleptotene spermatocytes are transported across the BTB at stages VII-VIII of the cycle. During this process a new BTB is first built behind the preleptotene spermatocyte and afterwards the old BTB is degraded to ensure a functional barrier at all times (Smith and Braun, 2012; Xiao et al., 2014). The BTB and the transport of germ cells across the BTB are crucial for spermatogenesis. Dramatic changes or disruption of the BTB lead to infertility.

5.4. Cell adhesion and cell adhesion molecules

As mentioned above, cell adhesion molecules (CAMs) play crucial roles for the proper function of the testis. One of the largest class of CAMs is formed by the immunoglobulin superfamily (IgSF) proteins, therefore also called immunoglobulin cell adhesion molecules (IgCAMs). IgSF proteins are implicated

in many different biological processes such as signaling pathways, immune system functions and cell-cell contacts. The IgCAMs can be classified in structural subgroups such as the CTX (cortical thymocyte marker in *Xenopus*) group. This group can be further divided into the CTX-subgroup, the JAM-subgroup and the CAR-subgroup. The latter contains four members which share a similar overall protein structure (Matthäus et al., 2016).

5.4.1. The CAR-subgroup

Besides the eponymous member CAR (coxsackie and adenovirus receptor), also ESAM (endothelial cell-selective adhesion molecule), CLMP (CAR-like membrane protein), and BT-IgSF (brain and testis-specific immunoglobulin superfamily protein), also known as IgSF11, belong to the CAR-subgroup (Figure 7).

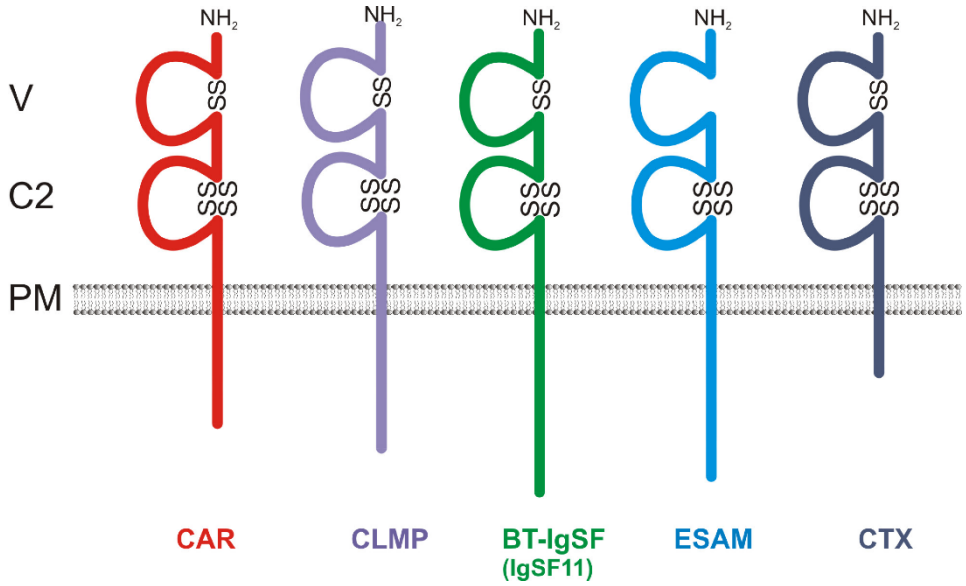

Figure 7: The CAR subgroup of IgCAMs
All members of the CAR subgroup exhibit the same overall protein structure. V: Ig-like domain of the V subtype; C2: Ig-like domain of the C2 subtype; PM: plasma membrane; CAR: coxsackievirus and adenovirus receptor; CLMP: CAR-like membrane protein; BT-IgSF: brain- and testis-specific immunoglobulin superfamily protein; ESAM: endothelial cell-selective adhesion molecule; CTX: marker for cortical thymocytes of Xenopus. Modified from Matthäus et al., 2014.

The CAR CAMs are single spanning transmembrane glycoproteins with extracellular, transmembrane and cytoplasmic domains. The extracellular part contains the two immunoglobulin domains (a variable V-type and a constant C2-type) which are connected by a linker (Raschperger et al., 2004). A crystallographic study of the extracellular part of CAR revealed complex homophilic and heterophilic interactions (Patzke et al., 2010). Based on these crystallographic data and due to high similarities in the amino acid sequence, three-dimensional structures for CLMP and BT-IgSF were predicted (Matthäus et al., 2016). In the cytoplasmic tail, all CAR-subgroup proteins carry a PDZ binding motif which allows interaction to PDZ domain-containing proteins (Matthäus et al., 2014). ESAM can bind to the scaffolding protein Na^+/H^+ exchange regulatory cofactor NHE-RF1 (Stalker et al., 2009) and to the

multidomain adaptor protein Membrane-associated guanylate kinase, WW and PDZ domain-containing protein 1 (MAGI-1) (Wegmann et al., 2004). CAR is able to bind to tight junction molecules like zonula occludens protein 1 (ZO-1) (Cohen et al., 2001), multiple PDZ domain protein (MUPP-1) (Coyne et al., 2004) and junctional adhesion molecule C (JAM-C) (Mirza et al., 2006). Other proteins containing a PDZ domain can co-localize with CAR, such as Postsynaptic density protein 95 (PSD-95), PRKCA-binding protein (PICK-1), MAGI-1b (Excoffon et al., 2004) and ligand-of-Numb protein-X 1 and 2 (LNX-1 and LNX-2) (Mirza et al., 2005; Sollerbrant et al., 2003). For CLMP, a co-localization with tight junction proteins like ZO-1 and Occludin could also be observed in epithelial cell lines (Raschperger et al., 2004).

All the above-mentioned proteins mediate cell-cell contacts. CAR can either act homophilic (Honda et al., 2000; Patzke et al., 2010) or heterophilic with other membrane proteins such as JAM-L (Verdino et al., 2010; Zen et al., 2005) as well as with extracellular matrix molecules like fibronectin (Patzke et al., 2010). CLMP and ESAM are both able to mediate cell adhesion in transfected cells in a homophilic manner (Eguchi et al., 2005; Hirata Ki et al., 2001; Nasdala et al., 2002; Raschperger et al., 2004).

All members of the CAR subgroup are expressed in the brain. ESAM is exclusively expressed in endothelial cells (Hirata Ki et al., 2001; Nasdala et al., 2002). For CAR, BT-IgSF and CLMP it was further shown that the expression in the brain is developmentally regulated (Langhorst, 2015; Jang et al., 2015; Honda et al., 2000). CAR, which is involved in the attachment and infection of coxsackie B viruses and many human adenoviruses, is additionally expressed in the developing heart (Dorner et al., 2005; Asher et al., 2005) but gets downregulated during maturation. In non-diseased adult human hearts, CAR is restricted to intercalated discs (Shaw et al., 2004). CAR deficient mice are embryonal lethal due to malformations and hemorrhages in the heart (Asher et al., 2005; Dorner et al., 2005). The expression sites of CLMP are still not fully elucidated. On mRNA level, some studies revealed an expression in the brain and in the heart of mice but only in a minor amount in the equivalent human tissues. Furthermore, CLMP is highly expressed in white adipose tissue of rats, mice and humans and in the small intestine and the placenta of humans (Raschperger et al., 2004; Eguchi et al., 2005). The expression might vary between species and uncertainties arise due to the absence of a reliable antibody to detect CLMP at the protein level (Langhorst, 2015).

5.4.2. BT-IgSF (IgSF11)

5.4.2.1. The *BTIGSF/Igsf11* gene and its transcript

The human *BTIGSF* gene is localized on chromosome 3, has 134 kb and is composed of 7 exons (NM_001015887.1). The encoded protein has 431 amino acids and the longest cytoplasmic tail among all CAR-subgroup members with 169 amino acid residues. The murine protein consists of 428 amino acids and is encoded by the 124 kb long *Igsf11* gene, which is localized on chromosome 16 and is also

composed of 7 exons (NM_170599). The amino acid sequences of murine and human BT-IgSF show a homology of 88% (Suzu et al., 2002). The murine amino acid sequence identity between BT-IgSF (P0C673) and the other CAR-subgroup members varies between 30% for ESAM (Q925F2) and 33% for CAR (P97792) and CLMP (Q8R373), when sequences were compared by BLASTP 2.6.0+ by NIH (Altschul et al., 1997). The length of the cytoplasmic tail between these proteins are variable but the C-terminal sequence is highly conserved, a region which probably enables interaction with PDZ containing proteins (Suzu et al., 2002).

5.4.2.2. Expression of BT-IgSF

BTIGSF mRNA was found in human testis, ovary, adrenal gland, kidney and brain. Also in mice *Igsf11* mRNA could be detected in neurons and glia cells as well as in the pyramidal layer of the dentate gyrus, the CA1 of the hippocampus and in the commissure fibers of the corpus callosum (Katoh and Katoh, 2003; Watanabe et al., 2005; Suzu et al., 2002). Consistent with these findings, it was also shown that *Igsf11* mRNA is expressed in rat olfactory bulbs, cortex, striatum, hippocampus and cerebellum. BT-IgSF protein was found in the correlated brain regions, where the expression increases during brain development. In 3 week old mice BT-IgSF expression in the dentate gyrus was threefold stronger than in the CA1 region of the hippocampus (Jang et al., 2015).

5.4.2.3. Biological functions of BT-IgSF

It has been reported that BT-IgSF can induce cell aggregation in a stably transfected human myeloid cell line, TF-1-fms cells, which normally grow in suspension. In U373MG cells, a transfected glioblastoma cell line, the cell adhesion effect of BT-IgSF could be shown. Furthermore, it was shown that this cell adhesion effect is independent from Ca^{2+} and Mg^{2+} and is mediated in a homophilic manner and is not mediated via integrins (Harada, 2005).

In zebrafish and *Neolamprologus meeli* BT-IgSF plays a role in the migration of melanophores (Eom et al., 2012; Ahi and Sefc, 2017). BT-IgSF is expressed in adult pigment cells and their precursors as well as in other organs like heart, brain and the testes. In BT-IgSF zebrafish mutants (*seurat* mutants), the melanophore precursors fails to migrate to the hypodermis to form a typical horizontal patterning, resulting in an irregular spotted pattern.

It has recently been elucidated that BT-IgSF regulates synaptic transmission and plasticity. By the interaction of BT-IgSF with PSD-95 and AMPARs in a tripartite manner, BT-IgSF recruits PSD-95 and AMPARs to homophilic cell adhesion sites. It was further shown that the interaction between BT-IgSF and PSD-95 takes place between the PDZ- binding domain of BT-IgSF and the first two PDZ domains of PSD-95. However, for the interaction between BT-IgSF and GluA1 the transmembrane domain of BT-IgSF is required. Knockdown studies of BT-IgSF in cultured neurons showed that BT-IgSF mediates

synaptic transmission via the stabilization of AMPARs. *In vivo* experiments with BT-IgSF knockout mice revealed a role for BT-IgSF in synaptic transmission. In BT-IgSF knockout granule cells from the dentate gyrus, the amplitude of mEPSCs was reduced, comparable with findings of shRNA knockdown of BT-IgSF in cultured rat neurons. Moreover, there were also changes in SC-CA1 (Schaffer collateral) synapses. The LTP was suppressed in these neurons, which indicates that BT-IgSF regulates plasticity in the hippocampus (Jang et al., 2015).

5.4.2.4. BT-IgSF in disease

Even though BT-IgSF is involved in different diseases, its biological importance is not well understood so far. BT-IgSF has been suspected to have an impact on neuronal development and health after three patients, which suffered from corpus callosum agenesis, were reported to exhibit interstitial deletion of the chromosomal area, in which also *BTIGSF* is localized (Suzu et al., 2002). In addition, neurons, derived from induced pluripotent stem cells from individuals with schizophrenia, showed reduced BT-IgSF expression, were less connected and exhibited a decreased neurite number, indicating that BT-IgSF could be important for neuronal development and synapse formation (Brennand et al., 2011).

BT-IgSF might also play a role in multiple types of cancer. BT-IgSF was reported to be upregulated in hepatocellular carcinomas as well as in intestinal-type gastric and colon cancer. Due to the expression site of BT-IgSF and its upregulation in several cancers, it was suggested that BT-IgSF could be an cancer-testis antigen (CTA), which are proteins, which are normally restricted to the testis but are also expressed in cancer (Scanlan et al., 2002; Watanabe et al., 2005). CTAs are often oncogenes supporting growth, survival and metastasis. It was shown that knockdown of *Igsf11* via siRNA lead to a reduced growth of gastric cancer cells, suggesting BT-IgSF as a promising target for the therapy of carcinomas (Watanabe et al., 2005). BT-IgSF also plays a role in breast cancer, since AP-2γ, a transcription factor activator, well known to be involved in neoplasia and overexpressed in most breast cancer types, enhances the expression of *BT-IGSF* by binding to the chromosomal binding site of AP-2γ on the *BTIGSF* gene. This study also proposed that BT-IgSF is a candidate for anticancer therapy (Ailan et al., 2009).

6. AIMS OF THE STUDY

The expression of BT-IgSF in the brain and the testis of mouse and man is already known. A function of BT-IgSF in the brain has recently been described, however, its role in the testis has been neglected until now. The aim of this thesis was to gain insight into the function of BT-IgSF in the murine testis. As a starting point for the analysis of BT-IgSF function, it is important to know the exact expression pattern. Therefore, the localization of BT-IgSF in the testis was investigated with immunofluorescence stainings of testis cryosections. Furthermore, the expression during different stages of the seminiferous epithelium was determined. To get a better understanding of the function of BT-IgSF, a non-conditional knockout was analyzed. After the observation that BT-IgSF knockout males were infertile, the major aim of the study was to characterize the reason for this phenotype. The infertility was characterized in detail and different probable causes, such as meiotic arrest, apoptosis or an impairment of the BTB, were analyzed to find the underlying pathomechanism and the role of BT-IgSF. The finding of a disrupted BTB and the major expression site of BT-IgSF in Sertoli cells, lead to the aim to selectively inactivate BT-IgSF in Sertoli cells. Therefore, a Sertoli cell-specific BT-IgSF knockout was analyzed in this study. It was also of interest, whether BT-IgSF is only necessary for the development of the testis and the BTB or if BT-IgSF also has a role in the maintenance of spermatogenesis and the BTB in adult males. To answer this question a tamoxifen inducible knockout of BT-IgSF of adult animals was generated and analyzed.

7. MATERIALS

7.1. Chemicals

Table 1: Chemicals used in this study

Substance	Company	Order number
30% acrylamide	Roth	3029.1
6-Carboxyfluorescein	Sigma	C0662
Acetic acid	Merck	1000631011
Agar-agar	Roth	2266.3
Agarose Neeo	Roth	22673
Ampicillin	Sigma	59349
Aprotinin	Sigma	A1153
APS	GE	17131101
Bacto Yeast Extract	BD	212750
Bacto-Tryptone	BD	211705
BODIPY 493/503	Thermo Scientific	D3922
BSA, Fraction V	Biomol	01400.100
$CaCl_2$	Merck	1023820500
Citric acid	Chemsolute	24321000
CNBr-Activated Sepharose 4B	GE Healthcare	17-0430-01
Corn oil	Sigma	C8267
DAPI	Sigma	D9542
DEA	Sigma	127744
dNTP Mix, 10 mM each	Thermo Scientific	R0191
DTT	Sigma	D9779
EDTA	Sigma	E6758
Eosin Y	Sigma	E4382
Ethanol	Merck	1009832511
Ethidiumbromid	Applichem	A1152
EZ-Link Sulfo-NHS-LC-Biotin	Pierce	21335
Glutathion sepharose 4B	GE Healthcare	17075601
Glycine	Merck	357002
Goat serum	Linaris	EZN1000-100H
Guanidinehydrochlorid	Merck	369080

Haematoxylin	Sigma	GHS332
HCl 32%	Merck	1003191011
IPTG	Roth	CN08.3
Isopropanol	Merck	1096342511
Ketanest	Pfizer	39944.00.00
Leupeptin	Sigma	L2884
Lipofectamine 2000	ThermoFisher	11668019
Mowiol	Merck	475904
Na_2HPO_4	Merck	106580
NaCl	Merck	1064041000
NaH_2PO_4	Merck	1063461000
NaOH	Merck	1064981000
PBS	Merck	L182-50
Pepstatin A	Sigma	77170
PFA	Merck	8187151000
PMSF	Enzo Life Sciences	ALX-270-184-G005
PNA-A488	Thermo Scientific	L21409
PNA-A568	Thermo Scientific	L32458
Protein A sepharose CL-4B	GE Healthcare	17-0780-01
Rompun 2%	Bayer	PZN 1320422
Sodium citrate	Merck	1064481000
Streptavidin-Cy5	Dianova	016-170-084
Sucrose	Merck	1076871000
Tamoxifen	Sigma	T5638
Technovit 3400	Haereus Kulzer	64708806
Technovit 7100	Haereus Kulzer	64709003
Technovit universal liquid	Haereus Kulzer	66022678
TEMED	Bio-Rad	1610800
Tissue-Tek OCT	Sakura	4583
Tris	Merck	1083821000
Triton X100	Merck	1086031000
Tween20	Sigma	P7949

7.2. Consumables

Table 2: Consumables used in this study

Product	Company	Order number
Amersham Protran 0.45 NC	GE Healthcare	10600002
Blotting paper, 400 g/m²	Macherey-Nagel	MN 440 B
Genomic-tip 500/G	Qiagen	10262
Gnome Pen Flat	Bar Naor Ltd	BN3525I
Hybond-N+	GE Healthcare	RPN203B
Illustra MicroSpin G-50	GE Healthcare	27-5330-01
PM 3 kDa membrane	Millipore	PLBC04310

7.3. Buffers and solutions

Table 3: Buffers and solutions used in this study

Solution	Recipe
10% Mowiol	2.4 g mowiol, 15.6 ml water, 2.4 ml 1 M Tris pH 8.5, 6 ml Glycerin
10x DNA sample buffer	250 g/l Ficoll-400, 200 ml/l 0.5 M EDTA, 10 ml/l 1M Tris pH 7.4, 2.5 g/l bromphenol blue
10x SSC buffer	1.5 M NaCl, 0.15 M, sodium citrate, pH 7
1x Running buffer	25 mM Tris, 190 mM glycine, 0.1% SDS, pH 8.3 with HCl
20x SSC buffer	3 M NaCl, 0.3 M sodium citrate, pH 7 with 0.1 M HCl
2x SSC buffer	0.3 M NaCl, 0.03 M, sodium citrate, pH 7
4% PFA	40 g/l PFA, 1x PBS, pH 7.2
50x TAE	242 g/l Tris, 57.2 ml/l acetic acid, 100 ml 0.5 M EDTA (pH 8.0)
5x Sample buffer with ß-ME	125 ml/l 1M Tris pH 6.8, 500 ml/l 100 mM EDTA pH7.0, 100 g/l SDS, 100 ml/l ß-mercaptoethanol, 0.5 g/l bromphenol blue, same amount glycerol was added
Agarose gel	2.5% agarose in 1xTAE buffer, 10 µl 1% ethidiumbromide
Anesthesia	12% Rompun (Bayer), 34% of Ketanest (Pfizer), 54% of a 0.9% sodium chloride solution
ASCM	136 mM NaCl, 2.5 mM KCl, 20 mM HEPES, 20 mM glucose, 2 mM $CaCl_2$, 1 mM $MgCl_2$, pH 7.3 with NaOH, osmolality 320 osmol/kg
Blocking solution IF	3% goat serum, 1% BSA, 0.1% Triton X100 in PBS
Blocking solution WB	3% BSA in TBST

Blotting buffer	100 ml/l 10x running buffer, 200 ml/l isopropanol
Church buffer	190 ml 0.5 M NaH_2PO_4 /1mM EDTA, pH 7.2 with NaOH, 1% BSA and 7% SDS were added and dissolved at 68 °C, filled up to 200 ml with H_2O, filtered through 0.8 µm, stored aliquots at -20 °C
Citrate buffer	10 mM Sodium Citrate Buffer, 0.05% Tween 20, pH 6.0
cleavage buffer	50 mM Tris-HCl pH 7.0, 150 mM NaCl, 1 mM EDTA, 1 mM DTT
Denaturation buffer	0.5 M NaOH, 1 M NaCl
Depurination buffer	250 mM HCl
ECL solution	Clarity Max, Bio-Rad
Elution buffer glutathione Sepharose	50 mM Tris-HCl pH 8.0, 10 mM reduced glutathione
Elution buffer protein A Sepharose column	150 mM NaCl, 0.58% acetic acid
LB medium	1% Bacto-Tryptone, 0.5% Bacto-Yeast-Extract, 1% NaCl dissolved in ddH_2O, autoclaved and stored at 4°C
LB-Agar	1.5% agar in LB-medium, autoclaved and stored at 4°C.
Proteinaseinhibitors	Aprotinin (1:500), Leupeptin (1:500), Pepstatin (1:500), PMSF (1:1000)
SDS-PAGE	**10%**: 2.8 ml water, 3.75 ml Tris pH 6.8, 100 µl SDS, 3.3 ml acrylamide, 100 µl 10% APS, 5 µl TEMED **Stacking gel**: 3.7 ml water, 0.625 ml Tris pH 6.8, 50 µl SDS, 0.65 ml acrylamide, 50 µl 10% APS, 5 µl TEMED
Solubilization-buffer	1% Chaps in TBS
Tail lysis buffer	3.752 g/l potassium chloride, 2 ml 1 M magnesium chloride, 10 ml 1 M Tris pH 8.0, 100 mg gelatin, 45 ml 10% TX-100, 45 ml 10% Tween 20, H_2O ad 1l
TBST	1x TBS, 0.5% Tween-20
Washing buffer IF	0.1% Triton X-100, 1X PBS
Washing buffer I	1x SSC with 1% SDS
Washing buffer II	1x SSC with 0.1% SDS
Washing buffer III	0.5x SSC with 0.1%SDS
Washing buffer IV	0.2x SSC with 0.1% SDS
Washing buffer V	0.1x SSC with 0.1% SDS
YT-media	16% Bacto-tryptone, 10% Bacto-Yeast-Extract, 5% NaCl, pH 7.0 with NaOH, autoclaved, stored at 4 °C

7.4. Cell culture media

Table 4: Cell culture media used in this study

Media	Recipe
COS7 cell media	DMEM (Gibco, 41966029), 1x PenStrep (Gibco, 15140122), 10% FCS (Gibco, 10270106)
MEM	Gibco, 31095029
Opti-MEM	Gibco, 31985047
Sertoli cell media	DMEM low glucose (Gibco, 31885023), 1x PenStrep (Gibco, 15140122), 10% FCS (Gibco, 10270106)

7.5. Primary Antibodies

Table 5: Primary antibodies used in this study for immunofluorescence stainings

Antibody target	Host	Dilution/Concentration	Company	Order number
BT-IgSF (Rb113)	Rabbit	1 µg/ml	AG Rathjen	
BT-IgSF (Rb95)	Rabbit	1 µg/ml	AG Rathjen	
Cx43	Rabbit	1:1000	Cell Signaling	3512
Cx43	Mouse (Mab)	1:250	B&D	610061
Espin	Mouse (Mab)	1:200	B&D	611656
SYCP3	Rabbit	1:500	abcam	15093
Vimentin	Rabbit	1:300	abcam	ab92547
WT1	Rabbit	1:300	abcam	ab15249
ZO-1	Rabbit	1:100	Invitrogen	40-2200
ZO-2	Rabbit	1:50	Cell signaling	2847S
γH2AX	Mouse (Mab)	3 µg/ml	Novus Biologicals	NB100-74435

7.6. Secondary Antibodies

Table 6: Secondary antibodies used in this study

Antibody	Conjugate	Dilution	Company	Order number
Goat anti mouse	A488	1:500	Invitrogen	A11029

Goat anti rabbit	Cy3	1:500	Jackson	111-165-144
Goat anti rabbit	A488	1:500	Invitrogen	A11034
Goat anti rabbit	HRP	1:20000	Jackson ImmunoResearch	111-035-144

7.7. Oligonucleotides

All oligonucleotides were purchased from Eurofins genomics. Stock concentrations are 50 µM.

Table 7: Oligonucleotides used in this study

Primer	Sequence 5´- 3´	Amplicon	Purpose
5´probe For **5´probe Rev**	GGGGGATCCAGGTTTGCAGTGAGGAGAATCA GGGGACGTCAGAAACAGTCAAGACAGCGGG	621 bp	Southern blot probe
Primer 1 **Primer 2**	ACATGCACAGGAAGGTCCTC TCATTCGAGCAATGCCTTTT	197 bp	Genotyping WT in BT-IgSF KO and BT-IgSF^{flx}
Primer 1 **Primer 3**	ACATGCACAGGAAGGTCCTC CTTCTGATGAGGTGGTCCCA	343 bp	Genotyping KO in BT-IgSF KO
Primer 1 **Primer 2**	ACATGCACAGGAAGGTCCTC TCATTCGAGCAATGCCTTTT	379 bp	Genotyping Flx allele in BT-IgSF^{flx}
Primer 4 **Primer 5**	GAACGCACTGATTTCGACCA AACCAGCGTTTTCGTTCTGC	200 bp	Genotyping Cre allele in all mice
GF1 **En2in**	GTAGAGAGCCTGAATAGACAGTTC TGGGACCACCTCATCAGAAG	6.58 kb	Long range PCR 5’ side
lacZ **GR1**	TCAACAGCAACTGATGGAAACCAG CTTCAGTGATGCTAAGTGGATGTC	6.54 kb	Long range PCR 3’ side
Rplp0	GGACCCGAGAAGACCTCCTT GCACATCACTCAGAATTTCAATGG	85 bp	qPCR housekeeping gene
BT-IgSF	TGCACTAATTTCAGGGGCGT GCCAGAGAAAGACTGGCGTA	268 bp	qPCR
Gja1 (Cx43)	GAACACGGCAAGGTGAAGAT GACGTGAGAGGAAGCAGTCC	187 bp	qPCR
Tjp1 (ZO-1)	GTTTAGGAGCACCAAGTGC TCCTGTACACCTTTGCTGG	96 bp	qPCR
Tjp2 (ZO-2)	GTCCTCTACCTGCTAGAAATCC	81 bp	qPCR

	GATATCTCTGTACACGTCTGCT		
Ocln	TGGCTGCTGCTGATGAATA CATCCT CTTGATCTGCGATAAT	116 bp	qPCR
Cldn11	TCCTTATTCTGCTGGCTCTC AGCTCACGATGGTGATCTC	84 bp	qPCR
Piwil2	GCACAGTCCACGTGGTGGAAA TCCATAGTCAGGACCGGAGGG	681 bp	qPCR
HoxA4	CACAAAATTCCACCTGCTCACA CATCGGTATCTGGCCATGGT	113 bp	qPCR
Cdc25c	GGCCACGTAGATGCAATTTTAAC GCGAAGACTCCACAGAATGACA	76 bp	qPCR
Hist1h1c	AGAAGCCTAAGAAGGCGACTG TCTTGGCCACTTTCTTGGTC	111 bp	qPCR
Sycp3	AGCCAGTAACCAGAAAATTGAGC CCACTGCTGCAACACATTCATA	105 bp	qPCR
Dazl	AATGTTCAGTTCATGATGCTGCTC TGTATGCTTCGGTCCACAGACT	73 bp	qPCR
Akap4	GACTGGTCTTGTTTTTCAGTGTCC TGCTGGTTCCAGGTCAGAAG	93 bp	qPCR
Prm1	CACAAAATTCCACCTGCTCACA CATCGGTATCTGGCCATGGT	103 bp	qPCR
pGEX for	ATAGCATGGCCTTTGCAGG		Sequencing of pGEX-6P-1 with BT-IgSF$_{cyt}$
pGEX rev	GAGCTGCATGTGTCAGAGG		Sequencing of pGEX-6P-1 with BT-IgSF$_{cyt}$
M13 uni (-21)	TGTAAAACGACGGCCAGT		Sequencing of pBluescript (II) KS (+) with 5’ probe
M13 rev (-29)	CAGGAAACAGCTATGACC		Sequencing of pBluescript (II) KS (+) with 5’ probe
BT-IgSF$_{cyt}$ For **BT-IgSF$_{cyt}$ Rev**	GCGGAATTCTCAGGGGCGTTCTTTTACTGG GCGGTCGACCTATACCAGGGACCCTGCTC		Amplification of BT-IgSF$_{cyt}$ for antibody generation

7.8. Molecular mass markers

Table 8: Molecular mass markers used in this study

Product	Company	Order number
SDS-PAGE Standard, High	Bio-Rad	161-0303
SDS-PAGE Standard, Low	Bio-Rad	161-0304

7.9. Molecular size markers

Table 9: Molecular size markers used in this study

Product	Company	Order number
1kb Plus	Thermo Fisher	SM1331
Lamda DNA/HindIII	Thermo Fisher	SM0101

7.10. Enzymes

Table 10: Enzymes used in this study

Enzyme	Company	Order number
Alkaline phosphatase from calf intestine (CIP)	NEB	M0290
BamHI-HF	NEB	R3136
BstEII/Eco91I	Thermo Fisher	ER0391
Collagenase IA	Sigma	C2674
EcoRI-HF	NEB	R3101
EcoRV-HF	NEB	R3195
GoTaq qPCR Master Mix	Promega	A6001
HindIII-HF	NEB	R3104
LA Taq	TaKaRa	RR002A
NotI-HF	NEB	R3189
PreScission Protease	GE Healthcare	27-0843-01
Proteinase K	Genaxxon	M3037
PstI-HF	NEB	R3140
Q5 High-Fidelity DNA Polymerase	New England Biolabs	M0491S
SuperScript II Reverse Transcriptase	Thermo Fisher Scientific	18064014
T4 DNA Ligase	NEB	M0202S

T4 Polynucleotide Kinase	NEB	M0201
***Taq* DNA Polymerase**	New England Biolabs	M0267L
Trypsin/EDTA (0.05%/0.02%)	ThermoFisher	25300054

7.11. Plasmids

Table 11: Plasmids used in this study

Plasmid	Company
pBluescript II KS (+)	Stratagene
pGEX-6P-1	Amersham
pIG2	Hansjürgen Volkmer
pYX-Asc-mBT-IgSF	I.M.A.G.E. Consortium

7.12. Bacteria

Table 12: Bacteria used in this study

Bacteria	Company
BL21	NEB
DH5α	NEB
MC1061/P3	ThermoFisher

7.13. Kits

Table 13: Kits used in this study

Kit	Company	Order number
Genomic DNA Buffer Set	Qiagen	19060
Invisorb Fragment CleanUp	Stratec Molecular	1020300900
NEBuilding HiFi DNA Assembly Cloning Kit	NEB	M5520
Plasmid Midi Kit	Qiagen	12143
Prime-IT RmT Random Primer Labeling Kit	Agilent Technologies	300392
RNeasy Mini Kit	Qiagen	74106

7.14. General lab devices

Table 14: General lab devices used in this study

Device	Company
7500 Fast Real-Time PCR System	Applied Biosystems
Balance XS40025	Mettler Toledo
Biozero, BZ 8100	Keyence
Canto II	BD
Centrifuge 5424 R	Eppendorf
Centrifuge 5804 R (cell culture)	Eppendorf
ChemiDoc XRS for Western Blot	Bio-Rad
Confocal microscope, LSM 700	Zeiss
Cryostat CM1950	Leica
Econo-Pump	Bio-Rad
EPC-9	Heka Elektronik
FACS Canto II	BD Biosciences
Fraction collector 2110	Bio-Rad
GelDoc XR+ for agarose gel imaging	Bio-Rad
Incubator	Binder
Mastercycler gradient	Eppendorf
Microtome HM360	Microm
Osmomat 3000 basic	Gonotec
PeqStar 96 universal gradient	PeqLab
Pipette puller P-97	Sutter Instrument Inc.
Precision Balance XS205	Mettler Toledo
SuperCycler Trinity	Kryatec
ThermoMixer C	eppendorf
ultra-centrifugal filter unit	Amicon
Ultracentrifuge RCM105GX	Sorvall
Ultra-sonic bath	Bandelin
UV cross-linker	Fisher Scientific
Water bath	GFL

7.15. Software

Table 15: Software used in this study

Software	Company
ApE	Wayne Davis
FlowJo	Treestar
Illustrator CS5	Adobe
ImageJ	NIH
Photoshop CS5	Adobe
Prism5	Graphpad
QuantityOne	Bio-Rad
Zen 2012	Zeiss

8. METHODS

8.1. Mouse models

Animals were housed on a 12/12 h light/dark cycle with free access to food and water. The animal procedures were performed according to the guidelines from directive 2010/63/EU of the European Parliament on the protection of animals used for scientific purposes. All experiments were approved by the local authorities of Berlin (LAGeSo) (numbers T0313/97, X 9007/16, O 0038/08, G 0188/16, S0032/03, 0143/07, H0237/04). Mice investigated were 8-12 weeks old. Littermates served as control.

8.1.1. BT-IgSF KO mice

The B6-Igsf11tm1e(KOMP)Wtsi mouse strain used for this research project was generated from targeted embryonic stem cells (JM8.N4) obtained from the KOMP Repository (clone EPD0297_2_B07) (Figure 8). Embryonic stem cells were injected into C57BL/6N blastocysts at the transgenic core facility of the MDC. Founders were crossed with C57BL/6N. To remove the neo cassette, mice were bread to 129S1-Hprttm1(cre)Mnn mice (Schwenk et al., 1995) and further backcrossed with C57BL/6. Correct insertion of the construct was tested on DNA level by Southern blot, long range PCR and genotyping (Figure 16 and Figure 17). Absence of *Igsf11* mRNA and BT-IgSF protein was tested by qPCR, immunofluorescence stainings and Western blotting (Figure 18, Figure 19 and Figure 20). The resulting animals are termed BT-IgSF KO mice in this study.

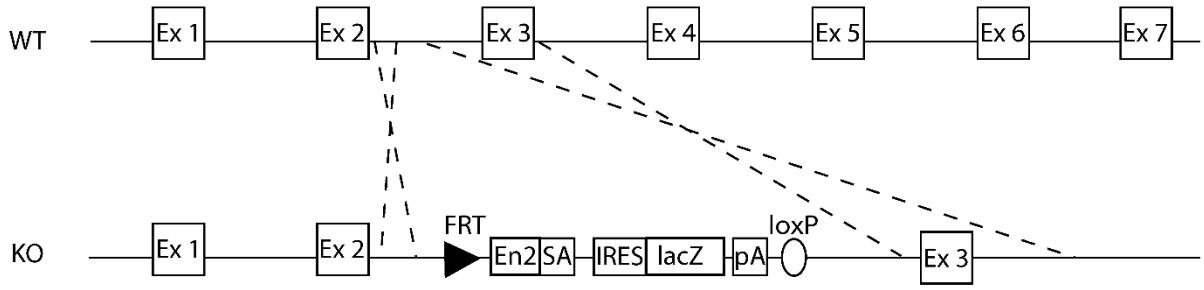

Figure 8: Scheme of the targeting-construct of the BT-IgSF non-conditional knockout mouse
Insertion of the targeting cassette leads to a frame-shift mutation and therefore to a premature STOP codon in the *Igsf11* gene. Ex: Exon, En2: intron of *EN2* gene, SA: splice acceptor, IRES: internal ribosome entry site, lacZ: ß-galactosidase gene, pA: poly A sequence, FRT: flippase recognition target, loxP: locus of X-over P1.

8.1.2. BT-IgSF^{flx}

For the BT-IgSF^{flx} mice (B6-Igsf11tm1a(KOMP)Wtsi/Fgr), sperm for the in vitro fertilization was derived from mice generated by KOMP Repository and the Mouse Biology Program at the University California Davis with embryonic stem cells from the Welcome Trust Sanger Institute (clone EPD0297_2_A07). The IVF was done by the transgenic core facility of the MDC. Resulting mice were crossed to

Tg(ACTFLPe)9205Dym (Dymecki, 1996), to remove the trapping cassette and to obtain a conditional allele. These animals are called BT-IgSF^{flx} (B6-Igsf11tm1c(KOMP)Wtsi/Fgr).

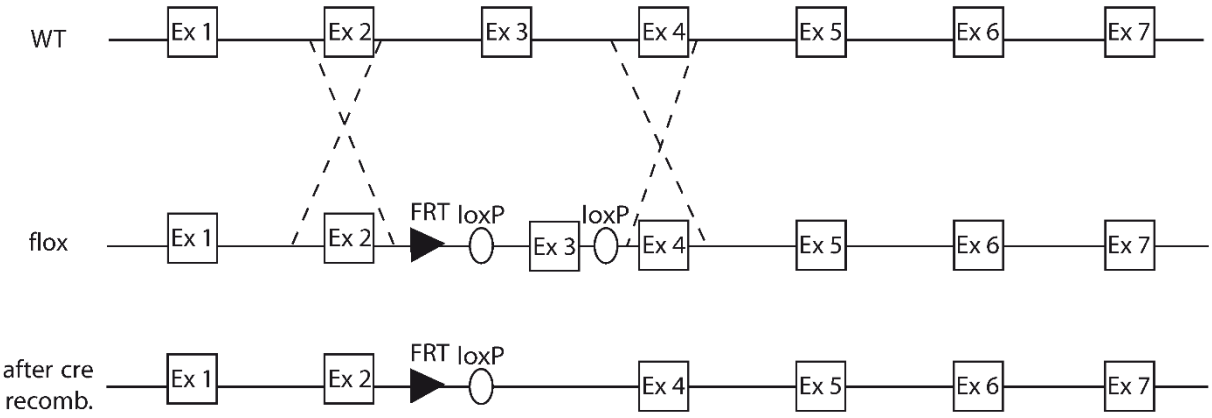

Figure 9: Scheme of the targeting-construct of the BT-IgSF^{flx} mice
The loxP sites flanking exon 3 enable an excision of exon 3 after recombination through a cre recombinase. Ex: Exon, FRT: flippase recognition target, loxP: locus of X-over P1.

8.1.3. Sertoli cell-specific knockout of BT-IgSF

To generate a Sertoli cell-specific BT-IgSF knockout, BT-IgSF$^{flx/flx}$ mice were bred to B6-Tg(Amh-cre)8815Reb/J mice (The National Institute for Agronomic Research, Gliki et al., 2004). The mice are designated Sertoli cell-specific KO (BT-IgSF$^{flx/flx}$; AMH^{cre+}).

8.1.4. Adult conditional BT-IgSF knockout

To generate a conditional, tamoxifen inducible BT-IgSF knockout mouse, a Rosa26creERT2 mouse line (B6.129-Gt(ROSA)26Sortm1(cre/ERT2)Tyj/J, Jackson Stock 008463) was crossed to BT-IgSF^{flx} mice resulting in animals called BT-IgSF$^{flx/flx}$; Rosa26creERT2. Tamoxifen treatments were performed at an age of 8-12 weeks with 1.5 mg tamoxifen on 5 consecutive days i.p. (Sultana et al., 2014) (Figure 10).

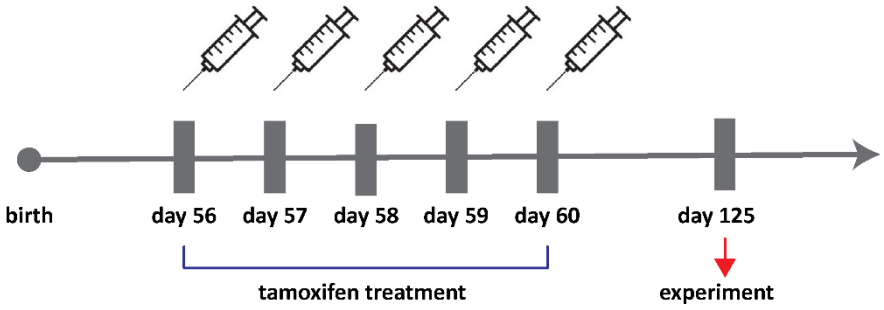

Figure 10: Time schedule of tamoxifen treatment of adult BT-IgSF$^{flx/flx}$; Rosa26creERT2 mice
Tamoxifen is administrated on 5 consecutive days i.p., 10 weeks after the first tamoxifen injection animals were used for experiments.

Tamoxifen was dissolved in corn oil and stored at -20 °C until used. Controls were treated with corn oil (vehicle) only. The experiment was terminated 10 weeks after the first tamoxifen administration. Mice

were killed via cervical dislocation or transcardial perfusion and testis were prepared for following analyses.

8.2. Southern Blot

To confirm the correct integration of the targeting construct in BT-IgSF KO mice, Southern blotting was performed. During this method, the fragments of digested genomic DNA are transferred to a membrane. Restriction sites were chosen to be directly 5' and 3' of a specific binding site of a probe in the target region (see Figure 17). The membrane was subsequently hybridized with the target-specific radiolabeled probe. The probe binds specifically to the digested target DNA fragment and can be visualized with a roentgen film or a photosensitive phosphor plate.

8.2.1. Generation of the 5´ probe

The probe was designed as an external probe recognizing a DNA section upstream from the 5´ homologous arm of the targeting construct (see Figure 17). The 5´probe was generated by PCR with genomic WT DNA from liver as template. The resulting amplicon of 621 bp was extracted from an agarose gel, digested with BamHI and PstI over night at 37 °C, loaded onto a 1% agarose gel and purified with the Invisorb Fragment CleanUp kit (Stratec).

The 5´end of the probe was phosphorylated with T4 polynucleotide kinase in ligation buffer for 1 h at 27 °C. The plasmid pBluescript KS+ was also digested with BamHI and PstI for 1 h at 37 °C to obtain matching ends and was dephosphorylated with alkaline phosphatase (CIP) at 37 °C for 1 h and subsequently loaded onto an 1% agarose gel, extracted and purified. Before setting up the ligation, a control gel with the Lambda DNA/HindIII marker for quantification of the plasmid and the insert (5' probe) was done. For the ligation, insert and vector were mixed at a 3:1 molar ratio. Seventy ng of the vector was used in the ligation at 27 °C for 2 h. After inactivation of the ligation mix for 10 min at 65 °C, 50 µl of competent DH5α were mixed with the ligation mix and incubated for 20 min on ice. After heat shock for 2 min at 42 °C, bacteria were placed on ice for 90 sec. After the addition of 440 µl LB media, bacteria were incubated at 37 °C for 1 h while shaking. Hundred µl of the transformed DH5α were plated on ampicillin containing agar plates and incubated over night at 37 °C. Colonies were picked and transferred into 100 ml LB media containing 100 µg/ml ampicillin. Midi preps were done with the Plasmid Midi Kit, followed by a test digestion with NotI and HindII which showed the presence of the correct fragments. The plasmid DNA was sequenced with standard primers M13 rev (-29) and M13 uni (-21). One clone contained a mutation, the other one was correct and was excised from the plasmid with BamHI and HindIII. The digestion was loaded onto a 2% agarose gel and the correct band was excised and purified.

8.2.2. Isolation of genomic DNA

Genomic DNA was isolated from 350 mg liver of adult mice with Qiagen Genomic-tip 500/G kit according to manufacturer's instructions. Isolated genomic DNA was incubated in an ultra-sonic bath for 6 hours to shear the DNA and frozen at -20 °C until usage.

8.2.3. Digestion of genomic DNA and electrophoresis

Twenty µg DNA was digested with 60 U BstEII (Eco91I) for 16 hours at 37 °C. The digested DNA and 15 µl of the 1kb plus ladder as size control were loaded onto a 1% agarose gel and run at 26-28 V for 19h. Afterwards the gel was incubated for 30 min in water containing ethidiumbromide to evaluate the separation and was then washed with water. The gel was depurinated for 8 min with depurination buffer, washed twice with water and denatured two times for 15 min with denaturation buffer. Afterwards the gel was neutralized twice with neutralization buffer for 1 h.

8.2.4. Blotting

The gel was placed in 20x SSC buffer and turned upside down. The positively charged nylon membrane was placed onto the gel after equilibration in 10x SSC buffer. Blotting paper soaked with 10x SSC buffer was placed on top of the membrane, followed by a pile of dry paper sheets and a glass plate. The whole sandwich was again turned upside down and a 1 kg weight was placed on top of it. The capillary transfer of DNA fragments from the gel to the membrane was carried out overnight and the membrane was subsequently washed briefly with 2x SSC and air-dried. The DNA was cross-linked to the membrane using UV exposure with 700 J/cm^2.

8.2.5. DNA detection by a ^{32}P- radiolabeled probe

Fifty ng of the probe was labeled with dCTP[α-^{32}P] with the Prime-It RmT Random Primer Labeling Kit according to manufacturer's instruction. Briefly, the probe was denatured at 95 °C for 10 min. Five µl of dCTP[α-^{32}P] and 3 µl of magenta polymerase were added to radiolabel the probe at 37 °C for 10 min. The reaction was stopped by adding 2 µl of the stop mix and excess nucleotides were removed by gel filtration via centrifugation in Illustra MicroSpin G-50 spin columns. The labeled probe was mixed with 10 µg of sheared mouse gDNA to block unspecific probe binding. One ml pre-warmed Church buffer was added to the mix and denatured at 95 °C for 10 min before the mix was placed in the hybridization oven for 1-2 h at 65 °C.

The membrane with the DNA was transferred into a hybridization glass bottle with pre-warmed Church buffer for pre-hybridization at 65 °C for 1 h. The radiolabeled probe was added to the membrane and hybridized at 65 °C overnight. After the hybridization, unbound probe was removed by several washing steps at 68 °C. First, the membrane was washed with washing buffer I for 10 min followed by washing with washing buffer II for 20 min until the radioactivity of the membrane was at background level.

Washing steps with washing buffer III-IV followed for 15 min each. The membrane was placed between one acetate sheet and a sheet of blotting paper, wrapped in foil and placed onto a photosensitive phosphor plate overnight.

8.3. Long range PCR

To double check correct homologous recombination, long range PCRs with primers outside of the insertion cassette and inside of the construct were performed. To check the 5' side of the inserted region, primers GF1 and En2in were used. For the confirmation of the 3' side, primers lacZ and GR1 were used. Both reactions were carried out in the Kryatec machine followed by a visualization of the amplicons on a 1% agarose gel. PCR conditions were:

Table 16: PCR conditions for generating the 5' probe

Solution	Volume	Concentration
Buffer	2.5 µl	1x
$MgCl_2$	1.5 µl	1.5 µM
dNTPs	0.25 µl	100 µM
LA Taq	0.25 µl	50 mU/µl
Primer	2 µl	4 µM
Primer	2 µl	4 µM
DNA Lysate	2 µl	variable
H_2O	14.625 µl	-

Temperature	Duration	Cycles
94 °C	3 min	1
94 °C	30 secs	
60 °C	30 secs	35
68 °C	8 min	
68 °C	10 min	1

8.4. Genotyping

Genotyping was performed by PCR amplification of genomic DNA isolated from tail cuts or ear punches. Tissue samples were lysed with 200 µl tail lysate buffer and 2 µl proteinase K (20 mg/ml) over night at 55 °C while shaking at 800 rpm. Inactivation was done at 95 °C for 5 minutes. For the BT-IgSF KO mice, primers P1 and P2 result in a fragment of 197 bp in the wildtype condition and primers P1 and P3 in a fragment of 343 bp in the knockout condition (Figure 11).

The floxed allele of the BT-$IgSF^{flx/flx}$ mouse was genotyped by primers P1 and P2, which leads to fragments of 197 bp in the wildtype and of 379 bp in the floxed condition, respectively (Figure 12).

The presence of the cre allele was tested with the primers P4 and P5 and results in a fragment of 200 bp (Figure 13). All PCR reactions were mixed with DNA sample buffer and 10 µl were loaded onto a 2.5% agarose gel. Gels were run at 100 V for 25 minutes.

8.4.1. PCR for BT-IgSF KO mice

For the BT-IgSF KO mouse strain a touchdown PCR with three primers was performed in the PeqStar (PeqLab) machine.

Table 17: PCR conditions for genotyping BT-IgSF WT and KO mice

Solution	Volume	Concentration	Temperature	Duration	Cycles
ThermoPol buffer	2.5 µl	1x	95 °C	3 min	1
dNTPs	0.2 µl	80 µM each	95 °C	20 secs	16
Taq (NEB)	0.16 µl	32 mU/µl	66 °C	20 secs	-0.5 °C/
Primer 1	2 µl	4 µM	70 °C	1 min	Cycle
Primer 2	2 µl	4 µM	95 °C	20 secs	
Primer 3	2 µl	4 µM	61 °C	20 secs	35
DNA Lysate	3 µl	variable	70 °C	1 min	
H_2O	13.14 µl		70 °C	5 min	1

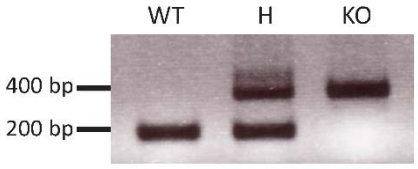

Figure 11: **PCR result of BT-IgSF KO mice genotyping**
Genotyping of BT-IgSF wildtype, heterozygous and knockout mice by PCR, wildtype fragment 197 bp, knockout fragment: 343 bp.

8.4.2. PCR for BT-IgSF^{flx} mice

For the BT-IgSF^{flx} mouse strain a touchdown PCR was performed in the PeqStar (PeqLab) machine.

Table 18: PCR conditions for genotyping BT-IgSF^{flx} mice

Solution	Volume	Concentration	Temperature	Duration	Cycles
ThermoPol buffer	2.5 µl	1x	95 °C	3 min	1
dNTPs	0.2 µl	80 µM each	95 °C	20 secs	16
Taq (NEB)	0.16 µl	32 mU/µl	66 °C	20 secs	-0.5 °C/
Primer 1	2 µl	4 µM	70 °C	1 min	Cycle
Primer 3	2 µl	4 µM	95 °C	20 secs	
DNA Lysate	3 µl	variable	61 °C	20 secs	35
H_2O	15.14 µl		70 °C	1 min	
			70 °C	5 min	1

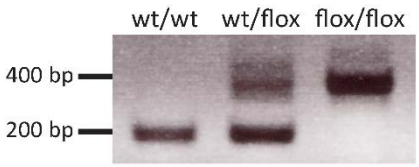

Figure 12: PCR result of BT-IgSF KO mice genotyping
Genotyping of BT-IgSF^{flx} wildtype, heterozygous and flox mice by PCR, wildtype fragment 197 bp, flox fragment: 379 bp.

8.4.3. PCR for cre strains (AMH-cre, Rosa26creERT2)

For these strains a PCR was performed in the Mastercycler (eppendorf) machine.

Table 19: PCR conditions for genotyping for mice containing a cre allele

Solution	Volume	Concentration
ThermoPol buffer	2.5 µl	1x
dNTPs	0.125 µl	80 µM each
Taq (NEB)	0.125 µl	32 mU/µl
Primer 4	2 µl	4 µM
Primer 5	2 µl	4 µM
DNA Lysate	2 µl	variable
H_2O	16.25 µl	

Temperature	Duration	Cycles
94 °C	2.5 min	1
96 °C	30 secs	
58 °C	30 secs	34
72 °C	40 secs	

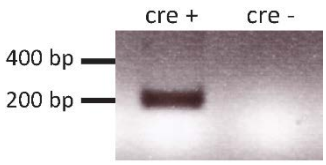

Figure 13:PCR result of cre mice genotyping
Genotyping of cre mice, presence of cre allele results in a fragment of 200 bp.

8.5. Antibody generation

8.5.1. Antibodies against the denatured extracellular part of BT-IgSF (Rb113 and Rb114)

The sequence encoding the extracellular part of BT-IgSF (BT-IgSF$_{ex}$) (aa residues 23 to 239, LEV … PRS) was cloned into the pIG2 vector and MC1061/P3 bacteria were used for amplification. The plasmid was used for transfection of COS7 cells. Transfection was done with Lipofectamine 2000 and Opti-MEM media when cells were 70% confluent. Culture media was exchanged against Opti-MEM media and plasmid and Lipofectamine 2000 were first diluted in Opti-MEM in different falcons. Both components were mixed, incubated for 20 min at room temperature and the solution was then added to the cells. The transfection mix was incubated for 5-6 h in the incubator at 37 °C with 5% CO_2. Afterwards, the transfection media was removed, replaced by DMEM with FCS and without P/S and replaced the next

day by DMEM with P/S and without FCS. 5 days after the transfection, the media containing the secreted extracellular part of BT-IgSF fused to a human Fc fragment of IgG1 was harvested. For this, the supernatant was loaded several times onto a protein A sepharose column, washed and eluted with

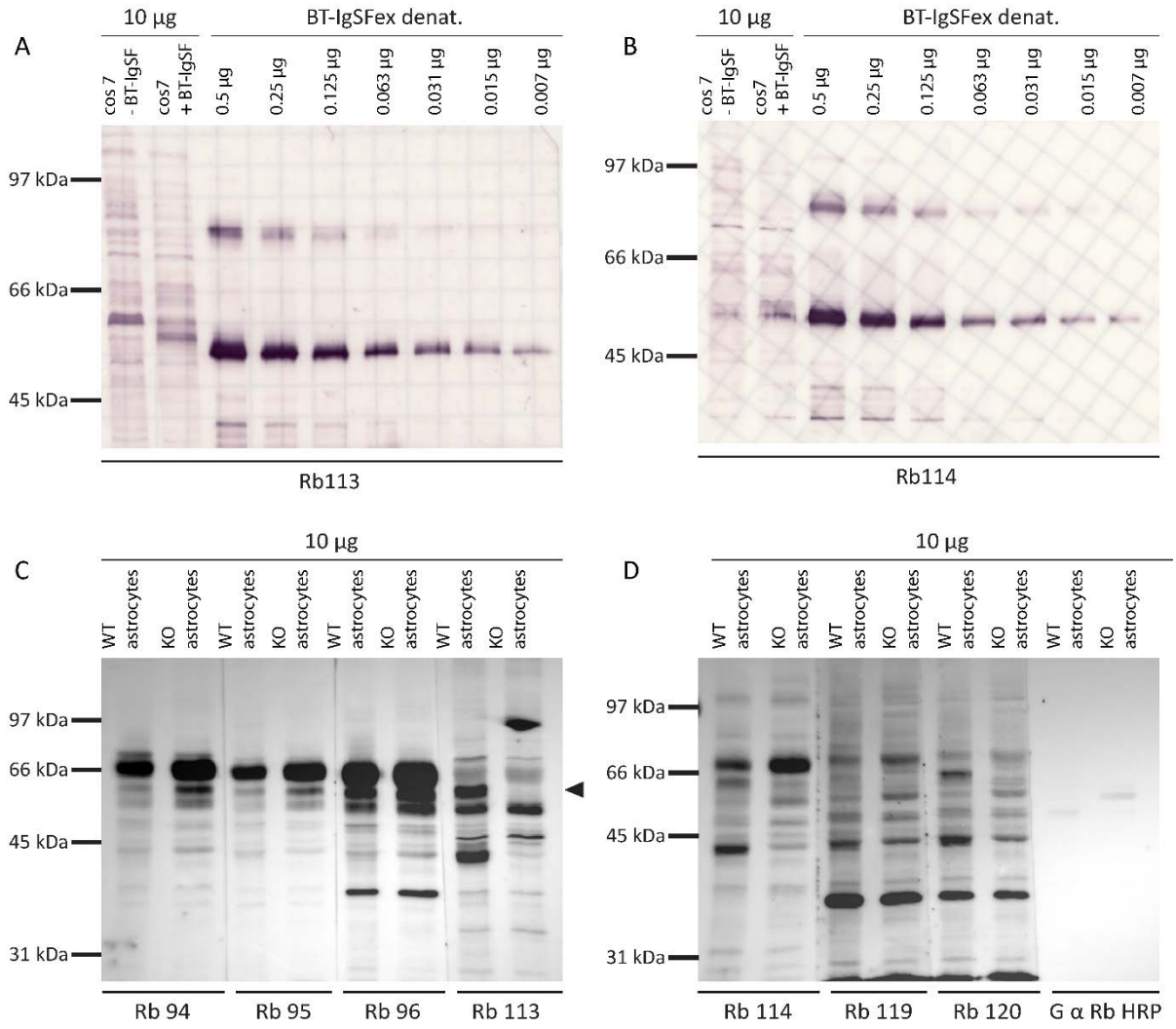

Figure 14*:* **Rb113 recognizes denatured BT-IgSF in Western Blots of tissue samples**
(A) Immunoblot with Rb113 against the pure antigen (denatured extracellular part of BT-IgSF). Rb113 was used in a concentration of 1 µg/ml and recognized the antigen with an input of 7 ng protein. (B) Immunoblot with Rb114 against the pure antigen (denatured extracellular part of BT-IgSF). Rb114 was used in a concentration of 1 µg/ml and recognized the antigen with an input of 7 ng protein. (C) and (D) all generated antibodies were tested in immunoblots. Membrane fractions of cultured astrocytes were analyzed for BT-IgSF expression with antibodies against the extracellular part of BT-IgSF (Rb94, Rb95 and Rb96) as well as against the denatured extracellular part of BT-IgSF (Rb113 and Rb114) and the cytoplasmic tail (Rb119 and Rb120). Rb113 shows a clear band of around 60 kDa (arrowhead) which is not detectable in astrocytes from BT-IgSF KO mice. The calculated molecular mass for BT-IgSF is 46 kDa but can potentially be glycosylated. The band at around 40 kDa could be a degraded form of BT-IgSF. All other antibodies have even higher background and are not as sensitive as Rb113. The Last two lanes in (D) are negative controls, showing only the secondary antibody.

elution buffer. Fractions with protein content, determined photometrically, were pooled, dialyzed against PBS and concentrated with an ultra-centrifugal filter unit. BT-IgSF$_{ex}$ was denatured with 20% SDS and 20 mM DTT at 95 °C for 3 min. 20 mM cysteine was added and aliquots of 100 µg were stored at -20 °C. Rabbits 113 and 114 were immunized five times with 1 ml containing 100 µg of antigen in

500 µl supplemented 1:1 with Freund's adjuvant at fortnightly intervals. Rabbit serum was loaded onto protein A sepharose columns to obtain IgGs and eluted with elution buffer. The eluate was dialyzed against PBS and concentrated with an ultra-centrifugal filter unit. Antibodies were first tested against the pure antigen (Figure 14 A and B). They both recognized a protein amount of 7 ng when used in a concentration of 1 µg/ml. Rb113 detected BT-IgSF in transfected COS7 cells (Figure 14 C, arrowhead). All generated antibodies were tested in an immunoblot with membrane fractions of WT and KO astrocytes (Figure 14 C and D). All tested antibodies had a very high background. However, Rb113 recognized a strong protein band at around 60 kDa which was not present in the KO (Figure 14 C, arrowhead). The calculated molecular weight of the amino acid sequence of BT-IgSF is 46 kDa (ExPASy, P0C673), but it is known that BT-IgSF can be N-glycosylated (Suzu et al., 2002) and Jang et al. also recognized BT-IgSF at around 60 kDa. A band in the wildtype of around 40 kDa was additionally recognized which could be a proteolytically degraded form of BT-IgSF.

8.5.2. Antibodies against the cytoplasmic part of BT-IgSF (Rb119 and Rb120)

The nucleotide sequence of the cytoplasmic tail of BT-IgSF (BT-IgSF$_{cyt}$) (aa residues 262 to 428, SGA … SLV) was generated by PCR using primers BT-IgSFcyt For and BT-IgSFcyt Rev and this amplicon was inserted into the pGEX-6P-1 vector. The whole procedure was done with the NEBuilding HiFi DNA Assembly Cloning Kit.

Table 20: PCR conditions for generating the sequence of BT-IgSF$_{cyt}$

Solution	Volume	Concentration
5x Q5 buffer	5 µl	1x
dNTPs	0.5 µl	200 µM each
Q5Taq	0.25 µl	32 mU/µl
Primer 4	1.25 µl	2.5 µM
Primer 5	1.25 µl	2.5 µM
DNA	1 µl	400 pg
H_2O	15.75 µl	

Temperature	Duration	Cycles
98 °C	30 secs	1
98 °C	10 secs	
65 °C	30 sec	40
72 °C	30 sec	
72 °C	2 min	1

The vector pGEX-6P-1 was digested with EcoRI-HF and Not-HI-HF for 1.5 h at 37 °C, loaded onto an 1% agarose gel and purified. Ligation was set up in a ratio of 1:2 (vector : insert) for 30 min at 50 °C. Fifty µl DH5α were transformed with 2 µl of the ligation mix, incubated at 37 °C for 1 h with SOC-media and plated onto ampicillin containing LB-plates. Four colonies were chosen for midi preparations. Test digestion of the 4 different clones with EcoRV-HF were performed and clones with the correct

fragment sizes were chosen for sequencing. For sequencing, primers pGEX for and pGEX rev were used. Clones with the correct insert without mutations were chosen for amplification in BL21. BL21 bacteria, transformed with pGEX-6P-1, containing BT-IgSF$_{cyt}$, were grown in YT-media until an OD$_{600}$ of 0.6 was reached. IPTG (1 mM) was added to induce expression of the protein BT-IgSF$_{cyt}$ with a GST tag and after

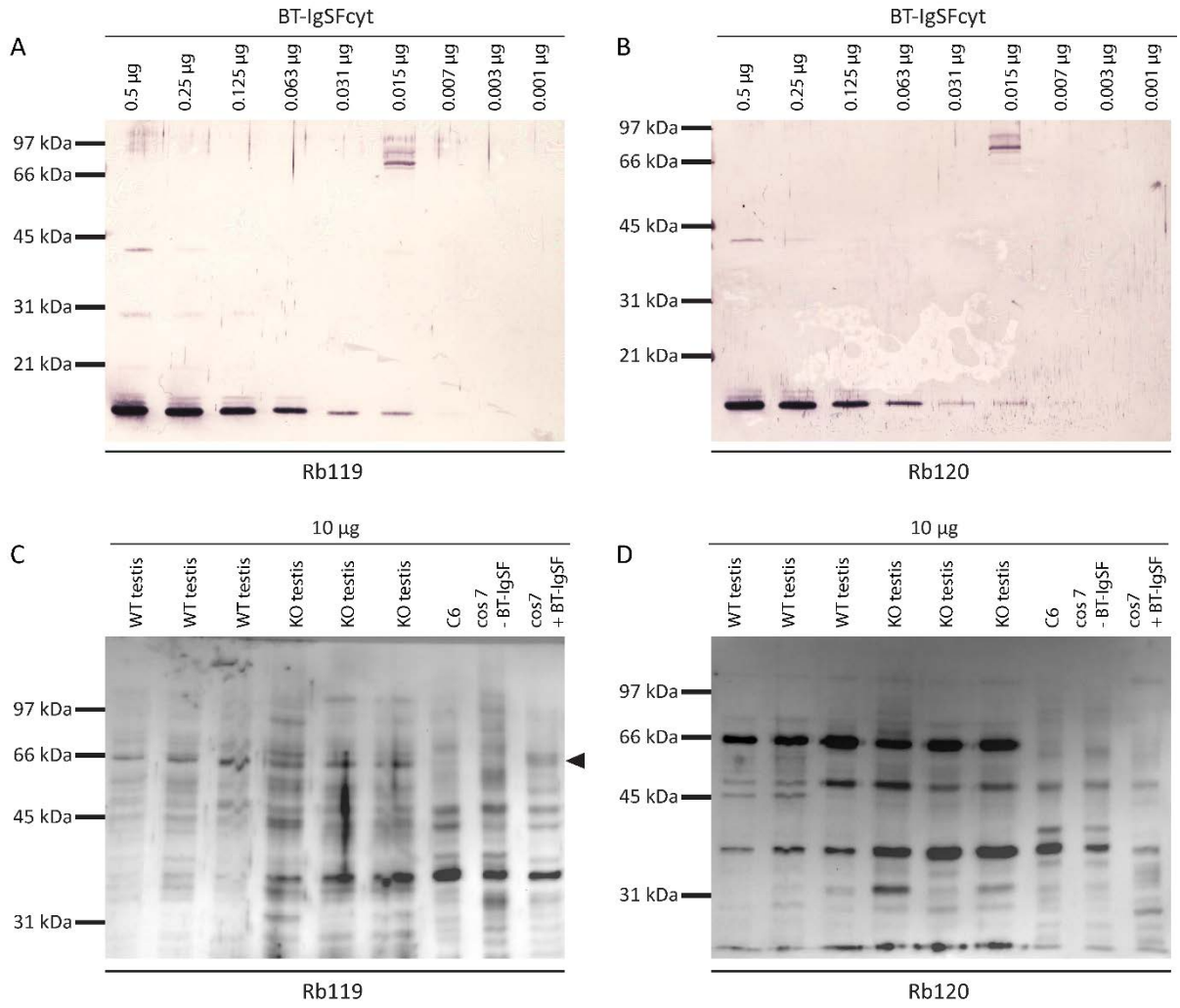

Figure 15: Neither Rb119 nor Rb120 are suitable to detect BT-IgSF in immunoblots
(A) Immunoblot with Rb119 against the pure antigen (cytoplasmic tail of BT-IgSF). Rb119 was used in a concentration of 1 µg/ml and recognized the antigen with an input of 15 ng protein. (B) Immunoblot with Rb120 against the pure antigen (cytoplasmic tail of BT-IgSF). Rb120 was used in a concentration of 1 µg/ml and recognized the antigen with an input of 7 ng protein. Rb119 (C) and Rb1120 (D) were tested against membrane fractions of WT and KO testes and against C6, untransfected COS7 cells and BT-IgSF transfected COS7 cells. None of the two tested antibodies was able to detect BT-IgSF, as no differences could be detected neither between WT and KO nor between untransfected and transfected cells.

7 h bacteria were pelleted and stored at -80 °C. Pellets were dissolved in PBS, proteinase inhibitors were added (pepstatin, leupeptin and aprotinin 1:500, PMSF 1:1000) and 1% Triton X100 were added before homogenization and ultra-sonic treatment. After centrifugation at 12,000 g for 20 mins, the supernatant was applied onto a glutathione sepharose column. After a washing step with PBS, BT-IgSF$_{cyt}$-GST was eluted from the column with elution buffer and fractions of 500 µl were collected with a fraction collector. The Column was regenerated with 0.1 M DEA pH 11.5, PBS and 6M

guanidinehydrochloride and again with PBS. Fractions were tested for protein content and pooled. The pooled fractions were dialyzed against cleavage buffer. PreScission protease was added (1:500) and incubated over night at 4 °C on a rotating wheel. The digestion mix was loaded onto the regenerated glutathione sepharose column. The column was eluted with elution buffer. Flow-through was collected and again loaded onto the column two more times. All eluates were pooled and concentrated with an ultra-centrifugal filter unit with a cut-off of 3 kDa. After gelfiltration of the solution, fractions were collected, tested for protein content and pooled. After concentration of the pooled fractions, 100 µg aliquots for immunization of rabbits were stored at -20 °C. Rabbits 119 and 120 were immunized six times with 100 µg antigen, supplemented with Freund's adjuvant at fortnightly intervals. Serum of rabbits was first loaded onto Protein A sepharose columns to obtain IgGs. The IgGs were then antigen-purified using a BT-IgSF$_{cyt}$-coupled CNBr sepharose column. Bound antibodies against BT-IgSF$_{cyt}$ were eluted using 0.1 M DEA pH 11.5. After dialysis against PBS, the antibodies were concentrated, aliquoted and stored at -80 °C. Antibodies were first tested against the pure antigen (Figure 15 A and B). They both recognized a protein amount of 15 ng when used in a concentration of 1 µg/ml. When tissue samples were tested, both antibodies did not detect BT-IgSF in testes lysates (Figure 15 C and D) but Rb119 seemed to be able to detect BT-IgSF in transfected COS7 cells (Figure 15 C, arrowhead). However, the background is very high and a difference between BT-IgSF WT and KO was not visible, suggesting that Rb119 and Rb120 are not suitable to detect BT-IgSF from tissue in immunoblots.

Table 21: Overview of antibodies against BT-IgSF generated by the Rathjen group

Labname	Antigen	Host	Tested applications	Suitable application
Rb94	aa 23 to 239, LEV …PRS extracellular part of mBT-IgSF fused to Fc of human IgG1	rabbit	WB, IF	-
Rb95	aa 23 to 239, LEV …PRS extracellular part of mBT-IgSF fused to Fc of human IgG1	rabbit	WB, IF	IF
Rb96	aa 23 to 239, LEV …PRS extracellular part of mBT-IgSF fused to Fc of human IgG1	rabbit	WB, IF	-
Rb113	aa 23 to 239, LEV …PRS extracellular part of mBT-IgSF fused to Fc of human IgG1	rabbit	WB	WB

	denatured with 20% SDS and 20 mM DTT			
Rb114	aa 23 to 239, LEV …PRS extracellular part of mBT-IgSF fused to Fc of human IgG1 denatured with 20% SDS and 20 mM DTT	rabbit	WB	-
Rb119	aa 262 to 428, SGA…SLV cytoplasmic part of mBT-IgSF	rabbit	WB	-
Rb120	aa 262 to 428, SGA…SLV cytoplasmic part of mBT-IgSF	rabbit	WB	-

8.6. Histology, testis weight, immunohistochemistry and generation of anti-BT-IgSF

For H&E stainings and immunofluorescence stainings, transcardial perfusion with 4% PFA in PBS was performed. Testes were post-fixed for H&E stainings overnight at 4 °C with 4% PFA in PBS. For immunofluorescence stainings against active Caspase-3, only 1% PFA in PBS was used as fixative. Gross morphology analysis of testes was performed on 5 µm methacrylate slices stained with H&E. Body weight and wet testis weight were measured directly after sacrificing the mice and only in non-perfused animals.

Stainings were performed on 16 µm paraformaldehyde-fixed cryosections. All used antibodies are listed in Table 5 and Table 6.

For WT1 stainings, an antigen-retrieval protocol with citrate buffer was performed (Brzica et al., 2011). Blocking was done at room temperature for 1 hour with 3% goat serum, 1% BSA in PBS with 0.1% Triton Tx100. Primary antibodies were incubated over night at 4 °C and secondary antibodies were incubated at room temperature for 2 hours.

H&E staining images were taken with a Biozero microscope.

Images from immunofluorescence stainings were obtained at room temperature by confocal imaging using a Carl Zeiss LSM 700 Laser Scanning Microscope equipped with ZEN 2011 software and the following lenses: a Plan-Neofluar 20x/0.30 NA objective or a Plan-Achromat 63x/1.40 NA oil objective (all from Carl Zeiss MicroImaging, GmbH). Images were imported into Photoshop CS5 (Adobe) for uniform adjustment of contrast and brightness. Figures were assembled using Illustrator CS5 (Adobe).

8.7. Apoptosis analysis

Apoptosis analysis was done on 15 µm cryosections stained against active Caspase-3 (Promega G7481, 1:400). Positive cells per tubuli were counted (40-50 tubuli per section, n=4 per genotype). Counting was done in ImageJ and statistical analysis was done with Prism5.

8.8. Staging of the seminiferous epithelium

For the staging of the seminiferous epithelium, 16 µm cryo-cross-sections of testes were stained with DAPI, PNA-A488 and anti-BT-IgSF antibody. Pictures of different tubules were taken using confocal microscopy. Tubules were analyzed according to the binary decision key (Meistrich and Hess, 2013). The first question of whether two generations (round and elongated) or a single generation (elongating or early elongated) of spermatids are present within the same tubuli cross section, allows to classify the tubule as being into early/middle or the late set of stages. PNA binds to the outer membrane of the acrosome and together with the DAPI staining a rough staging of the tubules is possible (Wakayama et al., 2015). The acrosome is formed from the Golgi apparatus and is then transported to the outside of the spermatid forming a cap-like structure. The developmental stage of the acrosome and the DNA in the germ cells together with the arrangement of the different germ cells to each other inside the tubuli allows a rough staging (Meistrich and Hess, 2013; Hess and De Franca, 2008).

8.9. Protein extraction and Western Blotting

Tissue samples (decapsulated testes or cultured astrocytes) were homogenized in 0.34 M Sucrose/PBS with proteinase inhibitors and membranes were enriched. For this, nuclei were removed after a first centrifugation of 10 min at 2000 rpm. The supernatant was further centrifuged at 44,000 rpm for 20 minutes. The pellet was then resuspended in 0.1M DEA pH 11.5 to remove peripheral proteins and centrifuged again at 44,000 rpm for 15 minutes. The pellet was resuspended in 1 ml PBS and centrifuged as before. The pellet was solubilized in solubilization-buffer and centrifuged again as before. The supernatant was kept as the membrane fraction and protein amount was measured with Nanodrop.

SDS-PAGE was performed on 10% gels for 1 h at 150 V. Blotting was done at 100 V for 1 h on nitrocellulose membranes. Blocking was done with 3% BSA/TBST for 1 h at room temperature. Primary antibodies were incubated over night at 4 °C. After three washing steps with TBST, secondary HRP coupled antibodies were incubated for 2 h at room temperature. After washing three times, membranes were developed with ECL solution and detected with ChemiDoc XRS.

For Western blotting the following antibodies were used: Rb113 (0.75 µg/ml), rabbit anti-Cx43 (Cell Signaling 3512, 1:1000) and as a loading control rabbit anti-pan-Cadherin (Sigma C3678, 1:1000). Analyses of three independent blots were done with Quantity One.

8.10. qRT- PCR

Total RNA was isolated from decapsulated testis using the RNeasy Mini Kit, including an on-column DNase I digestion according to manufacturer's instructions. RNA yield was measured by Nanodrop 1000 (Nanodrop). RNA was transcribed by SuperScript II using oligo(dT) Primers. The quantitative real time PCR was performed on a 7500 Fast Real-Time PCR System with GoTaq qPCR Master Mix. *Rplp0* was used as a housekeeping gene. Technical triplicates were performed with n=4 testes per genotype. Used primers are listed in Table 7. The relative fold change of BT-IgSF KO gene expression compared to WT was calculated by using the comparative real-time PCR method. All results were first normalized to *Rplp0* and then to WT.

8.11. Hormone status

Serum of male mice was analyzed by Laboklin (Bad Kissingen, Germany). FSH and testosterone were measured with a mouse-specific ELISA and LH with a mouse-specific Sandwich ELISA (LifeSPan BioSciences Inc., Seattle, USA).

8.12. Flow cytometry

Fifty mg of decapsulated testis were minced with a scissor in an 800 µl solution containing 0.1 M citric acid and 0.5% Tween-20 and incubated for 20 min under gentle agitation. Four ml of a 0.4 M Na_2HPO_4 solution with 1.75 µg/ml DAPI was added and incubated for 20 min in the dark. The filtered cell suspension (30 µm mesh) was measured and analyzed on a Canto II. Data were analyzed with FlowJo Software. Analyses were done in cooperation with Karin Müller, IZW Berlin, and Andreas Pelz, Charité Berlin.

8.13. Biotin *in vivo* assay

The biotin *in vivo* assay was used to examine the integrity of the blood-testis barrier (Meng et al., 2005). Fifty µl of 10 mg/ml EZ-Link Sulfo-NHS-LC-Biotin, freshly diluted in PBS containing 1 mM $CaCl_2$, was injected per testis of anaesthetized mice. The neighboring testis was injected with 50 µl of 1 mM $CaCl_2$ in PBS and served as a control. After 30 mins, animals were euthanized, and their testes were immediately frozen. Cryosections were stained with Strep-Cy5 (1:600) and 1 µg/ml DAPI.

8.14. Electron microscopy

Electron microscopy and post-fixation steps were done at the electron microscope facility of the Max Delbrück Center by Dr Bettina Purfürst. Mice were perfused with 2% FA / 2.5% GA in 0.1 M phosphate buffer, the testes were removed, incubated for two hours and then cut in two halves. The testes were further fixed for 24 hours in the same fixative. Samples were postfixed in 1% osmium tetroxide / 1.5% potassium ferrocyanide in water for 5 hours. Following washing with phosphate buffer, samples were stained with 1% tannic acid in phosphate buffer for 5 hours, dehydrated through a graded series of ethanol and embedded in Poly/Bed 812 (Polysciences, Inc., Eppelheim, Germany). Ultrathin sections were stained with uranyl acetate and lead citrate and examined with a FEI Morgagni electron microscope and the iTEM software (EMSIS GmbH, Münster, Germany).

8.15. Sertoli cell culture and dye coupling

The generation and culture of primary Sertoli cells were performed after the protocol from Veitinger et al., 2011. Briefly, both testes of a 7-day old mouse were decapsulated and digested with 1 mg/ml collagenase in MEM for 8 min at 37 °C. Digestion was stopped by adding DMEM with FCS. The solution was centrifuged at 400 g for 8 minutes and the supernatant was discarded. Cells were resuspended in Trypsin/EDTA (0.05%/0.2%) and incubated for 5 min at 37 °C. Digestion was stopped by adding DMEM with FCS and cells were centrifuged for 10 min at 400 g. Cells were resuspended in Sertoli cell media and seeded at $1x10^4$ cells per well in a 24-well plate with coverslips. Cells were cultured at 37 °C in an incubator with 5% CO_2. After three days, cells were transferred into an incubator with 34 °C and 5% CO_2. On day 7, when confluency was reached, cells were used for dye coupling. For this, coverslips were transferred into a submerged recording chamber and media was exchanged against ASCM. Glass capillaries prepared by a puller were filled with 2% solution (w/v) of 6-carboxyfluorescein. Individual Sertoli cells were injected with the dye by iontophoretical injection for 5 min, using negative voltage of -70 mV using EPC-9. Intracellular communication was monitored under fluorescence microscopy and pictures were taken with Axiovert 200M microscope and an Axiocam b/w. For fluorescence images, filter set 46 was used (Zeiss; Exc. 500/20 nm, FT 515 nm, Em. 535/30 nm). Spreading area was quantified using ImageJ and statistical analysis was done in Prism5.

8.16. Immunofluorescence staining of Sertoli cells

Sertoli cells were washed with 0.1% BSA/PBS and staining against BT-IgSF was done on living cells. For this, Sertoli cells were blocked at room temperature for 10 min with 1% BSA/PBS. Rb95 antibody was used to stain BT-IgSF and was incubated for 1 h at room temperature. After washing three times, cells were fixed for 10 min with 4% FA/PBS. After washing for three times, cells were blocked and

permeabilized with 1% BSA/PBS with 0.1% Triton TX100 for 10 min. Afterwards all other primary antibodies against intracellular antigens were applied for 1 h at room temperature. After washing, secondary antibodies were incubated for 45 min at room temperature. After another round of washing, DAPI and nilered or BODIPY were added and incubated for 10 min. Cells were washed in PBS and water and mounted onto slides with mowiol.

8.17. Statistical analysis

Statistical analyses were performed with Excel and Prism5. Normality was tested with Shapiro-Wilk normality test. Significance was determined by using the unpaired two-tailed Student's t-test, the one-way ANOVA or the Mann Whitney test. Significance was assumed for $p<0.05$. Asterisks indicate: *=$p<0.05$, **=$p<0.01$, ***=$p<0.001$, n.s.=not significant.

9. RESULTS

9.1. Verification of the BT-IgSF non-conditional knockout mouse

9.1.1. Correct insertion of the trapping cassette

To study the function of BT-IgSF in the mouse testis, initially a global knockout was characterized. Embryonic stem cells, in which the gene encoding *Igsf11* was inactivated by a trapping cassette, were obtained from the international mouse consortium and injected into mouse blastocysts by the transgenic core facility of the MDC. To validate the correct insertion of the trapping cassette into the genome of the chimera progeny, a Southern blot and long range PCRs were performed using a probe and primers indicated in Figure 16 and Figure 17, respectively.

Both analyses confirmed the correct integration of the trapping cassette (Figure 16 A and Figure 17 A) in the intron between exon 2 and 3 of the IgSF11 gene. In the Southern blot (Figure 16 B), the expected bands of 8.27 kb for the WT allele and 13.45 kb for the KO allele was detected with the 5' probe. In the long range PCR, the expected band of 6.58 kb of the 5' site of the construct and 8.46 kb of the 3' site of the construct were amplified (Figure 17 B).

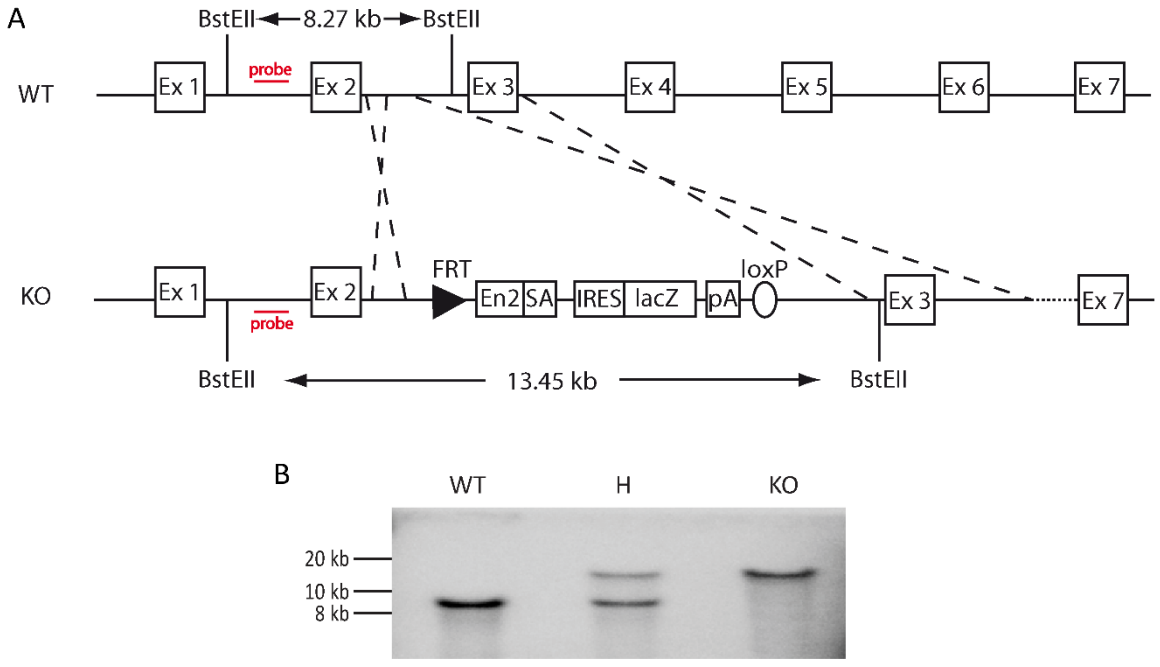

Figure 16: Correct insertion of the BT-IgSF non-conditional KO targeting cassette
(A) Correct integration of the targeting construct was assessed by Southern blotting. The probe was designed to hybridize outside of the homologous arm used for recombination. Genomic DNA was digested with BstEII leading to a fragment of 8.27 kb in case of WT DNA and of 13.45 kb in case of KO DNA. Position of the probe is indicated by a red bar. (B) The probe recognized the correct band in digested genomic DNA of WT, heterozygous (H) and KO animals. For more details of the construct see legend of Figure 8.

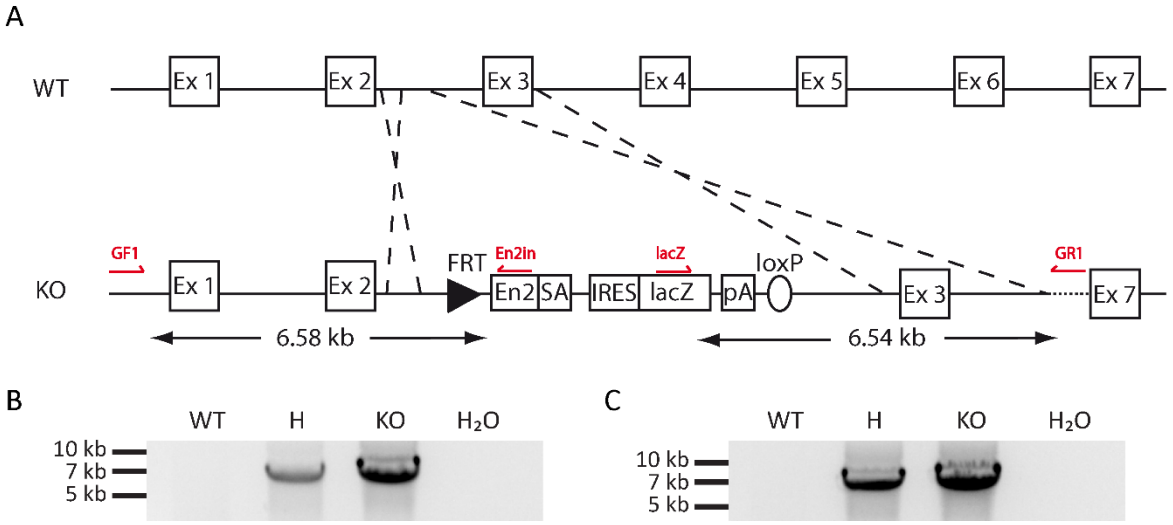

Figure 17: Confirmation of the correct insertion of the BT-IgSF non-conditional KO targeting construct by long range PCR
(A) Primers for the long range PCR are depicted in red. Primers were chosen to cover the 5' and 3' side of the construct. With both PCRs the correct integration of the targeting construct into the mouse genome was confirmed. In case of the knockout allele, fragments of 6.58 kbp (B) on the 5' side or 6.54 kbp (C) on the 3' side were amplified by PCR. For more details of the construct see legend of Figure 8.

9.1.2. *Igsf11* mRNA depletion in BT-IgSF KO mice

The insertion of the trapping cassette should result in a frame-shift mutation and therefore lead to a premature STOP codon in the *Igsf11* gene. It is possible that the frame-shift mutation results in a truncated mRNA, however, this shorter mRNA would then be degraded by nonsense-mediated mRNA

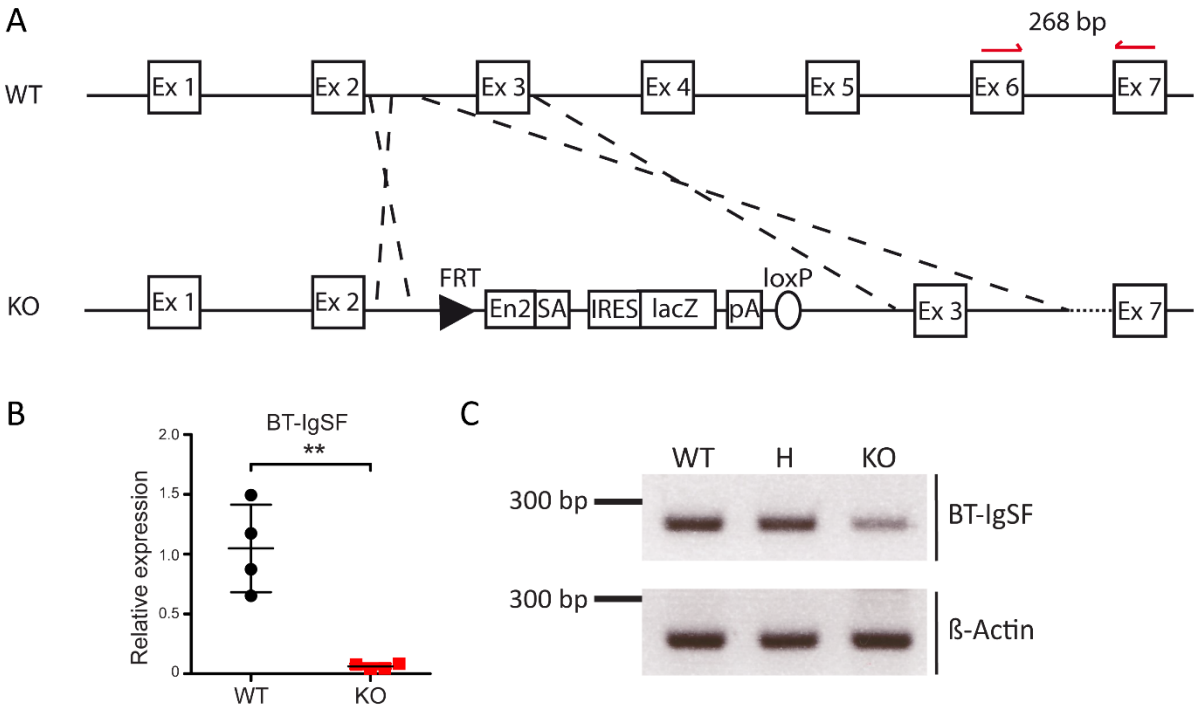

Figure 18: Residual mRNA fragments of *IgSF11* were detected in BT-IgSF KO animals
mRNA expression of *Igsf11* was tested in BT-IgSF KO animals. (A) Arrows in red show the position of the chosen primers in exon 6 and 7. mRNA of *Igsf11* is still detectable in minor amounts by qRT-PCR (B) and RT-PCR (C) in testes of BT-IgSF knockout males (n=4 per genotype). It is not clear whether the detected mRNA is the full-length mRNA or a truncated form.

decay. This means *Igsf11* mRNA should only be present, if at all, in truncated forms in the knockout animals. To check if mRNA of *Igsf11* is absent in the knockout animals, qPCRs were performed with intron-flanking primers for the last exons 6 and 7, after the introduced STOP codon (Figure 18 A). Surprisingly, in knockout testes around 6% of the wildtype mRNA amount was still present (Figure 18 B and C). However, the chosen primer pair is unable to distinguish wildtype full-length *Igsf11* mRNA from a truncated form, for example due to an alternative Start-Codon and open reading frame, since it amplifies only a fragment of the last two exons.

9.1.3. BT-IgSF depletion on protein level

To test whether the insertion of the trapping cassette leads to the absence of BT-IgSF at the protein level, Western blots were conducted with tissues, reported to have a strong BT-IgSF expression, to get maximal sensitivity. Therefore, membrane enriched fractions of testes and of cultivated astrocytes from cortices were tested with a polyclonal antibody raised against the denatured extracellular part of BT-IgSF (Rb113, see Table 21). The comparison of wildtype and knockout samples shows the absence of BT-IgSF protein in the knockouts (Figure 19), confirming the functional BT-IgSF knockout, despite remaining mRNA variants.

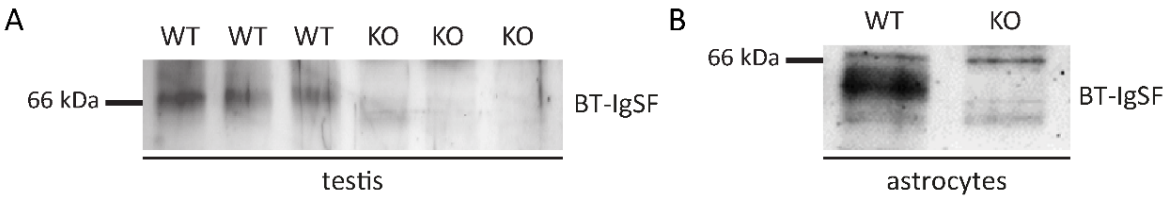

Figure 19: **BT-IgSF KO mice do not express BT-IgSF protein**
Neither in membrane fractions of testes (A) nor in astrocytes (B) BT-IgSF was detected in KO samples confirming a knockout at the protein level. (B) shows a magnified section of a blot shown in Figure 14 C. Note: Rb113 detects unspecific bands at around 66 and 55 kDa in cultivated astrocytes.

9.2. BT-IgSF expression in the murine testis

To analyze the localization of BT-IgSF inside the testes, an antibody which recognizes the native form of BT-IgSF is required. Therefore, a polyclonal antibody against the extracellular region of mBT-IgSF was used (Rb95, see Table 21), which showed the best staining results without high background. As seen in Figure 20, the BT-IgSF antibody is specific, showing no staining in the knockout tissue.

During the analysis of BT-IgSF expression in testis cross sections, differences in the expression between the different tubuli were observed. It is known that the expression of many proteins in the testis, e.g. Claudin 3, 5 and 11, is dependent on the stage of the cycle of the seminiferous epithelium (Meng et al., 2005). For the staging of seminiferi tubuli with BT-IgSF expression, co-stainings with peanut agglutinin (PNA) coupled to Alexa488 and DAPI were analyzed.

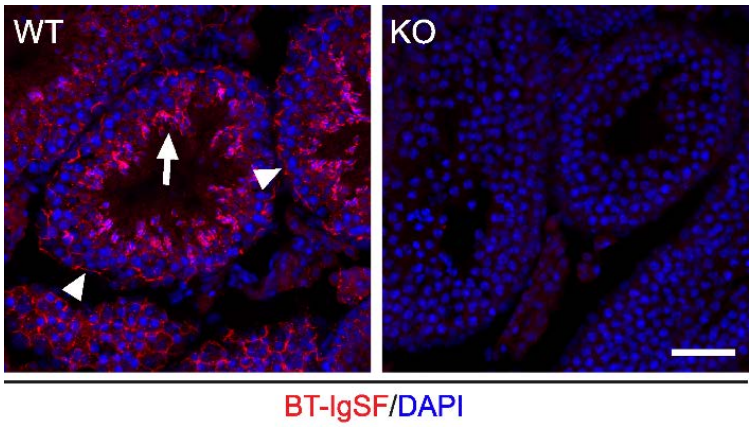

Figure 20: Antibody Rb95 against BT-IgSF used for immunofluorescence staining is specific
Immunofluorescence staining of wildtype and BT-IgSF knockout testis sections with a BT-IgSF antibody; specificity of the antibody was confirmed by a clear staining in WT sections and no signal in KO section. Arrow: expression at the adluminal side, in elongated spermatids; arrowhead: expression at the basal side, in Sertoli cells; scale bar: 50 µm.

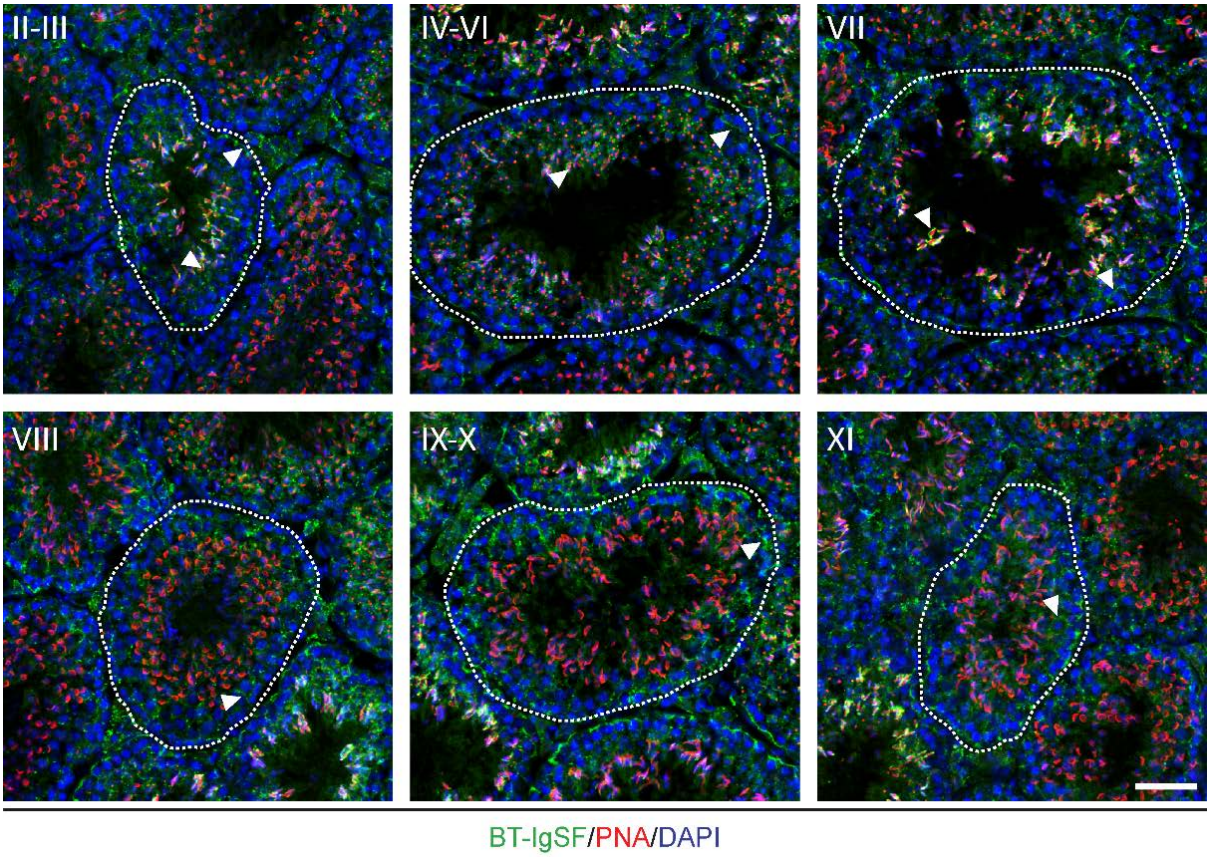

Figure 21*:* BT-IgSF is expressed in Sertoli cells in stages I-XII and additionally at the aES and the acrosomes of spermatids in stages I-VII
BT-IgSF is expressed at all stages in Sertoli cells. See arrowheads at the basal side of the tubuli. BT-IgSF is additionally found at the aES and the acrosomes of spermatids and sperm in stages I-VII, see arrowheads at the luminal side. Scale bar: 50 µm.

In all twelve stages, BT-IgSF is localized on the basal side of the seminiferi tubuli and associated with Sertoli cells close to the nucleus (Figure 21, arrowhead and Figure 24 A). BT-IgSF expression is found at the BTB, which is confirmed by a partial co-localization with the BTB protein connexin43 (Figure 22 A) and by a more extensive co-localization with ZO-1, which is also part of the BTB (Figure 22 B).

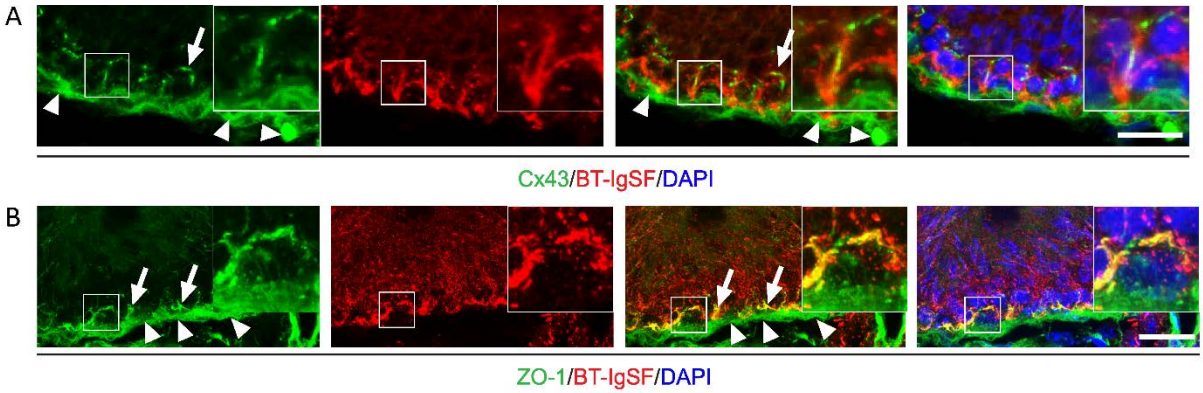

Figure 22: BT-IgSF co-localizes with Cx43 and ZO-1 at the BTB
(A) Immunofluorescence staining of wildtype testis sections against BT-IgSF and mouse anti-Cx43; Cx43 co-localizes partly with BT-IgSF; arrow: specific expression at the basal side; arrowheads: unspecific staining of the secondary goat anti-mouse-A488 antibody probably due to mouse-on-mouse cross reactions at the basement membrane; scale bar: 25 µm. (B) Immunofluorescence staining of wildtype testis sections against BT-IgSF and mouse anti-ZO-1; note the strong co-localization of BT-IgSF and ZO-1; arrow: specific expression at the basal side; arrowheads: unspecific staining of the secondary goat anti-mouse-A488 antibody probably due to mouse-on-mouse cross reactions at the basement membrane; scale bar: 20 µm.

Furthermore, early stages (I-V) and middle stages (VI-VII) but not in late stages (VIII-XII) show BT-IgSF expression at the adluminal compartment at or around the acrosome of elongated spermatids and sperms (Figure 21 and Figure 24 A).

At the adluminal side, between the head of the elongated spermatids and the Sertoli cells, the apical ES (aES) exists to ensure the adhesion of the maturating spermatids to the epithelium. The aES is only formed by Sertoli cells and the acrosome is part of the elongated spermatids. To analyze whether the BT-IgSF signal at or around the acrosomes is due to a localization on the acrosome or in the aES, co-stainings with the aES marker Espin were carried out, revealing a co-localization (Figure 23 B). This strongly suggests that BT-IgSF is expressed in Sertoli cells.

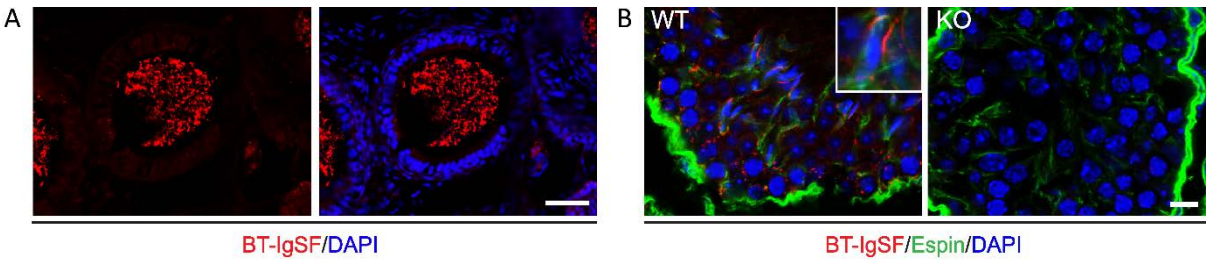

Figure 23: BT-IgSF is expressed at the acrosome of sperm and at the aES
(A) Immunofluorescence staining of epididymis sections show labeling of mature sperm; scale bar: 50 µm. (B) Immunofluorescence staining of testis sections show BT-IgSF co-localized with Espin at the apical ES; scale bar: 10 µm.

The expression of BT-IgSF on the acrosome of sperms was also tested by a staining of epididymis cross sections. In the ductules of the epididymis, mature sperms are stored until they are released and exist there without the contact to Sertoli cells. These sperms were also BT-IgSF positive at their acrosomes (Figure 23 A), clearly showing that BT-IgSF expression is not restricted to Sertoli cells but is also found in the acrosomes.

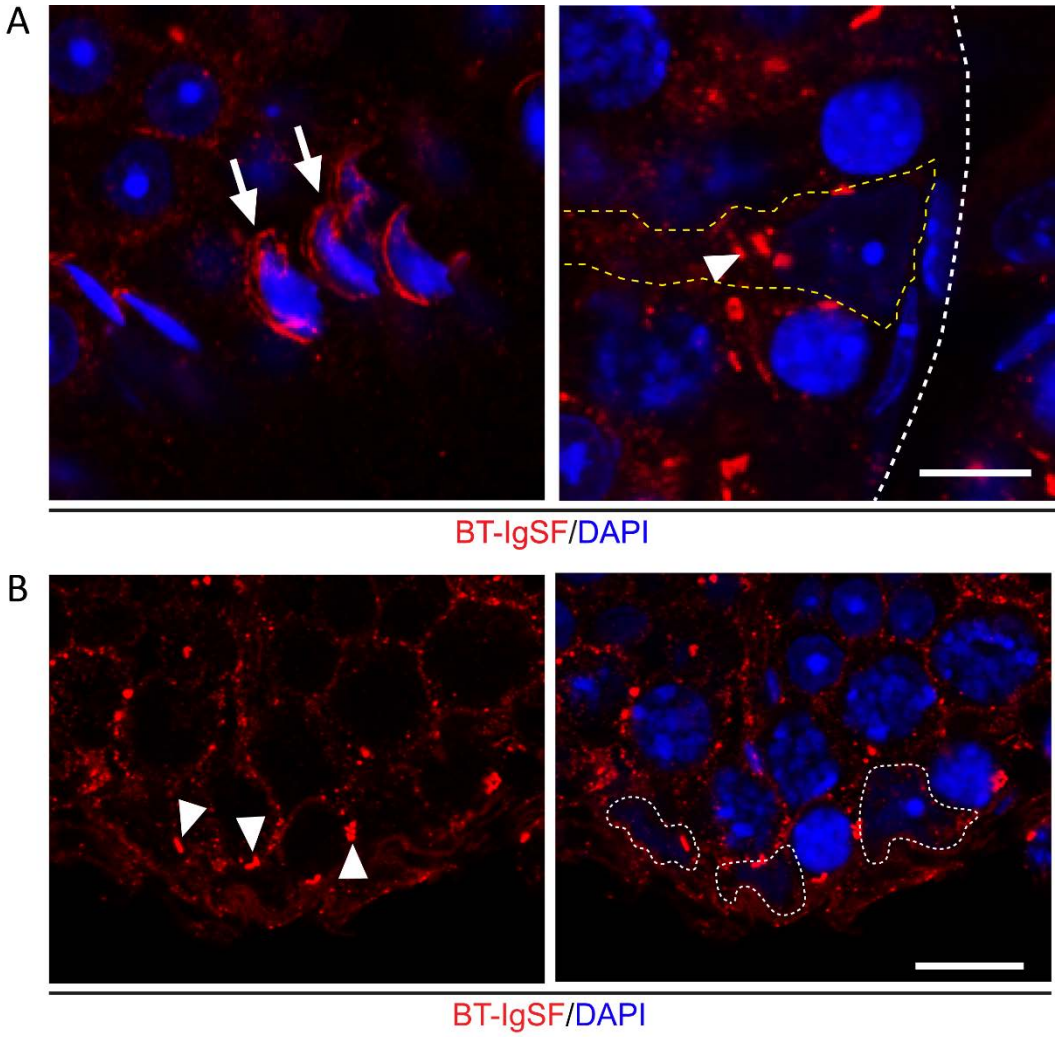

Figure 24: **BT-IgSF is expressed in Sertoli cells and at the aES and acrosomes of spermatids**
(A) Immunofluorescence staining of wildtype testis sections against BT-IgSF; arrow: expression at elongated spermatids at the apical ectoplasmic specialization (ES); arrowheads: expression at the basal side (marked by white dashed line), in Sertoli cells (indicated by yellow dashed line); scale bar: 5 µm. (B) Higher magnification of BT-IgSF immunofluorescence stainings of WT testes; arrowheads: strong BT-IgSF expression at Sertoli cells in the basal compartment; white outline indicates the nucleus of Sertoli cells; scale bar: 10µm.

The diffuse staining of BT-IgSF in the seminiferous epithelium suggests that BT-IgSF is not restricted to Sertoli cells. However, even at higher magnifications it remains unclear whether BT-IgSF protein is also expressed on germ cells since the thin cytoplasmic protrusions of Sertoli cells extend towards the lumen (Figure 24 B). Further electron microscopic investigations might clarify whether germ cells express BT-IgSF while migrating from the basal to the luminal side.

Taken together, the immunohistological studies show that BT-IgSF is expressed on Sertoli cells at the basal and apical side and on the acrosome of elongated spermatids and sperms.

9.3. BT-IgSF deficient males are infertile

During the breedings of BT-IgSF NC/lacZ mice it turned out that breedings of BT-IgSF knockout males with C57BL/6N wildtype females (5 cages with 1 male and 2 females each) did not result in any offspring, although vaginal plugs were observed, indicating normal mating behavior but infertility. Heterozygous males and BT-IgSF knockout females (9 females inspected) were fertile, suggesting that infertility is restricted to homozygous males.

Dissections of BT-IgSF knockout males showed that the testis size of BT-IgSF knockout mice was significantly reduced compared to wildtype and heterozygous animals (Figure 25 B), while other organs and the overall organ organization seemed not to be affected (Figure 25**Figure 25** A).

Figure 25: BT-IgSF KO testes are significantly smaller

(A) BT-IgSF knockout animals exhibit smaller testes; bl: bladder, e: epididymis, f:fat, p:penis, pg: preputial gland, sv: seminal vesicle, t:testis; scale bar 5mm. (B) Knockout testes showed a significantly decreased wet weight compared to wildtype and heterozygous testes; p value <0.001 (one-way ANOVA with Bonferroni correction); WT animals n=14, heterozygous animals n=22; KO animals n=30, data are shown as mean ± SD.

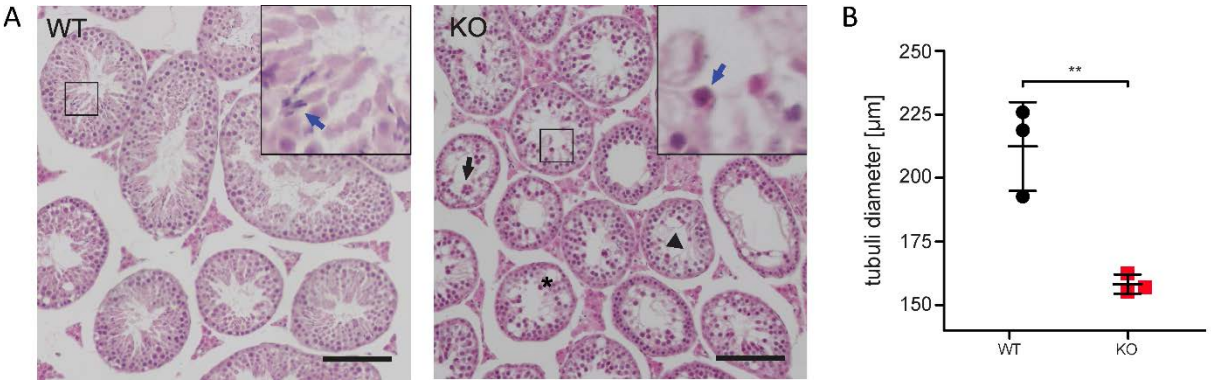

Figure 26: Atrophic testes in BT-IgSF knockout males

(A) H&E staining of methacrylate-sections show atrophic testes of BT-IgSF knockout animals; black arrow: multinucleated cells, arrowhead: Sertoli cell cytoplasmic extensions, asterisk: vacuolar degeneration, scale bar: 100 µm; higher magnification shows the lack of sperms in KO animals (blue arrow). (B) Tubuli diameter of BT-IgSF knockout males are significantly smaller compared to wildtype tubuli; data are shown as mean ± SD; **=p<0.01, n= 3 per genotype, 20-60 tubuli were analyzed.

To further characterize KO testis, the gross morphology was analyzed in H&E stained sections. Knockout males showed atrophic testes with vacuolar degeneration of the seminiferi tubuli (Figure 26 A, asterisk) and Sertoli cell cytoplasmic extensions (Figure 26, arrowhead). Diameter of BT-IgSF knockout tubuli were significantly smaller (158.22 µm ± 3.41) compared to wildtype tubuli (212.39 µm ± 2.83) (Figure 26 B). No sperms were detected in the lumen of homozygous knockout animals (Figure 26 A, enlarged image for details, blue arrow), in contrast, multinucleated cells were found at the luminal site (Figure 26 A, arrow).

The lack of sperms in BT-IgSF knockout males suggests a failure in spermatogenesis. To analyze in detail which cell types are missing in BT-IgSF knockout testes, testis preparations were stained for DNA with DAPI and were analyzed by flow cytometry.

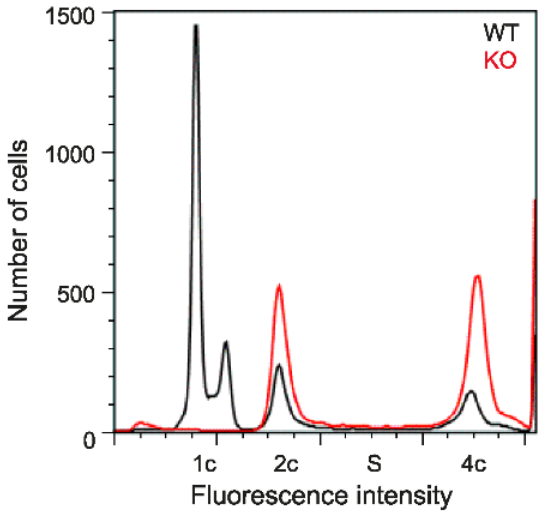

Figure 27: BT-IgSF KO testes lack spermatids and sperm
Flow cytometric analysis of testis cells, stained with DAPI, shows the lack of haploid chromatin containing cells in BT-IgSF knockouts (red), 1c: haploid, 23 chromatids; 2c: haploid, 23 chromosomes; S: S-phase; 4c: diploid, 46 chromosomes. Analysis was done in cooperation with Karin Müller, IZW Berlin.

During spermatogenesis, cells with different DNA content exist in the testes due to meiosis. Primary spermatocytes duplicate their chromatids reaching 4c chromatid content before they enter meiosis I. After meiosis I secondary spermatocytes exist with a chromatid content of 2c. After meiosis II the resulting spermatids and all following stages only have a chromatid content of 1c (see Figure 2). BT-IgSF-deficient testes completely lack haploid cells with 1c DNA content (Figure 27). This shows that no spermatids and sperms are present in the knockout testis and that meiosis II has no outcome, leading to azoospermia.

9.4. The loss of BT-IgSF leads to spermatogenic arrest after meiosis I

The lack of haploid cells in the seminiferi tubuli indicates an arrest in spermatogenesis, and a disturbance of meiosis. To determine the exact stage of arrest, expression of genes transcribed during

spermatogenesis were measured by qRT-PCR (Lee et al., 2006; Luangpraseuth-Prosper et al., 2015; Silva et al., 2009).

The expression of *Piwil2*, a specific marker for stem cells, did not significantly differ between wildtype and BT-IgSF knockout mice (Figure 28), suggesting that the number of stem cells are not changed in abundance. A slight tendency towards increased stem cell numbers in the knockout was detected.

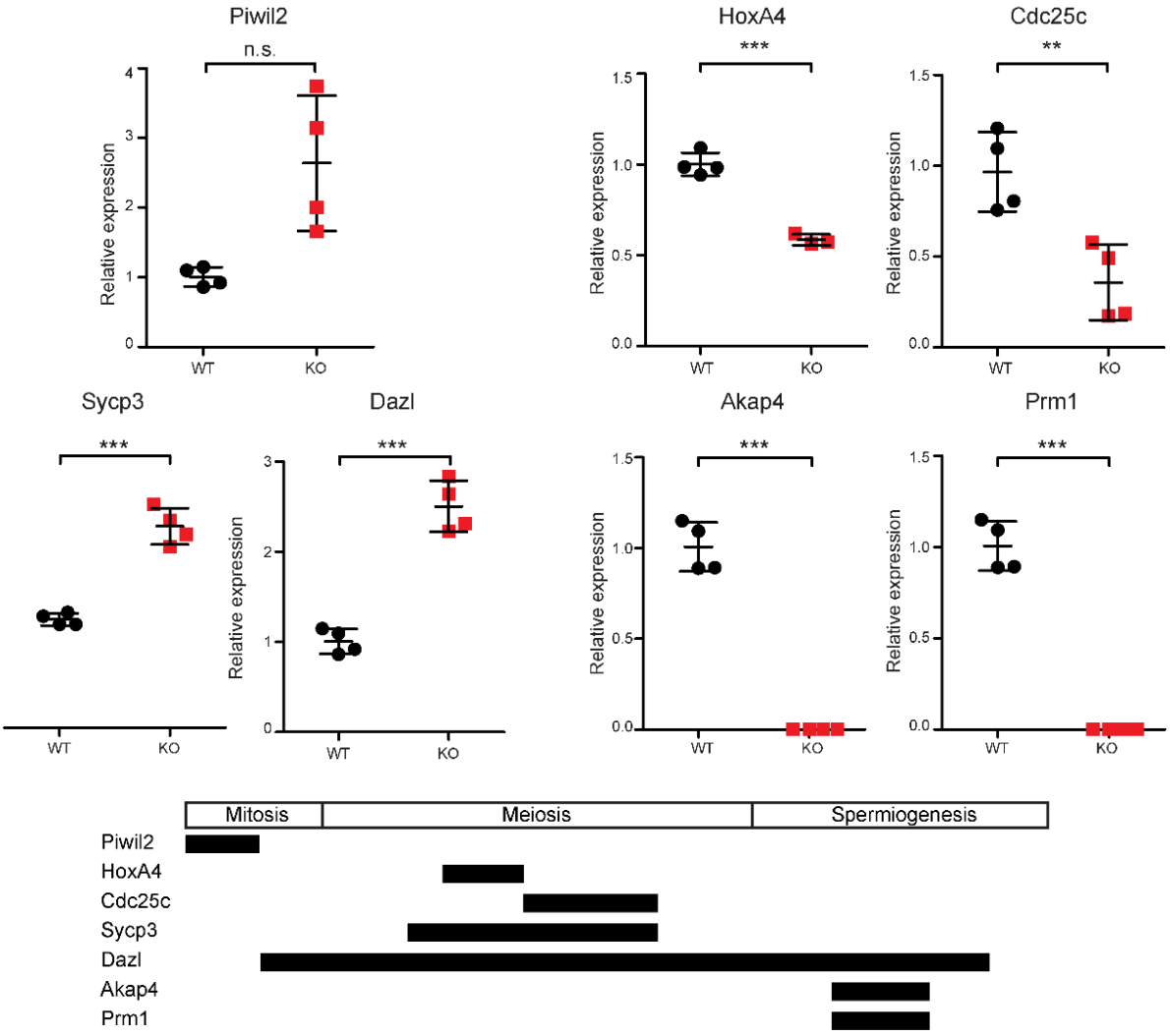

Figure 28: The lack of BT-IgSF leads to spermatogenic arrest

qRT-PCR analysis of meiotic genes from testis lysates of wildtype and BT-IgSF knockout mice. Gene expression was normalized to *Rplp0*, and indicated as fold change to WT. *Piwil2* was used as a marker for stem cells, *HoxA4* and *Cdc25c* were used as markers for mid-pachytene stage and late pachytene stage, for overall pachytene stage *SycP3* was used, for meiotic germ cells *Dazl* was used and for the post-meiotic haploid stages *Prm1* and *Akap4* were used; n=4 per genotype, data are shown as mean ± SD; n.s. = not significant, **= p<0.05, ***= p<0.001 (t-test).The scheme illustrates the pattern of expression of genes investigated during germ maturation.

However, the transcripts for germ cells in the mid-pachytene stage and late pachytene stage, *HoxA4* and *Cdc25c*, respectively, were significantly reduced. In contrast, marker genes for the overall pachytene stage (*Sycp3*) and for meiotic cells in general (*Dazl*) were upregulated, suggesting an increased cell number between the stem cell stage and the mid-pachytene stage. Transcripts for post-

meiotic markers (*Akap4* and *Prm1*), which are only expressed in haploid spermatids, were not detected at all in knockout testes. These expression data further confirm the observed complete lack of spermatids and sperms.

It is necessary to investigate whether the slight changes in gene expression have an impact on the molecular processes of meiosis I. Arrest in meiosis I is often caused by failed pairing of homologous chromosomes (Burgoyne et al., 2009). To examine whether this pairing works properly in BT-IgSF KO males, stainings against SYCP3 and γH2AX were performed on testis sections. SYCP3 is a marker for the axial element of the synaptonemal complex from zygotene to pachytene stage during meiosis I and phosphorylated H2AX (γH2AX) is expressed from leptotene on and later marks the silenced sex body, during meiotic sex chromosome inactivation (Handel, 2004; Lammers et al., 1994; Brower et al., 2009). Wildtype and knockout testis show SYCP3 expression, although in slightly different patterns, which can be attributed to the disturbed testis morphology in BT-IgSF deficient mice. In both genotypes γH2AX was co-expressed with SYCP3 at early pachytene, indicated by diffuse distribution (Figure 29 A, arrow), as well as late pachytene, implied by a restricted expression at the inactivated X-chromosome (Figure 29 A, arrowhead). In the knockout testes all meiotic cells expressed γH2AX, indicating that these cells are in meiosis I. In meiosis II, which represents a mitosis, γH2AX is normally not expressed (Figure 29 B).

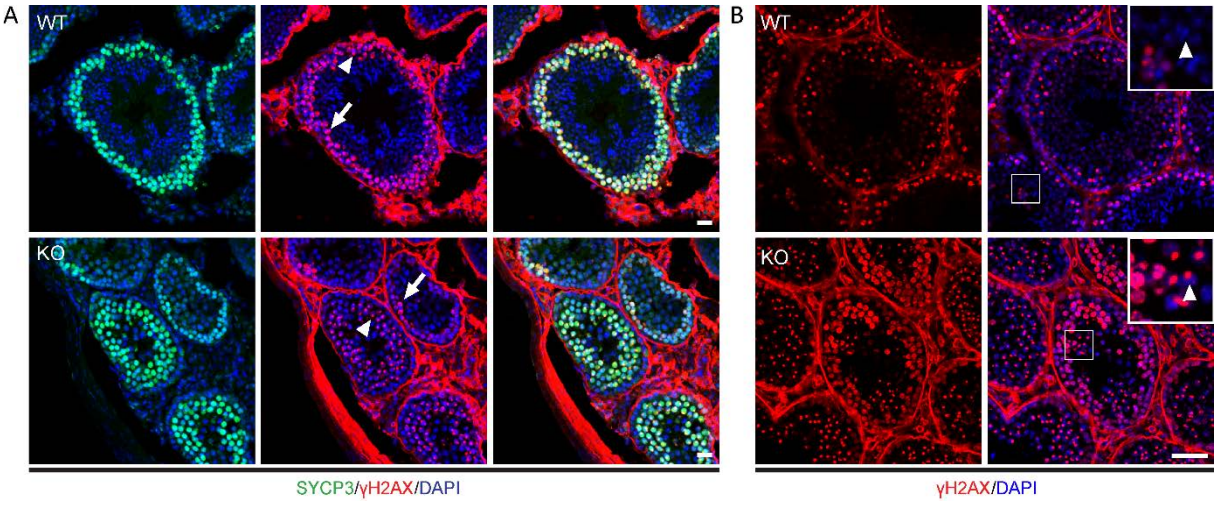

Figure 29: Meiotic arrest occurs after meiosis I
(A) Immunofluorescence staining of cryosections against γH2AX and SYCP3, arrow: leptotene stage, arrowhead: diplotene stage, scale bar: 20 µm. (B) Immunofluorescence staining against γH2AX. In the wildtype, meiotic cells with and without γH2AX expression are present (see arrow head in the insert); in contrast, in the KO, only γH2AX positive meiotic cells are present (see arrow head in the insert), indicating that all cells are in meiosis I; scale bar: 50µm.

These results show that in BT-IgSF deficient germ cells, meiosis I appears to be properly carried out and that the spermatogenic arrest most likely occurs after meiosis I.

9.5. Absence of BT-IgSF changes Sertoli cell morphology but does not affect hormonal balance

To assess implications of BT-IgSF absence on Sertoli cells, the localization of the intermediate filament vimentin in testis sections was analyzed. Immunostainings of testis sections showed irregular and disturbed cytoplasmic arms of Sertoli cells in BT-IgSF knockout mice (Figure 30 A). However, the localization and the number of Sertoli cells, as detected by nuclear staining with Wilms Tumor 1 (WT1), appeared not to be affected (Figure 30 B).

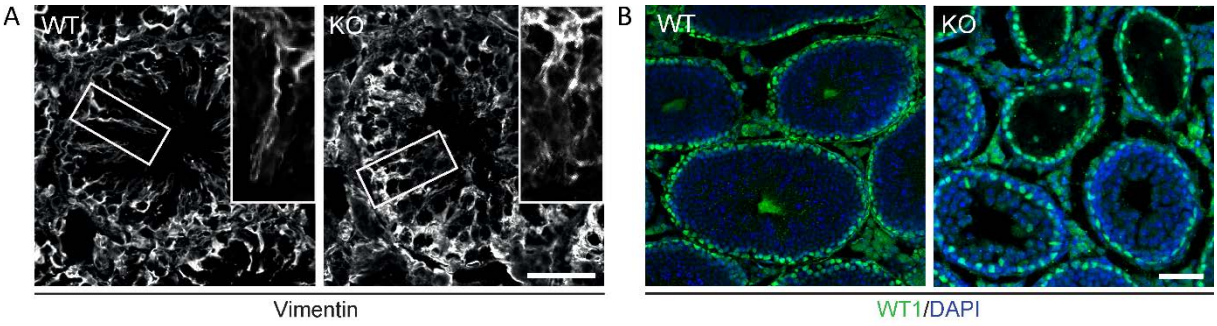

Figure 30: Loss of BT-IgSF influences the overall morphology of Sertoli cells
(A) Immunofluorescence stainings against vimentin, a cytoplasmic Sertoli cell marker. Note the irregular and disturbed cytoplasmic arms of Sertoli cells in BT-IgSF knockout mice; scale bar: 50µm. (B) Immunofluorescence stainings against Wilms Tumor 1 (WT1), a Sertoli cell marker located in the nucleus, show normal Sertoli cell number and localization in tubuli of knockout mice; scale bar: 50 µm.

Spermatogenic arrest is sometimes also associated with an increased apoptosis of germ cells. To investigate whether the absence of spermatids and sperms is caused by or associated with apoptosis, apoptotic cells were analyzed with an antibody staining against active Caspase-3, which is a key protein

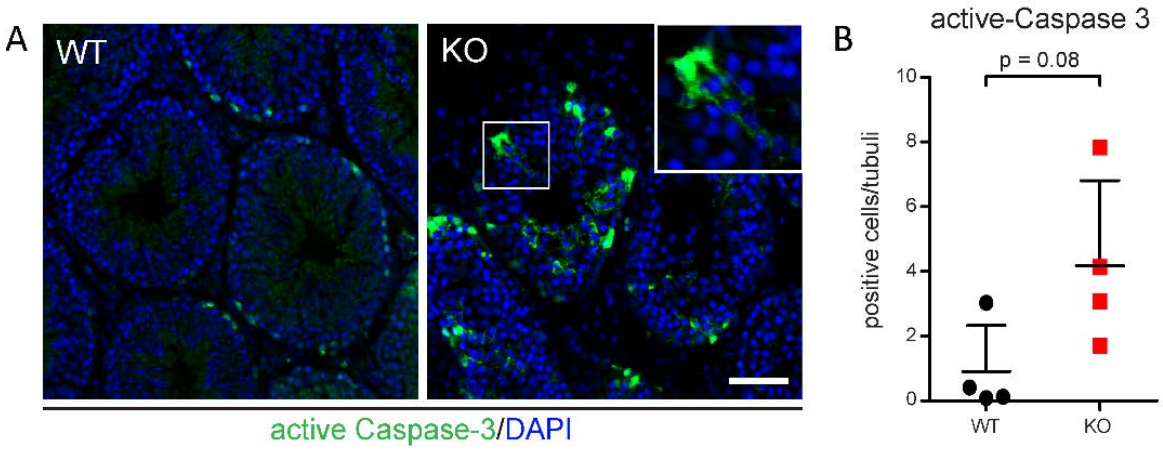

Figure 31: Loss of BT-IgSF does not increase apoptosis
(A) Immunofluorescence staining against active Caspase-3, a marker for apoptosis, show slightly more apoptotic cells in knockout testes, especially in Sertoli cells (insert); scale bar: 50 µm. (B) Quantitation of apoptotic cells per tubuli, no significant difference between knockout and wildtype testes was observed; n=5 per group, data are shown as mean + SD; p=0.08 (t-test).

in cell-death signaling. The analysis revealed a slight increase of Caspase-3 positive cells in BT-IgSF knockout testes, however, this tendency did not reach statistical significance (Figure 31 B). Based on their localization inside the tubuli and the presence of cytoplasmic arms, most apoptotic cells in knockout testes were considered to be Sertoli cells (Figure 31 A).

BT-IgSF deficiency could lead to changes in the hormonal hypothalamic-pituitary-axis, due to its expression in Sertoli cells, which are involved in the regulation of this hormonal axis. A misregulation of the hormonal system could either induce infertility or be a result of it. To analyze the hormonal status in BT-IgSF KO males, the level of LH, FSH and testosterone in the blood of wildtype and BT-IgSF knockout mice were measured by ELISA (performed by the company Laboklin, Germany). No significant differences in LH, FSH and testosterone between genotypes were detected (Figure 32). However, the LH values have a high variability, which is known, since LH varies episodically, in discontinuous pulses (Coquelin and Desjardins, 1982). These findings indicate that a disturbed hormonal balance does not contribute to, nor cause male infertility in BT-IgSF-deficient mice.

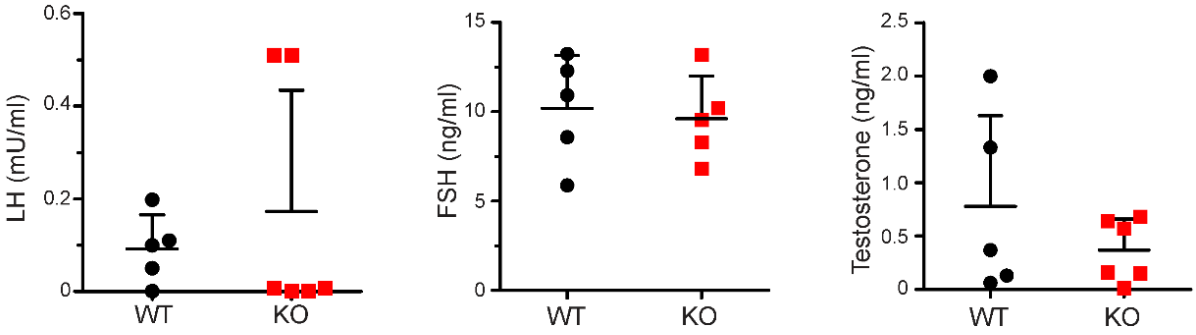

Figure 32: The lack of BT-IgSF does not lead to changes in the hormonal balance
No hormonal changes in LH (p=0.78), FSH (p=0.69) and testosterone (p=0.79) levels were detected in BT-IgSF knockout males, compared to wildtype; WT n=5, KO=6, data are shown as mean + SD; differences were not significant (Mann Whitney test).

9.6. Loss of BT-IgSF results in severe disruption of the BTB and an altered expression of BTB proteins

The expression and its subcellular localization of BT-IgSF in Sertoli cells strongly suggested to analyze BTB integrity in BT-IgSF knockout mice. This was carried out by injecting EZ-Link Sulfo-NHS-LC-Biotin, which is BTB impermeable, into the testis in an *in vivo* situation (Meng et al., 2005). After fixation, the injected EZ-Link Sulfo-NHS-LC-Biotin was visualized with Streptavidin-coupled Cy5 in cryostat sections. In wildtype testis, biotin staining outlined the basal spermatogonia but was not detectable in other cell layers (Figure 33). In contrast, in BT-IgSF KO testis, the biotin signal was less sharp in the basal compartment and was additionally detected in other cell layers, indicating a disruption of the BTB.

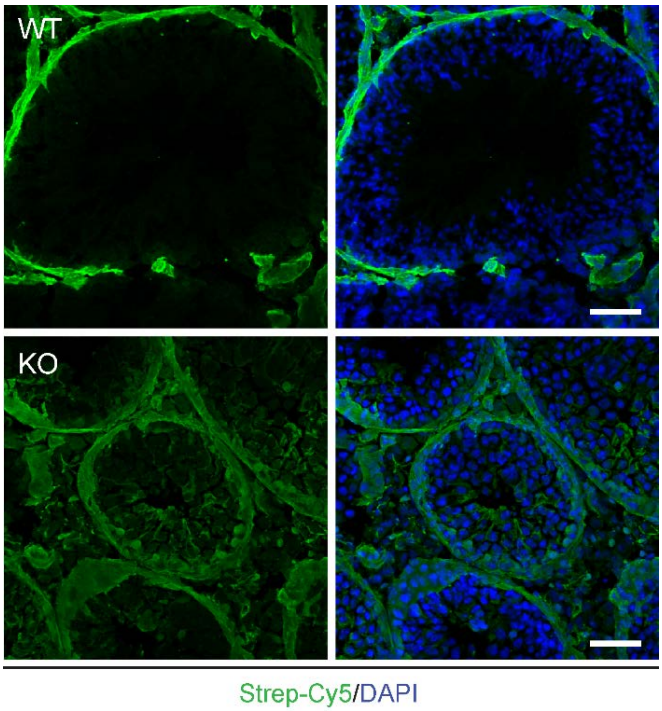

Figure 33: BT-IgSF loss leads to an impaired BTB
In vivo biotin assay to test the functionality of the BTB. After injection of a BTB-impermeable biotin tracer, its distribution is visualized by Streptavidin-Cy5 staining; knockout testis show distribution through all layers of the seminiferous epithelium, indicating an impaired BTB; n=3 per genotype; scale bar: 50 µm.

The BTB consists of several cell-cell contact proteins forming tight junctions, gap junctions and adherens junctions (for review see Cheng and Mruk, 2012; Xiao et al., 2014). Therefore, the mRNAs expression of proteins involved in the BTB formation were analyzed by qRT-PCR and revealed striking differences between wildtype and BT-IgSF knockout testes. The tight junction transcripts *Cldn11*, *Ocln* and *ZO-1* were significantly upregulated in knockout testes (Figure 34). *ZO-2* was not changed at the mRNA level and only slightly unorganized in immunofluorescence stainings (Figure 35 A). In immunofluorescence stainings of testis sections, ZO-1 protein appeared slightly enhanced and its localization was less organized at the BTB in comparison to the wildtype (Figure 35 B). Similarly, the mRNA of *Cx43*, the most abundantly expressed gap junctional protein in testes, was also upregulated in BT-IgSF knockouts (Figure 34).

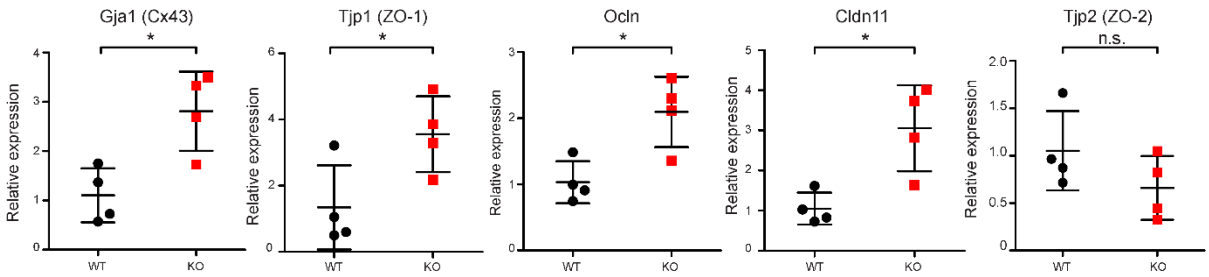

Figure 34: BT-IgSF deletion leads to upregulation of transcripts encoding BTB proteins
Analysis of BTB gene expression by qRT-PCR; Gja1, Tjp1, Ocln and Cldn11 are upregulated in knockout testes, Tjp2 is not changed; n=4 per group, data are shown as mean ± SD; *=p<0.05, n.s.= not significant (t-test).

This increase was also clearly detected in immunofluorescence stainings (Figure 35 C). Moreover, and most interestingly, Cx43 was found to localize throughout the knockout tubule and was not restricted to the BTB like in the wildtype, where Cx43 is sharply located at the basal site of the seminiferi tubuli (Figure 35 C). Furthermore, the phosphorylation status of Cx43 was increased in BT-IgSF deficient testes (Figure 35 D and E), although with some variability.

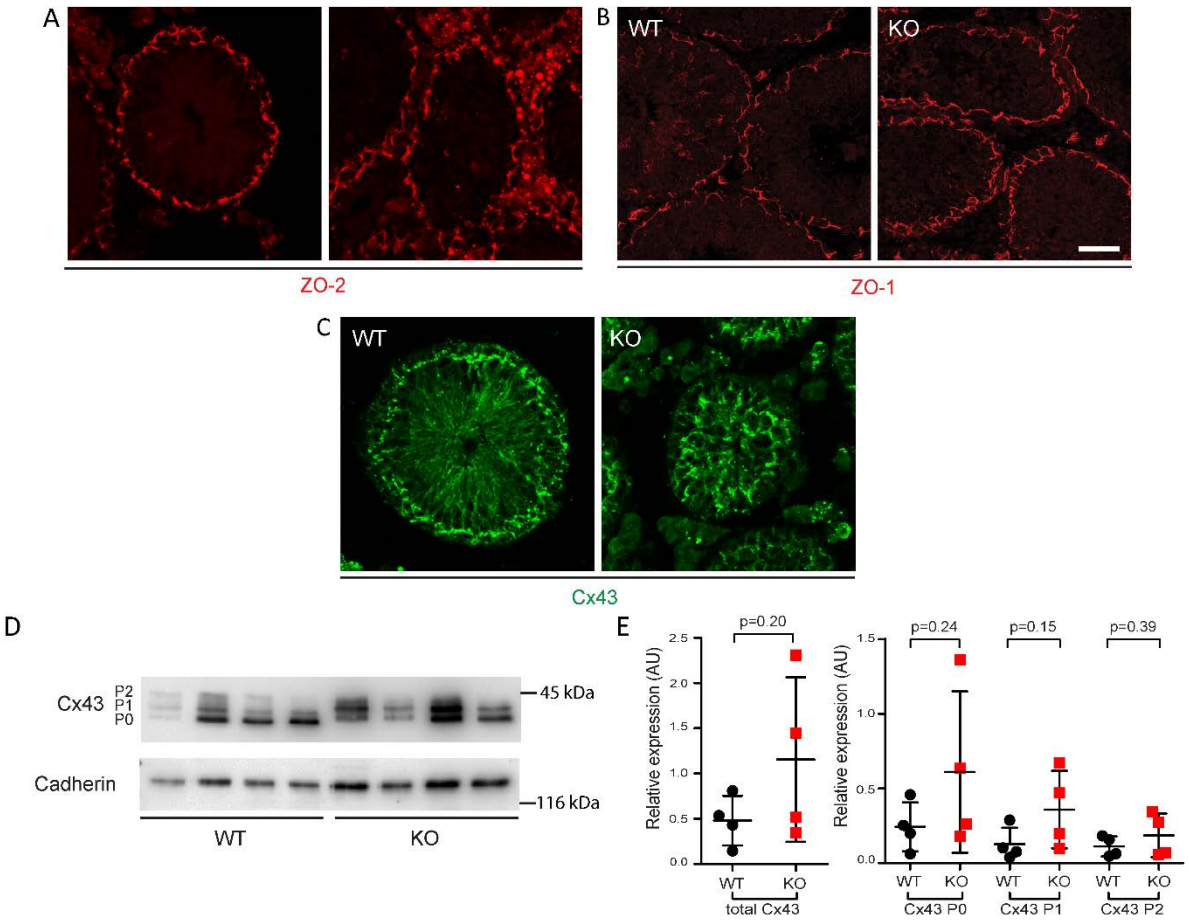

Figure 35: Cx43 is mislocalized and ZO-1 and ZO-2 are unorganized in the testes of BT-IgSF KO mice
(A) Immunofluorescence staining against ZO-2 of cryostat sections: expression and localization is normal in knockout testis, although less organized; scale bar: 50 µm. (B) Immunofluorescence staining against ZO-1, a tight junction protein of the BTB: note the slightly less organized localization of ZO-1 in knockout testis; scale bar: 50 µm. (C) Immunofluorescence staining against Cx43, a gap junction protein of the BTB: note the diffuse localization of Cx43 in knockout testis; scale bar: 20 µm. (D) and (E) Protein expression of Cx43; P0: unphosphorylated, P1 and P2: phosphorylated forms. Anti- pan-Cadherin was used as a loading control. Three independent blots were analyzed which showed no significant differences between WT and KO (t-test), data are shown as mean ± SD.

In electron microscopy of testis sections, vacuolation (Figure 36 A, red outline) as well as the lack of sperm and a disorganization of the epithelium was detected in BT-IgSF knockouts. However, no differences in the ultrastructure of the BTB of wildtype and knockout testis were detected at this level (Figure 36, arrowheads). All sections showed intact BTB structures including “new” and “old” BTBs behind and ahead of the pachytene spermatocytes, respectively, suggesting that BTB formation can occur in the absence of BT-IgSF, but its functionality is disturbed (Figure 36 B).

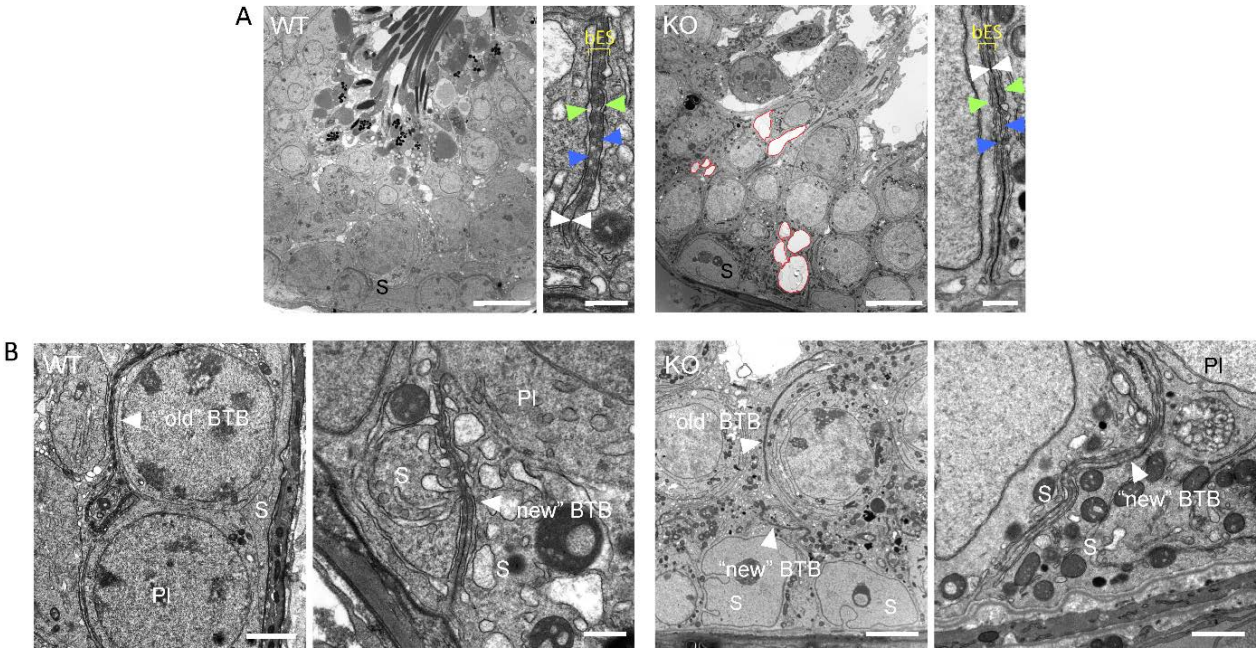

Figure 36: In BT-IgSF KO testes no structural differences of the BTB are detectable by electron microscopy
(A) Electron microscopy of adult testis; at higher magnifications no differences between WT and KO were observed in the basal ES, typified by the actin filament bundles (blue arrowheads) sandwiched between cisternae of the endoplasmic reticulum (green arrowheads) and the plasma membranes of two Sertoli cells, TJ (white arrowheads) coexisting with the basal ES, outlined in red: vacuoles, S: Sertoli cells; scale bar left panel WT and KO: 10 µm, right panel in WT and KO: 500 nm. (B) Electron microscopy of adult testes showing the "old" BTB ahead of the pachytene spermatocyte (Pl) and the "new" BTB behind the pachytene spermatocyte, suggesting a normal assembly and disassembly of the BTB; S: Sertoli cells, arrowhead: BTB, scale bar left panel WT: 2 µm, right panel WT: 500 nm, left panel KO: 10 µm, right panel KO: 1 µm. Electron microscopy was done in collaboration with Bettina Purfürst, core facility electron microscopy at the MDC.

9.7. Gap junction function is not altered *in vitro*

The change of Cx43 expression and localization in the BTB raises the question whether gap junction function in BT-IgSF knockout testes is impaired, which in turn results in an impaired BTB. To address this question, primary Sertoli cells were cultured and gap junction function was assessed by dye

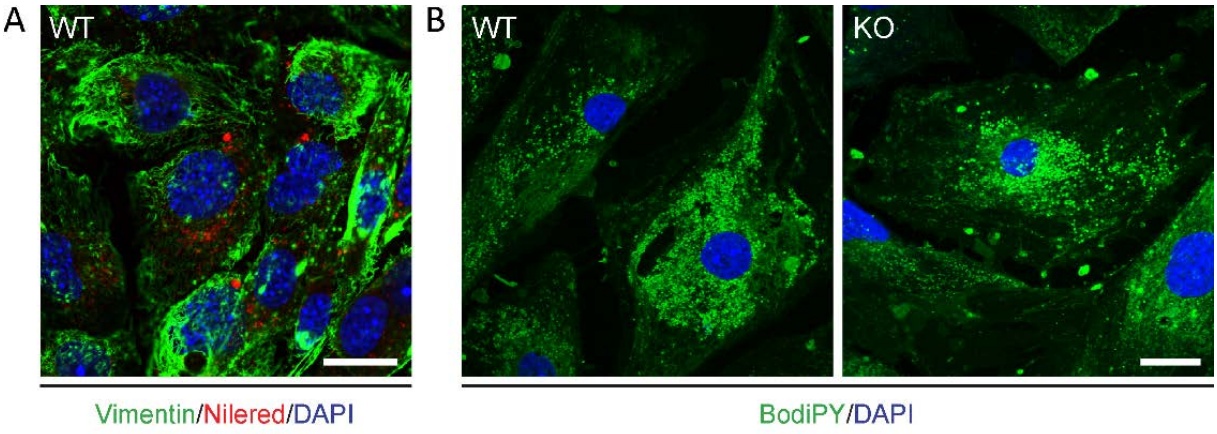

Figure 37: Primary isolated cells are positive for Sertoli cell markers
(A) Immunofluorescence staining of cultured Sertoli cells against vimentin and with nilered. Cells are positive for both markers, confirming identity of cells as Sertoli cells. Scale bar: 20 µm. (B) Staining of cultured Sertoli cells with BODIPY, a lipophilic dye, staining the lipid droplets inside Sertoli cells. Scale bar: 20 µm.

spreading using 6-carboxyfluorescein. First, the identity of the isolated cells was tested. Sertoli cells contain lipid droplets in their cytoplasm which can be stained by lipophilic dyes such as BODIPY or nilered (Figure 37 A and B) (Mather et al., 1990). Furthermore, Sertoli cells contain the intermediate filament vimentin (Figure 37 A). Both stainings confirmed that the cells cultured were Sertoli cells. Afterwards, the expression of BT-IgSF in Sertoli cells was analyzed and is shown in Figure 38. BT-IgSF is localized at the membrane of Sertoli cells and additionally appears to be present in special compartments of the cell membrane in puncta-like structures (Figure 38, arrow). Cx43 is also expressed in Sertoli cell cultures and co-localizes only partly with BT-IgSF (Figure 38). Sertoli cells, cultured at high density, can closely mimic the BTB functionally and structurally in *vitro* (Byers et al., 1986; Janecki et al., 1991; Cheng et al., 2011). The presence of BTB-like junctions at the day of gap junction assessment was tested by ZO-1 staining, which, however, is not a functional proof of tight junction barriers (Figure 39). In wildtype Sertoli cells, ZO-1 was localized at the membrane and appeared in a zigzag like form. In the KO cells, ZO-1 was also present at the membrane but the zigzag form was not detectable, and the expression appeared to be weaker.

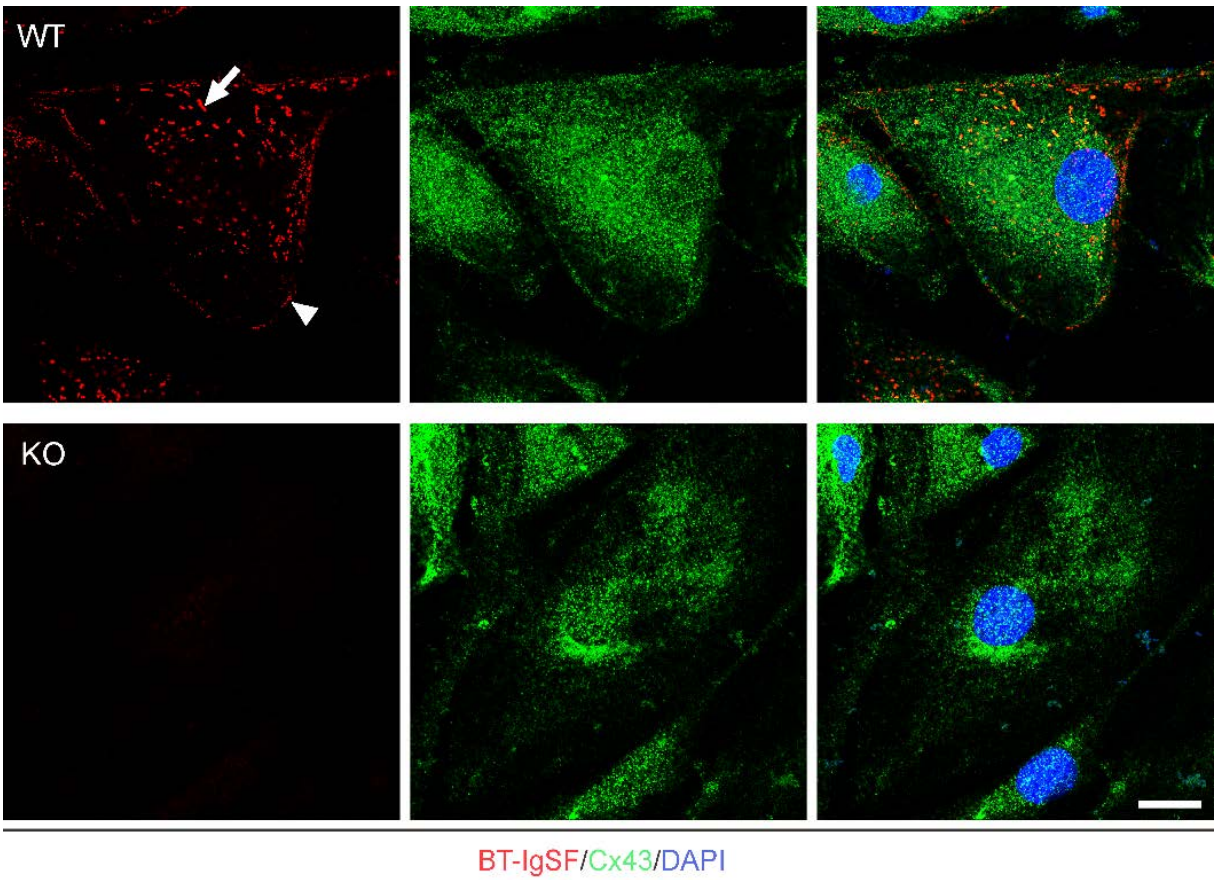

Figure 38: Cultured Sertoli cells express BT-IgSF and Cx43
Immunofluorescence staining of cultured WT and KO Sertoli cells stained against BT-IgSF (live staining) and Cx43 (after fixation). BT-IgSF is absent in KO cells. Note the partial co-localization of BT-IgSF and Cx43. Arrowhead: Localization of BT-IgSF at the membrane, arrow: localization of BT-IgSF in puncta like structures. Scale bar: 20 µm.

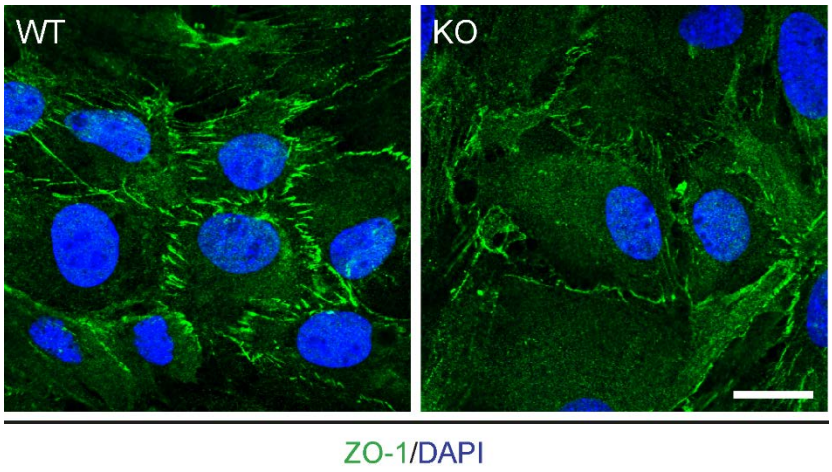

Figure 39: Sertoli cells form tight junctions *in vitro*
Immunofluorescence staining of cultured WT and KO Sertoli cells stained against ZO-1. Sertoli cells from both genotypes form tight junctions on the day of the dye spreading experiment. Scale bar: 20 µm.

For the analysis of gap junction function, a single Sertoli cell was microinjected with a fluorescent dye, 6-carboxyfluorescein, which is smaller (0.37 kDa) than 1kDa, the maximal size of a molecule to pass gap junctions (Lablack et al., 1998). Diffusion of the dye through gap junctions was analyzed after 5 minutes and the area of the spreading was measured. The injection and dye spreading worked well in all genotypes tested. However, there was no difference between WT and KO Sertoli cells in dye spreading area, indicating no impaired gap junction function of KO Sertoli cell *in vitro* (Figure 40).

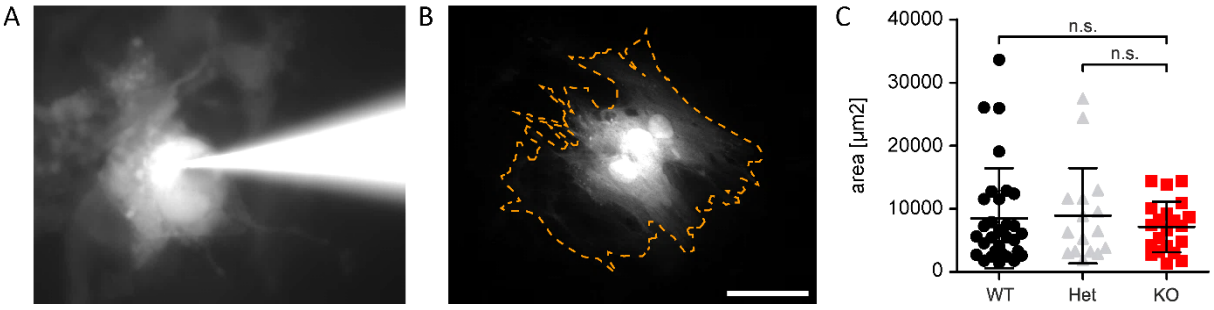

Figure 40: Loss of BT-IgSF does not lead to an altered coupling of Sertoli cells in vitro
(A) Injection of 6-carboxyfluorescein into one cell in an area of cells with high density. (B) Schematic presentation of a spreading area, 5 min after the loading with 6-carboxyfluorescein. Scale bar: 50 µm (C) No changes in the dye spreading area between WT, H and KO could be detected. n (WT)=31, n (H)=16, n (KO)=21, p (WT, KO)=0.472, p (H, KO)=0.363.

9.8. Sertoli cell-specific expression of BT-IgSF is essential for male fertility

To further substantiate that BT-IgSF expression in Sertoli cells is needed for proper testis morphology and fertility, BT-IgSF was inactivated by crossing mice with a floxed BT-IgSF allele to AMH^{Cre} mice in order to specifically knockout the BT-IgSF gene in Sertoli cells only. AMH is only expressed in fetal Sertoli cells in males. In $BT\text{-}IgSF^{flx/flx}$; AMH^{cre+} males, the exact same phenotype as in the global knockout was observed.

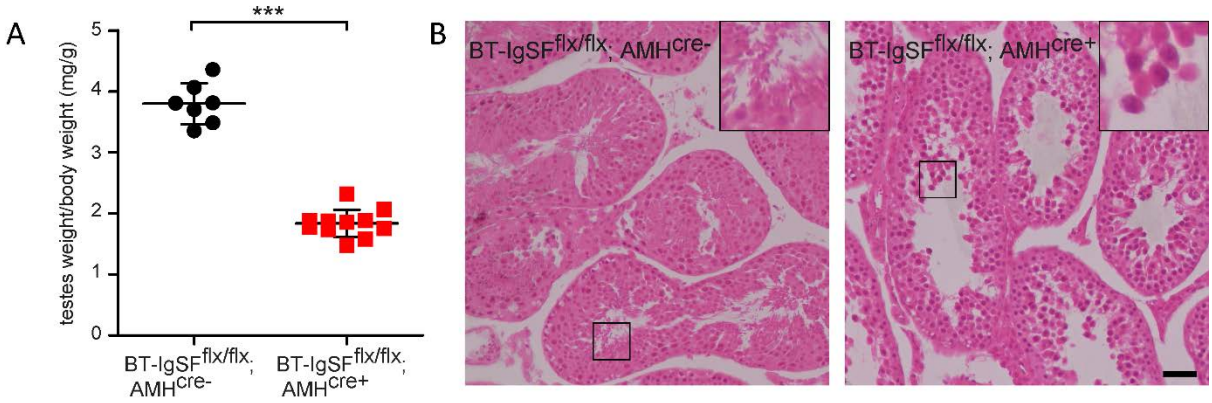

Figure 41: Sertoli cell-specific KO males have smaller and atrophic testes
(A) BT-IgSF$^{flx/flx}$; AMH^{cre+} testes show a significantly decreased wet weight compared to control animals; n=7 for control, n=11 for AMH^{Cre+}; data are shown as mean ± SD; ***= p<0.001 (t-test). (B) H&E stainings of methacrylate-sections show atrophic testes of AMH^{Cre+} mice compared to wildtype; scale bar: 50 µm.

The animals showed reduced testis weight (Figure 41 A) together with atrophic morphology in seminiferous tubules (Figure 41 B) and azoospermia (Figure 42 B). Knockout of BT-IgSF in Sertoli cells was proven by immunofluorescence stainings with antibodies to BT-IgSF (Figure 42 A, arrowhead). Interestingly, the stainings showed minimal residual BT-IgSF expression, but not in Sertoli cells, supporting the previous observations that also other cell types contain BT-IgSF protein. In summary, the results of the AMH-conditional knockout support the data on the global knockout that the expression of BT-IgSF in Sertoli cells is essential for male fertility.

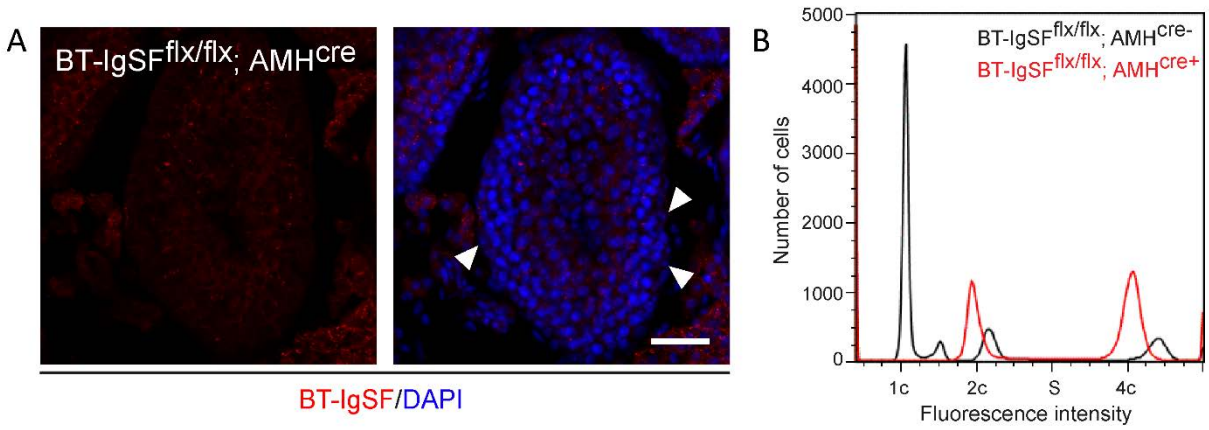

Figure 42: BT-IgSF is absent in Sertoli cells of the Sertoli cell-specific KO and testes have no spermatids and sperm
(A) Immunofluorescence staining against BT-IgSF in AMH-cKO showing the absence of BT-IgSF signal in Sertoli cells (arrowhead); scale bar: 50 µm. (B) Flow cytometric analysis of testis cells, stained with DAPI, shows the lack of haploid chromatin containing cells in AMH-conditional knockouts (red), compared to BT-IgSF$^{flx/flx}$ control (black); 1c: haploid, 23 chromatids; 2c: haploid, 23 chromosomes; S: S-phase; 4c: diploid, 46 chromosomes. FACS analysis was done in cooperation with Andreas Pelz, Charité Berlin.

9.9. Loss of BT-IgSF in adulthood affects spermatogenesis

To exclude overall developmental defects on the absence of BT-IgSF, a conditional knockout, in which BT-IgSF can be depleted at any chosen time point through the administration of tamoxifen (BT-IgSF$^{flx/flx}$; Rosa26creERT2), was developed. The Rosa26creERT2 mice express the cre recombinase ubiquitously in all cells but the cre recombinase is inactive and recombination can only occur in the presence of 4-hydroxytamoxifen, a synthetic estrogen receptor ligand. In the absence of the estrogen receptor agonist, cre is bound to the mutated form of the ligand-binding domain of the estrogen receptor and retained in the cytoplasm by HSP90. In the presence of 4-hydroxytamoxifen, creERT2 can translocate into the nucleus and recombine the floxed target gene (Feil et al., 2009).

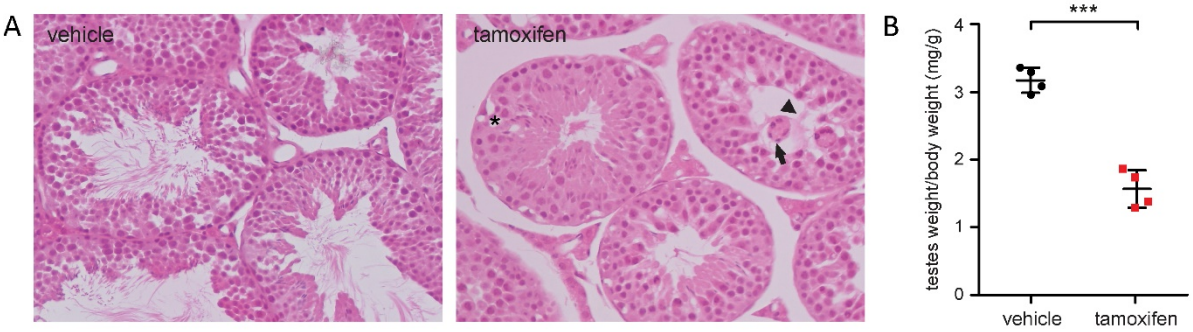

Figure 43: Loss of BT-IgSF in adulthood leads to smaller and atrophic testes
(A) H&E stainings of methacrylate-sections show atrophic testes of BT-IgSF$^{flx/flx}$; Rosa26CreERT2 mice treated with tamoxifen compared to vehicle control. (B) BT-IgSF$^{flx/flx}$; Rosa26CreERT2 testis treated with tamoxifen show a significantly decreased wet weight compared to vehicle treated animals; n=4 for vehicle, n=4 for tamoxifen; data are shown as mean ± SD; ***= p<0.001 (t-test).

Inactivation of BT-IgSF in sexually mature males (8-12 weeks old) by tamoxifen treatment, at 5 consecutive days, resulted in a reduction of testis weight to significantly lower levels compared to vehicle treated animals (Figure 43 B). In histological sections, vehicle treated animals had normal testis morphology (Figure 43 A, left panel), whereas tamoxifen treated animals showed testis with seminiferi

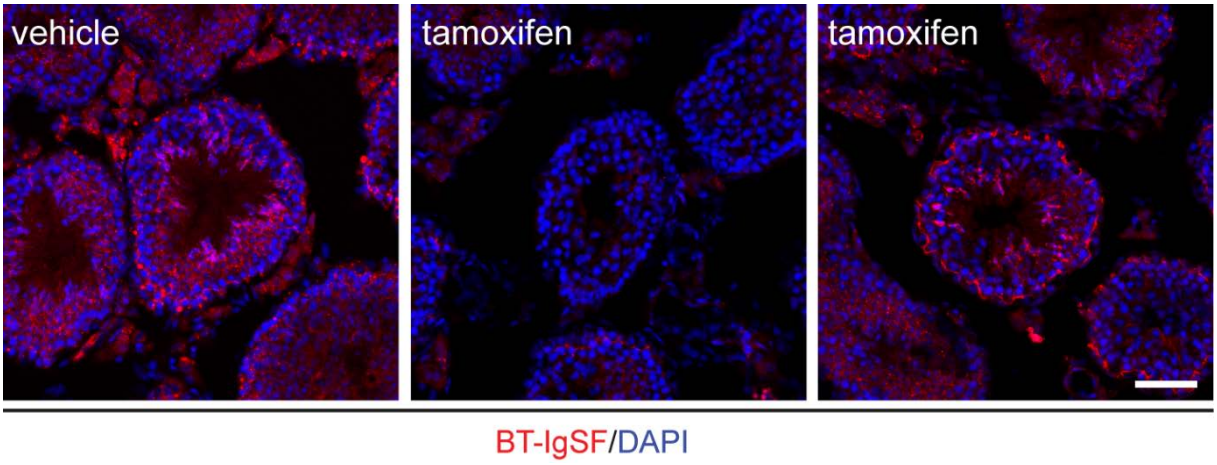

Figure 44: BT-IgSF deletion occurs not in all cells
Immunofluorescence staining of testes from vehicle and tamoxifen treated mice. Tubuli with and without BT-IgSF expression are present in tamoxifen treated mice, whereas all tubuli express BT-IgSF in the vehicle control. Scale bar: 50 µm.

tubuli resembling the morphology of BT-IgSF from non-conditional knockouts. They exhibited vacuolation, the lack of sperms and cytoplasmic extension of Sertoli cells (Figure 43 A, right panel). However, a proportion of normal seminiferi tubuli were still detectable and these tubuli still expressed BT-IgSF (Figure 44).

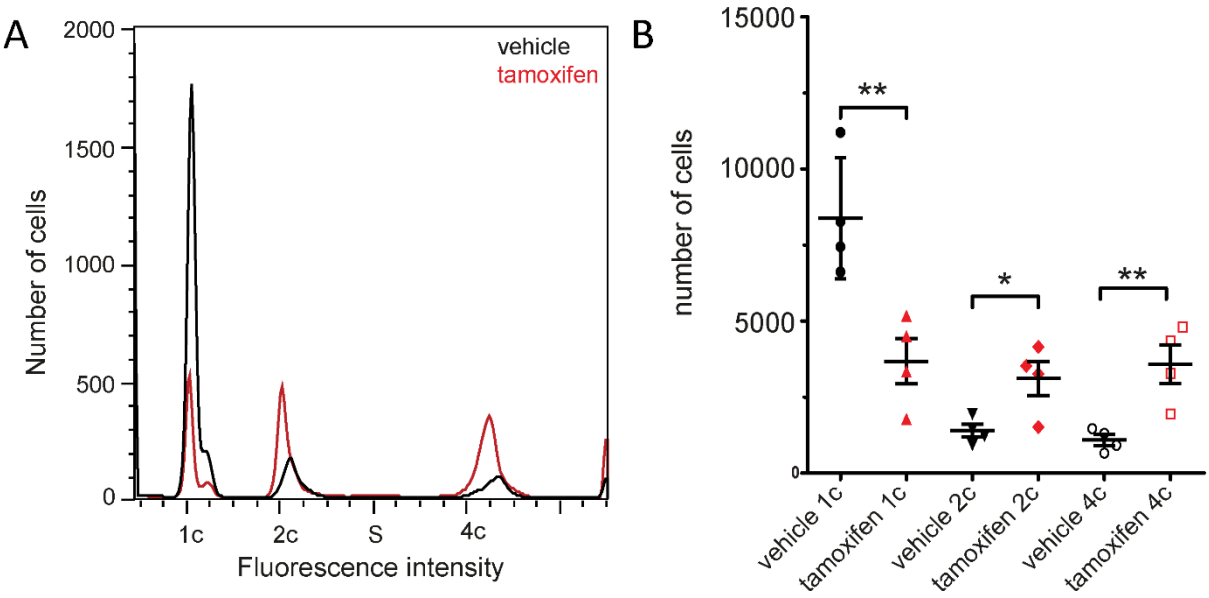

Figure 45: BT-IgSF deletion with tamoxifen leads to a reduction of spermatids and sperm
(A) Histogram and (B) quantification of a flow cytometric analysis of testis cells, stained with DAPI, showing the reduction of haploid chromatin containing cells by tamoxifen treatment of BT-IgSF$^{flx/flx}$;Rosa26CreERT2 (red) compared to vehicle control (black) and the increase in 2c and 4c cells; 1c: haploid, 23 chromatids; 2c: haploid, 23 chromosomes; S: S-phase; 4c: diploid, 46 chromosomes. FACS analysis was done in cooperation with Andreas Pelz, Charité Berlin.

In line with this, tamoxifen treated animals showed the same phenotype as the global and the Sertoli cell-specific KO, although not in the same extent. The composition of germ cells was changed in tamoxifen treated males. The testes of tamoxifen treated animals consisted of significantly less 1c cells than vehicle treated controls as determined by flow cytometry. A higher percentage of cells with 2c and 4c was measured, suggesting that more cells enter meiosis (Figure 45). This finding shows that spermatogenesis is arrested in some cells.

The fact that not all cells are affected required to test the efficiency of *Igsf11* knockout by tamoxifen. qRT-PCR analyses showed that the *Igsf11* expression on mRNA level was reduced by around 50%, which seems to be insufficient to maintain proper spermatogenesis (Figure 46, left panel). However, it was interesting to see, whether also other changes that were observed in the global knockout occur in this conditional knockout. Cx43 expression on mRNA level was upregulated and was again accompanied with altered localization throughout the tubule (Figure 47). The reduced number of spermatids and sperm with 1c DNA content was further confirmed by a reduced expression of Prm1

(Figure 45, right panel). The phenotype of this conditional knockout confirms the effect of BT-IgSF absence in the testes.

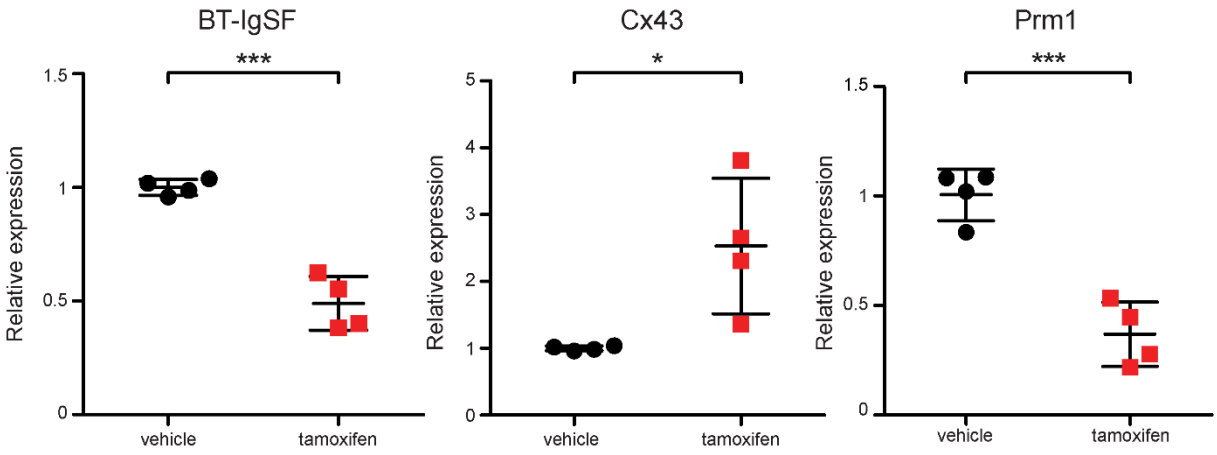

Figure 46: A reduction of BT-IgSF of around 50% leads to an increase of Cx43 and a reduction of sperm
Analysis of expression of Cx43 and Prm1 transcripts by qRT-PCR; BT-IgSF expression is reduced by around 50% in tamoxifen treated testes; Gja1 (Cx43) is upregulated in tamoxifen treated testes; Prm1, marker for spermatids and sperm, is significantly reduced; n=4 per group, data are shown as mean ± SD; *=p<0.05, ***=p<0.001 (t-test).

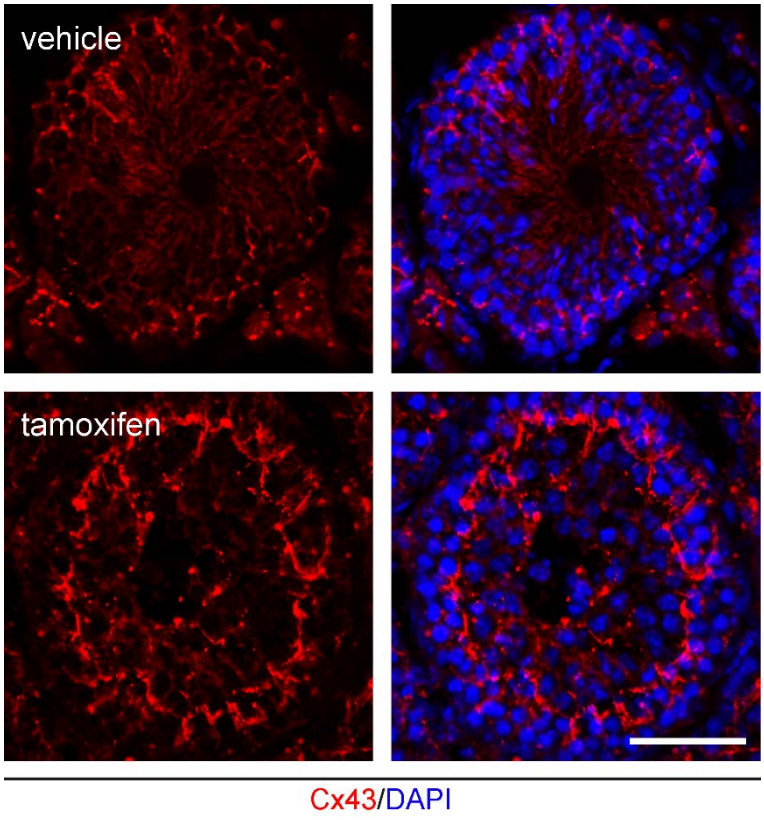

Figure 47: Cx43 is mislocalized in the testes when BT-IgSF is reduced
Immunofluorescence stainings of testes from vehicle and tamoxifen treated mice. Cx43 is normally located in vehicle treated mice. In tamoxifen treated animals, Cx43 is mislocalized. Scale bar: 50 µm.

In summary, BT-IgSF is not only necessary in the formation of the testis and the BTB, but it is also important in adult to maintain proper spermatogenesis and fertility in male mice.

10. DISCUSSION

BT-IgSF is known to be expressed in the brain and the testis of human and mice. Its function in testis was unknown until now. The aim of this study was to analyze the localization of BT-IgSF inside the testes and to characterize the function of BT-IgSF with the help of transgenic mouse models. BT-IgSF was shown to be expressed in Sertoli cells and in the aES and the acrosome of spermatids and sperm. During analyses of the BT-IgSF knockout mice, BT-IgSF was found to be essential for male fertility. BT-IgSF knockout males are infertile due to azoospermia with smaller and atrophic testes. The cause of this azoospermia is probably an impaired BTB along with mislocalization of BTB proteins. Furthermore, a Sertoli-cell specific knockout of BT-IgSF also exhibits this phenotype with smaller, atrophic testes and infertility with no spermatid and sperm production. It was additionally shown that BT-IgSF plays an essential role in the maintenance of the BTB and the spermatogenesis in adulthood as a conditional knockout of BT-IgSF in adult mice resulted in smaller testis with a disturbed spermatogenesis.

10.1. BT-IgSF, a member of the CAR subgroup

Spermatogenesis depends on intensive cross-talk between germ cells and Sertoli cells and intact cell-cell contacts. The disturbance of such cell junctions through the impairment of cell-cell adhesion can disrupt the BTB and lead to infertility.

One paradigmatic group of cell adhesion proteins expressed in the testis is the CAR subgroup of IgCAMs comprising CAR, CLMP and BT-IgSF (Sze et al., 2008; Wang et al., 2007; Pelz et al., 2017). Different studies described the localization of CAR in the testis. It was shown that CAR is expressed in all germ cell types, in Sertoli cells as well as in Leydig cells (Peters et al., 2001). Another study, using a different antibody, only detected CAR in more mature germ cells such as round spermatids, late elongating spermatids and in spermatozoa but not in early elongating spermatids (Mirza et al., 2006). The same group, one year later discovered that CAR is also expressed in Sertoli and germ cells in perinatal and postnatal stages, but not in Sertoli cells of adult testes (Mirza et al., 2007). However, there are also reports of CAR expression in Sertoli cells of adult testes at the site of the BTB and of co-localization with ZO-1 at the BTB (Wang et al., 2007). Furthermore, it was found that CAR is a regulatory protein of the BTB. In *in vitro* studies it was shown that CAR is essential for the integrity of the BTB and that a downregulation of CAR leads to a disruption of the tight junction barrier and an increased endocytosis of Occludin (Su et al., 2012).

CLMP is expressed in Sertoli TM4 cells and it co-localizes with ZO-1 in the testis at the BTB (Sze et al., 2008).

However, neither CAR nor CLMP have been found to be crucial for maintaining the integrity of the BTB

in vivo or being essential for male fertility (Sultana et al., 2014; Sze et al., 2008) although CAR interacts with JAM-C, which on the other hand is essential for male fertility (Gliki et al., 2004). Although BT-IgSF is a member of the CAR subgroup its expression pattern in the testis remained to be established. In this study, initially the localization of BT-IgSF inside the seminiferi tubuli was investigated, before functional questions were considered.

10.2. BT-IgSF expression in the testis

To date, no other study has analyzed BT-IgSF expression on protein level in the testes. To generate a solid basis for functional studies, knowledge of the timing and pattern of protein localization are of great importance. In this study, it was shown that BT-IgSF, another member of the CAR-subgroup, is also expressed at the BTB close to the Sertoli cell nucleus and co-localizes with ZO-1 and partially with Cx43 at the BTB. Furthermore, a co-localization of BT-IgSF with Espin, a marker for the ES, was observed. Similar expression patterns were also found for the close related proteins CLMP and CAR. CAR and CLMP co-localize with ZO-1 at the BTB and CAR additionally co-localizes with Espin at the aES.

Stainings with antibodies against BT-IgSF labeled Sertoli cells at the basal side of tubuli but also membranes of cells located at the adluminal side. Whether this labeling is restricted to the cytoplasmic arms of Sertoli cells, stretching into the lumen or whether BT-IgSF is also located at the membrane of germ cells, cannot be definitely decided based on these data. However, there is convincing evidence that the role of BT-IgSF in male fertility is largely dependent on its expression in Sertoli cells. BT-IgSF expression is strongest at the basal side at Sertoli cells. In the absence of BT-IgSF, defects in the BTB were observed which is constituted of cell junctions between Sertoli-Sertoli cells without the involvement of germ cells (Mruk and Cheng, 2015). The expression of BT-IgSF in Sertoli cells was further confirmed by a Sertoli-specific (AMH^{Cre}) knockout of BT-IgSF. AMH is only expressed in fetal Sertoli cells in males, enabling a Sertoli cell specific knockout of BT-IgSF (Lécureuil et al., 2002). In stainings against BT-IgSF in this Sertoli cell-specific knockout testes, no labeling of BT-IgSF was observed in Sertoli cells and only a very weak in the testes at all, showing the strong participation of Sertoli cells in BT-IgSF expression. Furthermore, the Sertoli cell-specific knockout of BT-IgSF shows the exact same phenotype as in the global knockout, leading to the conclusion that BT-IgSF is important for proper Sertoli cell function. Whether BT-IgSF is also present on germ cells might be determined by microscopy with higher resolution such as immunolabeled electron microscopy, for which however, appropriate antibodies are currently not available.

10.3. Staging of seminiferous tubules and BT-IgSF expression

During the analysis of BT-IgSF expression, it was observed that BT-IgSF is not uniformly expressed in testis cross-sections. There are several testis proteins known which follow a stage-dependent or stage-specific expression pattern. BT-IgSF however, is expressed in Sertoli cells in all stages from I-XII. Additionally, BT-IgSF can also be detected from stage I-VII at spermatids at the acrosome and the apical ES, respectively. This indicates an essential presence of BT-IgSF in Sertoli cells at all times and suggests that the major function takes place in the Sertoli cells. Interestingly, BT-IgSF is only expressed at the aES until stage VII. From stage VII and VIII on, spermiation occurs and elongated spermatids are released into the lumen to travel to the epididymis. The aES is the only anchor which attaches the elongated spermatids to the Sertoli cells and by this to the epithelium. BT-IgSF, as a cell adhesion protein in the aES, could be a component of this attachment structure and is probably necessary for retaining of elongated spermatids. When the spermiation starts, an attachment to the epithelium is no longer necessary and therefore also BT-IgSF expression is lost at the aES. Since the staging in this study was done in a rough way with cryosections without PAS staining, not every single stage could be unambiguously defined. Therefore, some stages were grouped together. However, the staging method was sufficient to determine the BT-IgSF expression during the cycle of the seminiferous epithelium and to get a deeper insight to the possible function of BT-IgSF. BT-IgSF was found to be expressed in all stages of the seminiferous epithelium and is therefore probably not involved in specific processes of germ cell differentiation.

10.4. Validation of the BT-IgSF knockout mouse

Beside the expression pattern, functional insights might be obtained by deletion of the gene in a knockout mouse. Therefore, a non-conditional knockout mouse of BT-IgSF was investigated. The correct integration of the trapping cassette in the intron between exon 2 and 3 was confirmed by Southern Blot and long range PCR. However, *Igsf11* mRNA of exon 6 and 7 was still detectable in qPCR analyses, which could be due to the presence of the wildtype full-length mRNA or due to the presence of a truncated form. Other start-codons with an alternative open reading frame could lead to a truncated transcript with exon 6 and 7. Behind the induced cassette, in exon 3, an additional start-codon, which is in-frame with the original sequence, exists and could lead to the production of a truncated mRNA of *Igsf11*. Truncated mRNAs are probable non-functional and therefore likely to be degraded. However, the existence of a full-length mRNA could lead to a hypomorphic phenotype. The knockout is supposed to happen on the transcript level due to the insertion of a splice acceptor which captures the transcript. In the knockout mice, a reduction of at least 93% of the full-length *Igsf11* mRNA occurred compared to the WT. To analyze whether the mouse is a knockout at the protein level,

Western blots and immunofluorescence stainings with wildtype and knockout tissue were performed. In these analyses, BT-IgSF could not be detected in BT-IgSF knockout animals, confirming a global knockout of BT-IgSF protein. The En2 splice acceptor used for the generation of this mouse is probably not completely efficient. Similar effects were reported for a Pannexin1 knockout mouse also generated by KOMP with the same strategy (Hanstein et al., 2013). In this study it was shown that Pannexin1 mRNA was only reduced by around 70% in the knockout animals in various tissues. In their study, Pannexin1 protein could not be detected in immunohistochemistry of the knockout animals. The authors concluded that their KO is a functional KO due to the absence of protein expression and the similarities to other Pannexin1 KO mouse models. The same conclusions can be drawn for the BT-IgSF KO mice in this study, which are assumed to be functional KOs. Although some residual mRNA is transcribed, no BT-IgSF protein can be detected with antibodies against the extracellular part in immunofluorescence stainings and Western blots. If protein is generated this amount is below the detection limit and might not have any influence as BT-IgSF KO animals have a striking phenotype of infertility.

10.5. BT-IgSF KO males are infertile

In breedings of BT-IgSF knockout animals, it was observed that male KOs did not produce offspring but resulted in vaginal plugs. This result suggests that no behavioral mating problems exist, but rather that there are problems with fertility. Female KO mice show normal fertility and can generate offspring. This finding indicates that BT-IgSF seems to be crucial for male fertility. Further analyses revealed that the loss of BT-IgSF in male mice leads to atrophic testes, an arrest of spermatogenesis and results in infertility. The testis size of BT-IgSF knockout mice is drastically reduced compared to control mice, accompanied by a lack of sperms and spermatids, vacuolation and mis-organized cytoplasmic arms of Sertoli cells. Identical results were obtained with a Sertoli cell-specific knockout of BT-IgSF (AMH^{Cre}). These males also exhibit smaller testis with no haploid spermatids and are infertile, confirming that the expression of BT-IgSF in Sertoli cells is essential for male fertility in mice. A similar phenotype was also observed in other mutants like the TAp73 knockout mouse (Holembowski et al., 2014). TAp73 is a transcription factors and acts as an adhesive homeostatic factor to ensure fertility by enabling sperm maturation. Tap73 knockout mice have nearly empty seminiferi tubuli due to defective cell-cell adhesions of germ cells to their nursing Sertoli cells. The loss of adhesion also leads to a defect BTB in these animals.

10.6. Spermatogenic arrest in BT-IgSF KO males occurs after meiosis I

Infertility due to azoospermia could have several reasons, one of which being meiotic arrest, which was subsequently analyzed in this study. Analyses of meiosis I specific genes and immunofluorescence

stainings against SYCP3 and γH2AX did not show major changes of meiosis I in the absence of BT-IgSF. SYCP3 is a marker for the axial element of the synaptonemal complex (Brower et al., 2009; Lammers et al., 1994). This complex is important for synapsis, recombination and segregation in meiosis I and SYCP3 is expressed from zygotene to pachytene stage. Mis-expression and mis-localization could indicate a failure in one of these processes. γH2AX is a marker for double-strand breaks and is involved in their repair. In meiosis I, where double-strand breaks associated with recombination occur, γH2AX is expressed from leptotene on and later marks the silenced sex body in the pachytene stage during meiotic sex chromosome inactivation (Blanco-Rodríguez, 2009; Handel, 2004). The presence of both markers in a correct pattern in knockout testes demonstrates that meiosis I occurs normally.

qPCR analysis of meiosis-related genes in BT-IgSF KO males demonstrated a normal meiosis I from leptotene to diplotene. Consistently, secondary spermatocytes with the chromosomal status of 2c and 1n were present whereas no 1c containing cells, sperm and spermatids, were detected. Furthermore, it was observed that all meiotic cells are positive for γH2AX, indicating that no cell enters meiosis II. Therefore, spermatogenesis arrest must occur after meiosis I. However, the investigation of meiosis II is complicated due to its strong similarity to mitosis. Further studies might clarify whether meiosis II is initiated at all.

10.7. Hormonal balance is not affected by the loss of BT-IgSF

Sperm production is hormonally driven and Sertoli cells are important to maintain a hormonal balance in the testis. Defects in Sertoli cells can lead to hormonal imbalance and infertility. Given that the lack of BT-IgSF affects Sertoli cells and that BT-IgSF is expressed in the brain and could interfere with the hypothalamic-pituitary-gonadal axis, suggested measuring the impact of BT-IgSF loss on hormonal balance.

The hypothalamus secrets GnRH which acts on the pituitary gland to produce FSH and LH. Both hormones act on Sertoli cells. FSH acts directly on Sertoli cells and triggers the production of inhibin B and initiates spermatogenesis. LH acts indirectly on Sertoli cells through the production of testosterone by Leydig cells. Testosterone has its target in the androgen receptor expressed mainly by Sertoli cells. Male mice with a Sertoli cell-specific knockout of the androgen receptor are infertile with an arrest in meiosis (Chang et al., 2004; Yeh et al., 2002). Therefore, Sertoli cells have a central role in this hormonal balance.

No changes between WT and BT-IgSF knockout males could be detected in the hormone levels of LH, FSH and testosterone. Differences in the LH levels between knockout individuals are probably due to episodical, discontinuous pulses of LH, which have been previously described (Coquelin and Desjardins, 1982). The unchanged hormone levels demonstrate that BT-IgSF expression in the brain has no impact

on the hypothalamic-pituitary-gonadal axis and hormonal control and that imbalance of hormone levels is not the cause for male infertility in mice lacking BT-IgSF.

10.8. BT-IgSF loss leads to a disruption of the BTB

Another common reason for azoospermia and infertility is a disturbed BTB. The BTB is a very sensitive structure which is damaged by several environmental toxins such as bisphenol A or by pharmaceuticals like cisplatin. Small alterations of BTB components could affect BTB integrity which is why BTB functionality was examined. The data presented in this work show that the spermatogenic arrest, which occurs in BT-IgSF KO males, is probably due to an impaired BTB accompanied with changes in the localization of BTB proteins. In the in vivo biotin assay, the biotin tracer was detected inside the seminiferi tubuli, indicative for a defect in the BTB. Transcripts of the major tight junction and gap junction proteins of the BTB such as ZO-1, Occludin and Cx43 were upregulated in BT-IgSF knockout testes and, additionally, a mislocalization of Cx43 and ZO-1 was observed in Sertoli cells. However, Sertoli cell-Sertoli cell junctions were unaffected as seen by electron microscopy.

Normally, Cx43 is predominantly expressed in Sertoli cells at the BTB. In contrast to wildtype, BT-IgSF knockout animals exhibit a disturbed Cx43 expression pattern. Cx43 is not only expressed at the basal BTB barrier but is irregularly distributed and also found in adluminal compartments. Similar findings were also detected in *Fads2*- (Fatty acid desaturase 2) knockout mice (Stoffel et al., 2008). The loss of FADS2 leads to smaller testes, mislocalization of several BTB proteins such as Cx43, Occludin and ZO-1 and to a disrupted BTB, similar to the observations in the BT-IgSF mutant mice, presented here. Cx43 is the predominant connexin in the testis and its importance for male fertility was shown by several studies. The global knockout of Cx43 leads to death soon after birth due to heart defects. However, already at early developmental stages Cx43 has an impact on fertility. From E11.5 on, the testes of Cx43 knockouts are smaller compared to wildtype testes which is caused by a germ cell deficiency (Juneja et al., 1999; Gerber et al., 2014). To study the function of Cx43 in adult males, a Sertoli cell-specific Cx43 knockout was analyzed by Brehm et al., 2007. Sertoli cells exhibited vacuolation and an arrest of spermatogenesis at spermatogonia, leading to male infertility. In electron microscopic images, no changes were detected in the BTB but these knockout animals revealed an overexpression of BTB proteins and their localization in the tubuli was more diffuse (Carette et al., 2010) - findings that are similar to the phenotype described here for BT-IgSF.

A number of studies have shown that knockout of BTB proteins including Claudin11, ZO-2 and Occludin lead to infertility (Mazaud-Guittot et al., 2010; Gow et al., 1999; Saitou et al., 2000; Xu et al., 2009). The phenotypes are very similar to those observed in BT-IgSF knockout males. Claudin11 knockout males have smaller testes, no spermatids, Sertoli cell aggregates and show apoptosis of germ cells

(Mazaud-Guittot et al., 2010). The BT-IgSF knockout also showed smaller testes, no spermatids and multinucleated cell aggregates in the lumen. However, no significant increase in apoptosis could be detected for BT-IgSF-deficient males. ZO-2 knockout males have an impaired BTB and Occludin knockouts revealed atrophic testes in old males. The defects in the BTB of Occludin knockout males are comparable to the impaired BTB of BT-IgSF deficient animals. Taken together the cell adhesion molecule BT-IgSF is expressed at the BTB and is important for its integrity.

Whether the increase in expression of the BTB proteins Cx43, ZO-1, Occludin and Claudin11 is due to a direct effect of BT-IgSF loss or a compensation mechanism to make up for the lack of one cell adhesion molecule, remains to be determined. It will also interesting to elucidate whether the loss of BT-IgSF directly leads to an impaired BTB or whether altered gap junction activity is the major reason for an impaired BTB. Cx43 phosphorylation is important to regulate gap junction function and the localization of Cx43 molecules (de Feijter et al., 1996). A tendency towards an increased Cx43 phosphorylation was observed, which might change gap junction position and activity.

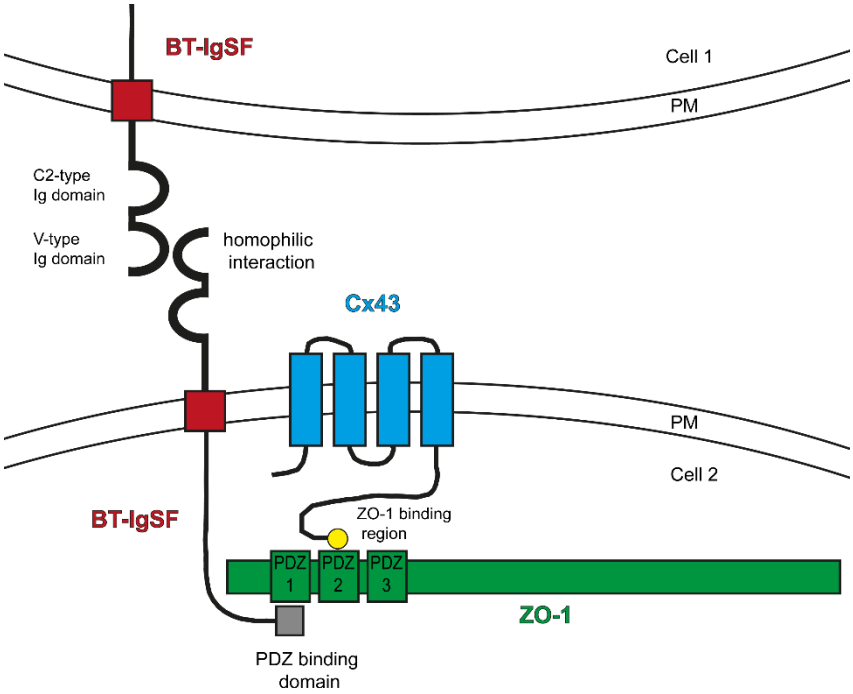

Figure 48: Hypothetical model of the indirect interaction of BT-IgSF with Cx43 through ZO-1
BT-IgSF establishes cell-cell contacts through homophilic interaction with the extracellular domain between cell 1 and 2. It is possible that BT-IgSF interacts via its first Ig-domains or the first Ig domain can also bind to the second Ig domain (not shown). The intracellular tail with its PDZ binding motif on the C-terminus (grey box) enables a binding to ZO-1 with one of its PDZ domains. Here the theoretical binding to the first PDZ domain is illustrated. This binding has still to be proven with yeast-two-hybrid or immunoprecipitation assays. ZO-1 is known to interact with the second PDZ domain with Cx43 on its C-terminus (yellow dot). This model shows that the absence of BT-IgSF could have an impact on Cx43 localization. The red box shows the transmembrane domain of BT-IgSF, blue boxes show transmembrane spanning parts of Cx43. PM: plasma membrane.

Interestingly, it is known that ZO-1 interacts with connexins such as Cx43 and Cx45 through the PDZ domains of ZO-1 (Giepmans and Moolenaar; Laing et al., 2005; Kausalya et al., 2001; Duffy et al., 2002). An interaction between ZO-1 and BT-IgSF is conceivable, since a strong co-localization was detected

(Figure 22). Addtionally, a co-localization of BT-IgSF and Cx43 was observed, enabling a close proximity and a possible indirect interaction through ZO-1. Furthermore, an interaction of ZO-1 with the cytoplasmic segments of the closely related cell adhesion proteins CLMP and CAR have been published (Raschperger et al., 2004; Cohen et al., 2001; Sze et al., 2008). Therefore, it seems reasonable to hypothesize that BT-IgSF establishes cell-cell contacts through homophilic interaction on the extracellular domain, via the first Ig domains or via the first Ig domain and the second Ig domain (Patzke et al., 2010), and that the intracellular PDZ-binding domain of BT-IgSF interacts with one PDZ domain of ZO-1, which in turn interacts through its second PDZ domain with Cx43 (Figure 48). Binding of BT-IgSF to ZO-1 could be further analyzed by a yeast-two-hybrid screen, immunoprecipitation assays and FLIM-FRET.

The described complex between BT-IgSF, ZO-1 and Cx43 might be formed in Sertoli cells and could explain why the absence of BT-IgSF has an impact on the Cx43 localization.

10.9. Gap junction function of BT-IgSF deficient Sertoli cells is not affected *in vitro*

In electron microscopy, the presence of a structurally normal BTB was shown. However, it is not clear whether this structurally normal barrier is functional. One of the BTB functions is cell communication via gap junctions. It was shown that Cx43 expression and localization is altered. Cx43 is the most important gap junction protein in the testis and therefore an alteration of gap junction function is feasible. Sertoli cells cultured at high density can almost mimic a BTB *in vitro* structurally and functionally. They form functional tight junction barriers and other structures such as gap junctions, ES and desmosomes , which can be observed in electron microscopy (Byers et al., 1993; Janecki et al., 1991).

Most studies use rat testes and younger aged animals to generate primary Sertoli cells. The isolation of adult Sertoli cells is time consuming, the yield is low due to contaminations with spermatids and the procedure is very expensive (Mruk and Cheng, 2011). Due to challenges in culturing adult Sertoli cells, Sertoli cells from P7 old mice were prepared in this study. At this time point Sertoli cells are still dividing mitotically before they stop proliferating at P10-12 (Kluin et al., 1984). Moreover, at P7 the spermatogenesis has not yet started in mice, which happens between P8 to P10 (Nebel et al., 1961). This fact is an advantage for the yield of the Sertoli cell culture because only spermatogonia can contaminate the cell culture. On the other hand, the BTB, which is only formed at around P17 in mice, is not yet present (Hosoi et al., 2002). Thus, the immature Sertoli cells do not have the same physiological properties as adult Sertoli cells. For the study of the function of BT-IgSF, a more mature culture would be of interest because expression is strongest in adult testes. Another disadvantage of

the *in vitro* monolayer culture is that Sertoli cells lose their polarity and their complex structure with multiple cytoplasmic arms and become rather large and flat cells. Nevertheless, the identity of Sertoli cells was confirmed by Vimentin staining and the presence of lipid droplets.

To see whether the conditions in the cultured Sertoli cells could mimic the in vivo situation, the expression of BT-IgSF and Cx43 expression was tested. BT-IgSF expression could be observed at the membrane of WT Sertoli cells and a partial co-localization with Cx43 could be seen. Tight junctions also seemed to be developed and were readily identified by a staining against ZO-1. However, the presence of ZO-1 is not a proof for functionality of these tight junctions, which would for example require electron microscopy.

Assessment of gap junction function was done with the cultured mature Sertoli cells. No differences in cell-cell communication via gap junction between WT and KO Sertoli cells were seen. This is in contrast to the *in vivo* findings, where more and mislocalized Cx43 was detected. Together with the disrupted BTB it was conceivable that these changes have an impact on gap junction function. There are reports of differences between the BTB *in vivo* and *in vitro*. The transepithelial electrical resistance of the *in vitro* BTB is lower than the expected value *in vivo*, suggesting a leakier barrier (Mruk and Cheng, 2015). Furthermore, in the cell culture no germ cells and peritubular myoid cells are present, which also contribute to the BTB (Su et al., 2013; Dym and Fawcett, 1970). Another aspect is, that biological substances which could modulate the BTB are missing *in vitro*. The used Sertoli cells in this study are immature and were generated before the BTB was formed. These differences between *in vivo* and *in vitro* could contribute to an explanation why no differences between WT and KO gap junction function was detected.

10.10. BT-IgSF expression is important for fully developed testes

The results discussed so far were generated from non-conditional knockout mice, in which the lack of BT-IgSF is already present at the beginning of testis development. However, spermatogenesis is a constant process and the development of a single sperm takes about 5 weeks in mice. Therefore, it was asked whether BT-IgSF is also important for the maintenance of the BTB and of spermatogenesis. The conditional knockout mice develop normally until they reach adulthood and only in the mature organism, BT-IgSF is removed to analyze the function of BT-IgSF in the sexually mature mice. The tamoxifen inducible BT-IgSF knockout mice revealed that loss of BT-IgSF in mature male mice with fully developed testes caused the occurrence of the same phenotype as in the global and Sertoli cell-specific KOs, even though not all tubuli were affected. The loss of 50% of BT-IgSF mRNA lead to an increase of Cx43 expression and a decrease of haploid spermatids, indicating the importance of BT-IgSF for proper spermatogenesis and BTB integrity in adulthood.

Tamoxifen was given i.p. in a dose of 1.5 mg/day. Originally, a dose of 3 mg/day was intended, however, this caused several deaths one week after the last tamoxifen administration. Therefore, the lower dose was chosen to prevent lethal effects. However, the reduced tamoxifen amount could potentially not be enough to bind to the estrogen receptor in every cell. This could be an explanation for the observed “mosaic” phenotype with normal tubuli co-existing with atrophic azoospermic tubuli. For future experiments, a dose of 2 or 2.5 mg/day could be tested to reach more cells without lethality.

This experiment shows that BT-IgSF is not only necessary for the formation of the testes and the initial BTB but also for maintenance of the functionality.

10.11. Impact of this study on human infertility in men

Male infertility is an important issue in the whole world and is not only a problem of highly industrialized societies but also in developing countries (ORC Macro and the World Health Organization, 2004). In 30-40% of all men with abnormal semen parameters such as lower sperm count or decreased sperm motility, no reason can be found (Jiang et al., 2014). 1% of the male world population suffers from azoospermia (Gudeloglu and Parekattil, 2013). 49-93% of all azoospermia cases are caused by testicular defects (non-obstructive azoospermia) (Jarvi et al., 2010). This defect is related to multifactorial reasons like environmental pollution, genetic and epigenetic factors and disorders in the hormonal system. One probable reason for non-obstructive azoospermia is an impaired blood-testis barrier.

In this study a new blood-testis barrier protein, BT-IgSF, was identified and its absence leads to infertility due to non-obstructive azoospermia.

Since, in the absence of BT-IgSF, the ultrastructure of the BTB appears normal in electron microscopic images, it is reasonable that BT-IgSF might be essential for a functional BTB and appears to interfere with barrier dynamics including the localization of Cx43 and the expression of junctional proteins. It is of note that changes in Cx43 expression also lead to infertility in humans. In patients with secretory azoospermia, Cx43 expression was shown to be reduced (Defamie et al., 2003).

It would be of interest to analyze whether BT-IgSF expression is changed in patients with azoospermia, especially in patients with a spermatogenic arrest at the level of secondary spermatocytes. Further investigations on the mechanistic regulation of BT-IgSF might help to better understand unknown causes of human male infertility.

11. FUTURE PERSPECTIVES

The presented data of this study still leave some open questions.

To analyze the expression site of BT-IgSF in more detail, microscopic methods with higher resolution such as immunolabeled electron microscopy are essential. This investigation might help to determine whether BT-IgSF is expressed on the aES and the acrosome of the spermatids and sperm.

The Sertoli cell-specific knockout of BT-IgSF showed that the expression of BT-IgSF in Sertoli cells is crucial to maintain fertility. Whether BT-IgSF expression on germ cells on the acrosome is of similar importance has to be determined. Therefore, a germ cell specific knockout e.g. with a Stra8-cre mouse line might answer this question.

In order to get more insights into the molecular mechanism of BT-IgSF function, the possible interaction of BT-IgSF with ZO-1 and Cx43 should be investigated. One might hypothesize that the C-terminal segment of BT-IgSF binds to one of the PDZ domains of ZO-1 which in turn interacts with Connexin43. Previous studies have shown that several Connexins including Connexin43 and 45 bind to ZO-1 (Giepmans and Moolenaar; Laing et al., 2005; Kausalya et al., 2001; Duffy et al., 2002). Immunoprecipitations and yeast two-hybrid screens could elucidate binding partners of BT-IgSF. One hypothesis is that the loss of BT-IgSF leads to a mislocalization of Cx43 and a disorganized localization of ZO-1 because of the lack of interaction with BT-IgSF, which might help to establish the correct intracellular localization. This could be confirmed by a transgene mouse containing BT-IgSF without the PDZ binding motif, which is necessary to bind e.g. to ZO-1. This mouse might show the same phenotype as the total BT-IgSF knockout mouse.

Sertoli cell cultures could be improved to better mimic the *in vivo* situation. Therefore, matrigel or bicameral chambers would maintain the polarity properties of Sertoli cells and enable the measurement of the transepithelial electrical resistance, which gives information about the BTB functionality. Also the preparation of mature Sertoli cells could improve the similarities to the *in vivo* situation.

To confirm that the infertity of BT-IgSF KO males is only caused by the absence of BT-IgSF in the testes, a rescue with wildtype BT-IgSF could be done in KO mice. A virus, carrying a vector with the BT-IgSF gene, directly injected into the testis could restore BT-IgSF expression and it would be interesting, to see whether spermatogenesis and fertility could be reverted in these mice. For a more specific approach BT-IgSF could be driven by a Sertoli cell-specific promoter. Another approach would be to generate a transgenic mouse with a Tet-On expression system. In this case BT-IgSF transcription would be inactive until tetracycline or doxycyclien is present. With this system it would be possible to

generate mice without BT-IgSF until they reach adulthood and then to active BT-IgSF expression through the administration of tetracycline/doxycycline.

The results of these future experiments might be used to enrich knowledge of ongoing processes during spermatogenesis and to analyze the BT-IgSF expression in patients suffering from azoospermia.

12. REFERENCES

Ahi, E.P., and K.M. Sefc. 2017. A gene expression study of dorso-ventrally restricted pigment pattern in adult fins of Neolamprologus meeli, an African cichlid species. *PeerJ*. 5:e2843. doi:10.7717/peerj.2843.

Ailan, H., X. Xiangwen, R. Daolong, G. Lu, D. Xiaofeng, Q. Xi, H. Xingwang, L. Rushi, Z. Jian, and X. Shuanglin. 2009. Identification of target genes of transcription factor activator protein 2 gamma in breast cancer cells. *BMC Cancer*. 9:279. doi:10.1186/1471-2407-9-279.

Altschul, S.F., T.L. Madden, A.A. Schäffer, J. Zhang, Z. Zhang, W. Miller, and D.J. Lipman. 1997. Gapped BLAST and PSI-BLAST: a new generation of protein database search programs. *Nucleic Acids Res.* 25:3389–3402.

Asher, D.R., A.M. Cerny, S.R. Weiler, J.W. Horner, M.L. Keeler, M.A. Neptune, S.N. Jones, R.T. Bronson, R.A. DePinho, and R.W. Finberg. 2005. Coxsackievirus and adenovirus receptor is essential for cardiomyocyte development. *genesis*. 42:77–85. doi:10.1002/gene.20127.

Blanco-Rodríguez, J. 2009. γH2AX marks the main events of the spermatogenic process. *Microsc. Res. Tech.* 72:823–832. doi:10.1002/jemt.20730.

Borg, C.L., K.M. Wolski, G.M. Gibbs, and M.K. O'Bryan. 2010. Phenotyping male infertility in the mouse: how to get the most out of a "non-performer". *Hum. Reprod. Update*. 16:205–24. doi:10.1093/humupd/dmp032.

Boussouar, F., and M. Benahmed. 2004. Lactate and energy metabolism in male germ cells. *Trends Endocrinol. Metab.* 15:345–350. doi:10.1016/j.tem.2004.07.003.

Brehm, R., M. Zeiler, C. Rüttinger, K. Herde, M. Kibschull, E. Winterhager, K. Willecke, F. Guillou, C. Lécureuil, K. Steger, L. Konrad, K. Biermann, K. Failing, and M. Bergmann. 2007. A Sertoli Cell-Specific Knockout of Connexin43 Prevents Initiation of Spermatogenesis. *Am. J. Pathol.* 171:19–31. doi:10.2353/ajpath.2007.061171.

Brennand, K.J., A. Simone, J. Jou, C. Gelboin-Burkhart, N. Tran, S. Sangar, Y. Li, Y. Mu, G. Chen, D. Yu, S. McCarthy, J. Sebat, and F.H. Gage. 2011. Modelling schizophrenia using human induced pluripotent stem cells. *Nature*. 473:221–225. doi:10.1038/nature09915.

Brower, J. V, C.H. Lim, M. Jorgensen, S.P. Oh, and N. Terada. 2009. Adenine nucleotide translocase 4 deficiency leads to early meiotic arrest of murine male germ cells. *Reproduction*. 138:463–470. doi:10.1530/REP-09-0201.

Brzica, H., D. Breljak, I. Vrhovac, and I. Sabolić. 2011. Role of Microwave Heating in Antigen Retrieval in Cryosections of Formalin-Fixed Tissues. *IN-TECH Open, Rijeka, Croat.* 41–62. doi:10.5772/825.

Burgoyne, P.S., S.K. Mahadevaiah, and J.M.A. Turner. 2009. The consequences of asynapsis for mammalian meiosis. *Nat. Rev. Genet.* 10:207–216. doi:10.1038/nrg2505.

Byers, S., R. Pelletier, and C. Suarez-Quain. 1993. Sertoli cell junctions and the seminiferous epithelium barrier. *In* The Sertoli Cell. L.. Russell and M. Griswold, editors. Cache River Press, Clearwater. 431–446.

Byers, S.W., M.A. Hadley, D. Djakiew, and M. Dym. 1986. Growth and characterization of polarized monolayers of epididymal epithelial cells and Sertoli cells in dual environment culture chambers. *J. Androl.* 7:59–68.

Carette, D., K. Weider, J. Gilleron, S. Giese, J. Dompierre, M. Bergmann, R. Brehm, J.-P. Denizot, D. Segretain, and G. Pointis. 2010. Major involvement of connexin 43 in seminiferous epithelial

junction dynamics and male fertility. *Dev. Biol.* 346:54–67. doi:10.1016/j.ydbio.2010.07.014.

Chang, C., Y.-T. Chen, S.-D. Yeh, Q. Xu, R.-S. Wang, F. Guillou, H. Lardy, and S. Yeh. 2004. Infertility with defective spermatogenesis and hypotestosteronemia in male mice lacking the androgen receptor in Sertoli cells. *Proc. Natl. Acad. Sci.* 101:6876–6881. doi:10.1073/pnas.0307306101.

Chen, S.-R., and Y.-X. Liu. 2015. Regulation of spermatogonial stem cell self-renewal and spermatocyte meiosis by Sertoli cell signaling. *Reproduction*. 149:R159-67. doi:10.1530/REP-14-0481.

Cheng, C.Y., and D.D. Mruk. 2012. The Blood-Testis Barrier and Its Implications for Male Contraception. *Pharmacol. Rev.* 64:16–64. doi:10.1124/pr.110.002790.

Cheng, C.Y., E.W. Wong, P.P. Lie, M.W. Li, D.D. Mruk, H.H. Yan, K.-W. Mok, J. Mannu, P.P. Mathur, W.-Y. Lui, W.M. Lee, M. Bonanomi, and B. Silvestrini. 2011. Regulation of blood-testis barrier dynamics by desmosome, gap junction, hemidesmosome and polarity proteins: An unexpected turn of events. *Spermatogenesis*. 1:105–115. doi:10.4161/spmg.1.2.15745.

Cohen, C.J., J.T.C. Shieh, R.J. Pickles, T. Okegawa, J.-T. Hsieh, and J.M. Bergelson. 2001. The coxsackievirus and adenovirus receptor is a transmembrane component of the tight junction. *Proc. Natl. Acad. Sci.* 98:15191–15196. doi:10.1073/pnas.261452898.

Cooke, H.J., and P.T.K. Saunders. 2002. Mouse models of male infertility. *Nat. Rev. Genet.* 3:790–801.

Coquelin, A., and C. Desjardins. 1982. Luteinizing hormone and testosterone secretion in young and old male mice. *Am. J. Physiol.* 243:E257-63.

Coyne, C.B., T. Voelker, S.L. Pichla, and J.M. Bergelson. 2004. The Coxsackievirus and Adenovirus Receptor Interacts with the Multi-PDZ Domain Protein-1 (MUPP-1) within the Tight Junction. *J. Biol. Chem.* 279:48079–48084. doi:10.1074/jbc.M409061200.

Defamie, N., I. Berthaut, B. Mograbi, D. Chevallier, J.-P. Dadoune, P. Fénichel, D. Segretain, and G. Pointis. 2003. Impaired Gap Junction Connexin43 in Sertoli Cells of Patients with Secretory Azoospermia: A Marker of Undifferentiated Sertoli Cells. *Lab. Investig.* 83:449–456. doi:10.1097/01.LAB.0000059928.82702.6D.

Dorner, A.A., F. Wegmann, S. Butz, K. Wolburg-Buchholz, H. Wolburg, A. Mack, I. Nasdala, B. August, J. Westermann, F.G. Rathjen, and D. Vestweber. 2005. Coxsackievirus-adenovirus receptor (CAR) is essential for early embryonic cardiac development. *J. Cell Sci.* 118:3509–3521.

Duffy, H.S., M. Delmar, and D.C. Spray. 2002. Formation of the gap junction nexus: binding partners for connexins. *J. Physiol.* 96:243–249. doi:10.1016/S0928-4257(02)00012-8.

Dym, M., and D.W. Fawcett. 1970. The Blood-Testis Barrier in the Rat and the Physiological Compartmentation of the Seminiferous Epithelium1. *Biol. Reprod.* 3:308–326. doi:10.1093/biolreprod/3.3.308.

Dymecki, S.M. 1996. Flp recombinase promotes site-specific DNA recombination in embryonic stem cells and transgenic mice. *Proc. Natl. Acad. Sci. U. S. A.* 93:6191–6196.

Eguchi, J., J. Wada, K. Hida, H. Zhang, T. Matsuoka, M. Baba, I. Hashimoto, K. Shikata, N. Ogawa, and H. Makino. 2005. Identification of adipocyte adhesion molecule (ACAM), a novel CTX gene family, implicated in adipocyte maturation and development of obesity. *Biochem. J.* 387:343–353. doi:10.1042/BJ20041709.

Eom, D.S., S. Inoue, L.B. Patterson, T.N. Gordon, R. Slingwine, S. Kondo, M. Watanabe, and D.M. Parichy. 2012. Melanophore migration and survival during zebrafish adult pigment stripe development require the immunoglobulin superfamily adhesion molecule Igsf11. *PLoS Genet.*

8:e1002899. doi:10.1371/journal.pgen.1002899.

Excoffon, K.J.D.A., A. Hruska-Hageman, M. Klotz, G.L. Traver, and J. Zabner. 2004. A role for the PDZ-binding domain of the coxsackie B virus and adenovirus receptor (CAR) in cell adhesion and growth. *J. Cell Sci.* 117:4401–4409. doi:10.1242/jcs.01300.

de Feijter, A.W., D.F. Matesic, R.J. Ruch, X. Guan, C.C. Chang, and J.E. Trosko. 1996. Localization and function of the connexin 43 gap-junction protein in normal and various oncogene-expressing rat liver epithelial cells. *Mol. Carcinog.* 16:203–212. doi:10.1002/(SICI)1098-2744(199608)16:4<203::AID-MC4>3.0.CO;2-G.

Feil, S., N. Valtcheva, and R. Feil. 2009. Inducible Cre Mice. 343–363.

França, L.R., R.A. Hess, J.M. Dufour, M.C. Hofmann, and M.D. Griswold. 2016. The Sertoli cell: one hundred fifty years of beauty and plasticity. *Andrology*. 4:189–212. doi:10.1111/andr.12165.

Gerber, J., K. Weider, N. Hambruch, and R. Brehm. 2014. Loss of connexin43 (Cx43) in Sertoli cells leads to spatio-temporal alterations in occludin expression. *Histol. Histopathol.* 29:935–948.

Giepmans, B.N., and W.H. Moolenaar. The gap junction protein connexin43 interacts with the second PDZ domain of the zona occludens-1 protein. *Curr. Biol.* 8:931–4.

Ginsburg, M., M.H. Snow, and A. McLaren. 1990. Primordial germ cells in the mouse embryo during gastrulation. *Development*. 110:521–528.

Gliki, G., K. Ebnet, M. Aurrand-Lions, B.A. Imhof, and R.H. Adams. 2004. Spermatid differentiation requires the assembly of a cell polarity complex downstream of junctional adhesion molecule-C. *Nature*. 431:320–324. doi:10.1038/nature02877.

Gow, A., C.M. Southwood, J.S. Li, M. Pariali, G.P. Riordan, S.E. Brodie, J. Danias, J.M. Bronstein, B. Kachar, and R.A. Lazzarini. 1999. CNS Myelin and Sertoli Cell Tight Junction Strands Are Absent in Osp/Claudin-11 Null Mice. *Cell*. 99:649–659. doi:10.1016/S0092-8674(00)81553-6.

Griswold, M.D. 1988. Protein secretions of Sertoli cells. *Int. Rev. Cytol.* 110:133–56.

Gudeloglu, A., and S.J. Parekattil. 2013. Update in the evaluation of the azoospermic male. *Clin. (São Paulo, Brazil)*. 68 Suppl 1:27–34. doi:10.6061/clinics/2013(Sup01)04.

Handel, M.A. 2004. The XY body: a specialized meiotic chromatin domain. *Exp. Cell Res.* 296:57–63. doi:10.1016/j.yexcr.2004.03.008.

Hanstein, R., H. Negoro, N.K. Patel, A. Charollais, P. Meda, D.C. Spray, S.O. Suadicani, and E. Scemes. 2013. Promises and pitfalls of a Pannexin1 transgenic mouse line. *Front. Pharmacol.* 4:61. doi:10.3389/fphar.2013.00061.

Harada, H., S. Suzu, Y. Hayashi, and S. Okada. 2005. BT-IgSF, a novel immunoglobulin superfamily protein, functions as a cell adhesion molecule. *J. Cell. Physiol.* 204:919–926.

Hess, R.A., and L.R. De Franca. 2008. Spermatogenesis and cycle of the seminiferous epithelium. *Adv. Exp. Med. Biol.* 636:1–15. doi:10.1007/978-0-387-09597-4_1.

Hirata Ki, K., T. Ishida, K. Penta, M. Rezaee, E. Yang, J. Wohlgemuth, and T. Quertermous. 2001. Cloning of an immunoglobulin family adhesion molecule selectively expressed by endothelial cells. *J. Biol. Chem.* 276:16223–16231. doi:10.1074/jbc.M100630200.

Holembowski, L., D. Kramer, D. Riedel, R. Sordella, A. Nemajerova, M. Dobbelstein, and U.M. Moll. 2014. TAp73 is essential for germ cell adhesion and maturation in testis. *J. Cell Biol.* 204:1173–1190. doi:10.1083/jcb.201306066.

Honda, T., H. Saitoh, M. Masuko, T. Katagiri-Abe, K. Tominaga, I. Kozakai, K. Kobayashi, T. Kumanishi,

Y.G. Watanabe, S. Odani, and R. Kuwano. 2000. The coxsackievirus-adenovirus receptor protein as a cell adhesion molecule in the developing mouse brain. *Brain Res. Mol. Brain Res.* 77:19–28.

Hosoi, I., Y. Toyama, M. Maekawa, H. Ito, and S. Yuasa. 2002. Development of the blood-testis barrier in the mouse is delayed by neonatally administered diethylstilbestrol but not by beta-estradiol 3-benzoate. *Andrologia*. 34:255–262. doi:10.1046/j.1439-0272.2002.00502.x.

Janecki, A., A. Jakubowiak, and A. Steinberger. 1991. Regulation of Transepithelial Electrical Resistance in Two-Compartment Sertoli Cell Cultures: In Vitro Model of the Blood-Testis Barrier. *Endocrinology*. 129:1489–1496. doi:10.1210/endo-129-3-1489.

Jang, S., D. Oh, Y. Lee, E. Hosy, H. Shin, C. van Riesen, D. Whitcomb, J.M. Warburton, J. Jo, D. Kim, S.G. Kim, S.M. Um, S.-K. Kwon, M.-H. Kim, J.D. Roh, J. Woo, H. Jun, D. Lee, W. Mah, H. Kim, B.-K. Kaang, K. Cho, J.-S. Rhee, D. Choquet, and E. Kim. 2015. Synaptic adhesion molecule IgSF11 regulates synaptic transmission and plasticity. *Nat. Neurosci.* 19:84–93. doi:10.1038/nn.4176.

Jarvi, K., K. Lo, A. Fischer, J. Grantmyre, A. Zini, V. Chow, and V. Mak. 2010. CUA Guideline: The workup of azoospermic males. *Can. Urol. Assoc. J.* 4:163–167.

Jiang, X.-H., I. Bukhari, W. Zheng, S. Yin, Z. Wang, H.J. Cooke, and Q.-H. Shi. 2014. Blood-testis barrier and spermatogenesis: lessons from genetically-modified mice. *Asian J. Androl.* 16:572–580. doi:10.4103/1008-682X.125401.

Juneja, S.C., K.J. Barr, G.C. Enders, and G.M. Kidder. 1999. Defects in the germ line and gonads of mice lacking connexin43. *Biol. Reprod.* 60:1263–1270.

Katoh, M.M., and M.M. Katoh. 2003. IGSF11 gene, frequently up-regulated in intestinal-type gastric cancer, encodes adhesion molecule homologous to CXADR, FLJ22415 and ESAM. *Int. J. Oncol.* 23:525–531.

Kausalya, P.J., M. Reichert, and W. Hunziker. 2001. Connexin45 directly binds to ZO-1 and localizes to the tight junction region in epithelial MDCK cells. *FEBS Lett.* 505:92–6.

Kerr, J.B., M. Millar, S. Maddocks, and R.M. Sharpe. 1993. Stage-dependent changes in spermatogenesis and Sertoli cells in relation to the onset of spermatogenic failure following withdrawal of testosterone. *Anat. Rec.* 235:547–59. doi:10.1002/ar.1092350407.

Kluin, P.M., M.F. Kramer, and D.G. de Rooij. 1984. Proliferation of spermatogonia and Sertoli cells in maturing mice. *Anat. Embryol. (Berl).* 169:73–8.

Koopman, P., J. Gubbay, N. Vivian, P. Goodfellow, and R. Lovell-Badge. 1991. Male development of chromosomally female mice transgenic for Sry. *Nature*. 351:117–121.

de Kretser, D.M., K. Loveland, and M. O'Bryan. 2016. Spermatogenesis. *In* Endocrinology: Adult and Pediatric. Elsevier. 2325–2353.e9.

Kushida, T., H. Iijima, Y. Nagato, and H. Kushida. 1993. Studies on thick sections of the nucleus of mouse Sertoli cells using an electron microscope operating at 300 kV. *Okajimas Folia Anat. Jpn.* 70:41–50.

Lablack, A., V. Bourdon, N. Defamie, C. Batias, M. Mesnil, P. Fenichel, G. Pointis, and D. Segretain. 1998. Ultrastructural and biochemical evidence for gap junction and connexin 43 expression in a clonal Sertoli cell line: a potential model in the study of junctional complex formation. *Cell Tissue Res.* 294:279–287. doi:10.1007/s004410051178.

Laing, J.G., B.C. Chou, and T.H. Steinberg. 2005. ZO-1 alters the plasma membrane localization and function of Cx43 in osteoblastic cells. *J. Cell Sci.* 118:2167–76. doi:10.1242/jcs.02329.

Lammers, J.H., H.H. Offenberg, M. van Aalderen, A.C. Vink, A.J. Dietrich, and C. Heyting. 1994. The

gene encoding a major component of the lateral elements of synaptonemal complexes of the rat is related to X-linked lymphocyte-regulated genes. *Mol. Cell. Biol.* 14:1137–1146.

Langhorst, H. 2015. Deletion of Clmp in Mice Reveals Essential Roles for CLMP in Growth, Survival, Gastrointestinal and Urinary Tract Functions. 144 pp.

Leblond, C.P., and Y. Clermont. 1952. Definition of the stages of the cycle of the seminiferous epithelium in the rat. *Ann. N. Y. Acad. Sci.* 55:548–573.

Lécureuil, C., I. Fontaine, P. Crepieux, and F. Guillou. 2002. Sertoli and granulosa cell-specific Cre recombinase activity in transgenic mice. *Genesis*. 33:114–118. doi:10.1002/gene.10100.

Lee, J.H., W. Engel, and K. Nayernia. 2006. Stem cell protein Piwil2 modulates expression of murine spermatogonial stem cell expressed genes. *Mol. Reprod. Dev.* 73:173–179. doi:10.1002/mrd.20391.

Luangpraseuth-Prosper, A., E. Lesueur, L. Jouneau, E. Pailhoux, C. Cotinot, and B. Mandon-Pépin. 2015. TOPAZ1, a germ cell specific factor, is essential for male meiotic progression. *Dev. Biol.* 406:158–171. doi:10.1016/j.ydbio.2015.09.002.

Mather, J.P., K.M. Attie, T.K. Woodruff, G.C. Rice, and D.M. Phillips. 1990. Activin stimulates spermatogonial proliferation in germ-Sertoli cell cocultures from immature rat testis. *Endocrinology*. 127:3206–14. doi:10.1210/endo-127-6-3206.

Matthäus, C., H. Langhorst, L. Schütz, R. Jüttner, and F.G. Rathjen. 2016. Cell-cell communication mediated by the CAR subgroup of immunoglobulin cell adhesion molecules in health and disease. *Mol. Cell. Neurosci.* doi:10.1016/j.mcn.2016.11.009.

Matthäus, C., J. Schreiber, R. Jüttner, and F.G. Rathjen. 2014. The Ig CAM CAR is Implicated in Cardiac Development and Modulates Electrical Conduction in the Mature Heart. *J. Cardiovasc. Dev. Dis.* 1:111–120. doi:10.3390/jcdd1010111.

Mazaud-Guittot, S., E. Meugnier, S. Pesenti, X. Wu, H. Vidal, A. Gow, and B. Le Magueresse-Battistoni. 2010. Claudin 11 deficiency in mice results in loss of the Sertoli cell epithelial phenotype in the testis. *Biol. Reprod.* 82:202–213. doi:10.1095/biolreprod.109.078907.

Meistrich, M.L., and R.A. Hess. 2013. Assessment of Spermatogenesis Through Staging of Seminiferous Tubules. *Spermatogenesis*. 927:299–307. doi:10.1007/978-1-62703-038-0.

Meng, J., R.W. Holdcraft, J.E. Shima, M.D. Griswold, and R.E. Braun. 2005. Androgens regulate the permeability of the blood-testis barrier. *Proc. Natl. Acad. Sci. U. S. A.* 102:16696–16700. doi:10.1073/pnas.0506084102.

Meng, X., M. Lindahl, M.E. Hyvönen, M. Parvinen, D.G. de Rooij, M.W. Hess, A. Raatikainen-Ahokas, K. Sainio, H. Rauvala, M. Lakso, J.G. Pichel, H. Westphal, M. Saarma, and H. Sariola. 2000. Regulation of cell fate decision of undifferentiated spermatogonia by GDNF. *Science*. 287:1489–93.

Mirza, M., J. Hreinsson, M.-L. Strand, O. Hovatta, O. Söder, L. Philipson, R.F. Pettersson, and K. Sollerbrant. 2006. Coxsackievirus and adenovirus receptor (CAR) is expressed in male germ cells and forms a complex with the differentiation factor JAM-C in mouse testis. *Exp. Cell Res.* 312:817–830. doi:10.1016/j.yexcr.2005.11.030.

Mirza, M., C. Petersen, K. Nordqvist, and K. Sollerbrant. 2007. Coxsackievirus and Adenovirus Receptor Is Up-Regulated in Migratory Germ Cells during Passage of the Blood-Testis Barrier. *Endocrinology*. 148:5459–5469. doi:10.1210/en.2007-0359.

Mirza, M., E. Raschperger, L. Philipson, R.F. Pettersson, and K. Sollerbrant. 2005. The cell surface

protein coxsackie- and adenovirus receptor (CAR) directly associates with the Ligand-of-Numb Protein-X2 (LNX2). *Exp. Cell Res.* 309:110–120. doi:10.1016/j.yexcr.2005.05.023.

Mital, P., G. Kaur, and J.M. Dufour. 2010. Immunoprotective Sertoli cells: making allogeneic and xenogeneic transplantation feasible. *Reproduction*. 139:495–504. doi:10.1530/REP-09-0384.

Morrow, C.M.K., D. Mruk, C.Y. Cheng, and R.A. Hess. 2010. Claudin and occludin expression and function in the seminiferous epithelium. *Philos. Trans. R. Soc. Lond. B. Biol. Sci.* 365:1679–96. doi:10.1098/rstb.2010.0025.

Mruk, D.D., and C.Y. Cheng. 2011. An in vitro system to study Sertoli cell blood-testis barrier dynamics. *Methods Mol. Biol.* 763:237–252. doi:10.1007/978-1-61779-191-8_16.

Mruk, D.D., and C.Y. Cheng. 2015. The Mammalian Blood-Testis Barrier: Its Biology and Regulation. *Endocr. Rev.* 36:564–91. doi:10.1210/er.2014-1101.

Mullaney, B.P., and M.K. Skinner. 1992. Basic fibroblast growth factor (bFGF) gene expression and protein production during pubertal development of the seminiferous tubule: follicle-stimulating hormone-induced Sertoli cell bFGF expression. *Endocrinology*. 131:2928–2934. doi:10.1210/endo.131.6.1446630.

Nasdala, I., K. Wolburg-Buchholz, H. Wolburg, A. Kuhn, K. Ebnet, G. Brachtendorf, U. Samulowitz, B. Kuster, B. Engelhardt, D. Vestweber, and S. Butz. 2002. A transmembrane tight junction protein selectively expressed on endothelial cells and platelets. *J. Biol. Chem.* 277:16294–16303. doi:10.1074/jbc.M111999200.

Nebel, B.R., A.P. Amarose, and E.M. Hacket. 1961. Calendar of gametogenic development in the prepuberal male mouse. *Science*. 134:832–3.

Oakberg, E.F. 1956a. A description of spermiogenesis in the mouse and its use in analysis of the cycle of the seminiferous epithelium and germ cell renewal. *Am. J. Anat.* 99:391–413. doi:10.1002/aja.1000990303.

Oakberg, E.F. 1956b. Duration of spermatogenesis in the mouse and timing of stages of the cycle of the seminiferous epithelium. *Am. J. Anat.* 99:507–516.

ORC Macro and the World Health Organization. 2004. WHO | Infecundity, infertility, and childlessness in developing countries. Demographic and Health Surveys (DHS) Comparative reports No. 9. *WHO*.

Patzke, C., K.E. a Max, J. Behlke, J. Schreiber, H. Schmidt, A. a Dorner, S. Kröger, M. Henning, A. Otto, U. Heinemann, and F.G. Rathjen. 2010. The coxsackievirus-adenovirus receptor reveals complex homophilic and heterophilic interactions on neural cells. *J. Neurosci.* 30:2897–2910. doi:10.1523/JNEUROSCI.5725-09.2010.

Pelz, L., B. Purfürst, and F.G. Rathjen. 2017. The cell adhesion molecule BT-IgSF is essential for a functional blood–testis barrier and male fertility in mice. *J. Biol. Chem.* jbc.RA117.000113. doi:10.1074/jbc.RA117.000113.

Peters, A., J. Drumm, C. Ferrell, D.A. Roth, D.M. Roth, M. McCaman, P. Novak, J. Friedman, R. Engler, and R. Braun. 2001. Absence of Germline Infection in Male Mice Following Intraventricular Injection of Adenovirus. *Mol. Ther.* 4:603–613. doi:10.1006/MTHE.2001.0500.

Pointis, G., and D. Segretain. 2005. Role of connexin-based gap junction channels in testis. *Trends Endocrinol. Metab.* 16:300–306. doi:10.1016/j.tem.2005.07.001.

Raschperger, E., U. Engstrom, R.F. Pettersson, and J. Fuxe. 2004. CLMP, a novel member of the CTX family and a new component of epithelial tight junctions. *J. Biol. Chem.* 279:796–804.

doi:10.1074/jbc.M308249200.

Rex A. Hess, and Luiz R. França. 2015. Sertoli Cell Biology (Second edition). M.K. Skinner and M.D. Griswold, editors. 1-55 pp.

Saitou, M., M. Furuse, H. Sasaki, J.D. Schulzke, M. Fromm, H. Takano, T. Noda, and S. Tsukita. 2000. Complex phenotype of mice lacking occludin, a component of tight junction strands. *Mol. Biol. Cell*. 11:4131–4142.

Scanlan, M.J., A.O. Gure, A.A. Jungbluth, L.J. Old, and Y.-T. Chen. 2002. Cancer/testis antigens: an expanding family of targets for cancer immunotherapy. *Immunol. Rev.* 188:22–32.

Schwenk, F., U. Baron, and K. Rajewsky. 1995. A cre-transgenic mouse strain for the ubiquitous deletion of loxP-flanked gene segments including deletion in germ cells. *Nucleic Acids Res.* 23:5080–5081.

Sertoli, E. 1987. Historical tribute: On the existence of specialized branching cells in the seminiferous canaliculi of the human testis. By Enrico Sertoli. 1865. *Hum. Reprod.* 2:83–4.

Shaw, C.A., P.C. Holland, M. Sinnreich, C. Allen, K. Sollerbrant, G. Karpati, and J. Nalbantoglu. 2004. Isoform-specific expression of the Coxsackie and adenovirus receptor (CAR) in neuromuscular junction and cardiac intercalated discs. *BMC Cell Biol.* 5:42. doi:10.1186/1471-2121-5-42.

Silva, C., J.R. Wood, L. Salvador, Z. Zhang, I. Kostetskii, C.J. Williams, and J.F. Strauss. 2009. Expression profile of male germ cell-associated genes in mouse embryonic stem cell cultures treated with all-trans retinoic acid and testosterone. *Mol. Reprod. Dev.* 76:11–21. doi:10.1002/mrd.20925.

Smith, B.E., and R.E. Braun. 2012. Germ cell migration across Sertoli cell tight junctions. *Science*. 338:798–802. doi:10.1126/science.1219969.

Sollerbrant, K., E. Raschperger, M. Mirza, U. Engstrom, L. Philipson, P.O. Ljungdahl, and R.F. Pettersson. 2003. The Coxsackievirus and adenovirus receptor (CAR) forms a complex with the PDZ domain-containing protein ligand-of-numb protein-X (LNX). *J. Biol. Chem.* 278:7439–7444. doi:10.1074/jbc.M205927200.

Stalker, T.J., J. Wu, A. Morgans, E.A. Traxler, L. Wang, M.S. Chatterjee, D. Lee, T. Quertermous, R.A. Hall, D.A. Hammer, S.L. Diamond, and L.F. Brass. 2009. Endothelial cell specific adhesion molecule (ESAM) localizes to platelet-platelet contacts and regulates thrombus formation in vivo. *J. Thromb. Haemost.* 7:1886–1896. doi:10.1111/j.1538-7836.2009.03606.x.

Stoffel, W., B. Holz, B. Jenke, E. Binczek, R.H. Günter, C. Kiss, I. Karakesisoglou, M. Thevis, A.-A. Weber, S. Arnhold, and K. Addicks. 2008. Delta6-desaturase (FADS2) deficiency unveils the role of omega3- and omega6-polyunsaturated fatty acids. *EMBO J.* 27:2281–2292. doi:10.1038/emboj.2008.156.

Su, L., I.A. Kopera-Sobota, B. Bilinska, C.Y. Cheng, and D.D. Mruk. 2013. Germ cells contribute to the function of the Sertoli cell barrier. *Spermatogenesis*. 3:e26460. doi:10.4161/spmg.26460.

Su, L., D.D. Mruk, and C. Yan Cheng. 2012. Regulation of the blood-testis barrier by coxsackievirus and adenovirus receptor. *AJP Cell Physiol.* 303:C843–C853. doi:10.1152/ajpcell.00218.2012.

Sultana, T., M. Hou, J.-B. Stukenborg, V. Tohonen, J.H.A. Inzunza Figueroa, A. Chagin, and K. Sollerbrant. 2014. Mice depleted of CAR display normal spermatogenesis and an intact Blood-Testis Barrier. *Reproduction*. doi:10.1530/REP-13-0653.

Suzu, S., Y. Hayashi, T. Harumi, K. Nomaguchi, M. Yamada, H. Hayasawa, and K. Motoyoshi. 2002. Molecular cloning of a novel immunoglobulin superfamily gene preferentially expressed by brain and testis. *Biochem. Biophys. Res. Commun.* 296:1215–1221.

Sze, K.-L., W.M. Lee, and W.-Y. Lui. 2008. Expression of CLMP, a novel tight junction protein, is mediated via the interaction of GATA with the Kruppel family proteins, KLF4 and Sp1, in mouse TM4 Sertoli cells. *J. Cell. Physiol.* 214:334–344. doi:10.1002/jcp.21201.

Tadokoro, Y., K. Yomogida, H. Ohta, A. Tohda, and Y. Nishimune. 2002. Homeostatic regulation of germinal stem cell proliferation by the GDNF/FSH pathway. *Mech. Dev.* 113:29–39.

Veitinger, S., T. Veitinger, S. Cainarca, D. Fluegge, C.H. Engelhardt, S. Lohmer, H. Hatt, S. Corazza, J. Spehr, E.M. Neuhaus, and M. Spehr. 2011. Purinergic signalling mobilizes mitochondrial Ca^{2+} in mouse Sertoli cells. *J. Physiol.* 589:5033–5055. doi:10.1113/jphysiol.2011.216309.

Verdino, P., D.A. Witherden, W.L. Havran, and I.A. Wilson. 2010. The Molecular Interaction of CAR and JAML Recruits the Central Cell Signal Transducer PI3K. *Science (80-.).* 329:1210–1214. doi:10.1126/science.1187996.

Vogl, R.A.H. and A.W. 2015. Sertoli Cell Biology. M.D. Griswold, editor. 1-31 pp.

Wan, H.-T., D.D. Mruk, C.K.C. Wong, and C.Y. Cheng. 2013. The apical ES–BTB–BM functional axis is an emerging target for toxicant-induced infertility. *Trends Mol. Med.* 19:396–405. doi:10.1016/j.molmed.2013.03.006.

Wang, C.Q.F., D.D. Mruk, W.M. Lee, and C.Y. Cheng. 2007. Coxsackie and adenovirus receptor (CAR) is a product of Sertoli and germ cells in rat testes which is localized at the Sertoli-Sertoli and Sertoli-germ cell interface. *Exp. Cell Res.* 313:1373–1392. doi:10.1016/j.yexcr.2007.01.017.

Watanabe, T., T. Suda, T. Tsunoda, N. Uchida, K. Ura, T. Kato, S. Hasegawa, S. Satoh, S. Ohgi, H. Tahara, Y. Furukawa, and Y. Nakamura. 2005. Identification of immunoglobulin superfamily 11 (IGSF11) as a novel target for cancer immunotherapy of gastrointestinal and hepatocellular carcinomas. *Cancer Sci.* 96:498–506. doi:10.1111/j.1349-7006.2005.00073.x.

Wegmann, F., K. Ebnet, L. Du Pasquier, D. Vestweber, and S. Butz. 2004. Endothelial adhesion molecule ESAM binds directly to the multidomain adaptor MAGI-1 and recruits it to cell contacts. *Exp. Cell Res.* 300:121–133. doi:10.1016/j.yexcr.2004.07.010.

Wong, V., and L.D. Russell. 1983. Three-dimensional reconstruction of a rat stage V Sertoli cell: I. Methods, basic configuration, and dimensions. *Am. J. Anat.* 167:143–161. doi:10.1002/aja.1001670202.

Xiao, X., D.D. Mruk, C.K.C. Wong, and C.Y. Cheng. 2014. Germ cell transport across the seminiferous epithelium during spermatogenesis. *Physiology (Bethesda).* 29:286–298. doi:10.1152/physiol.00001.2014.

Xu, J., F. Anuar, S.M. Ali, M.Y. Ng, D.C.Y. Phua, and W. Hunziker. 2009. Zona occludens-2 is critical for blood-testis barrier integrity and male fertility. *Mol. Biol. Cell*. 20:4268–4277. doi:10.1091/mbc.E08-12-1236.

Yeh, S., M.-Y. Tsai, Q. Xu, X.-M. Mu, H. Lardy, K.-E. Huang, H. Lin, S.-D. Yeh, S. Altuwaijri, X. Zhou, L. Xing, B.F. Boyce, M.-C. Hung, S. Zhang, L. Gan, C. Chang, and M.-C. Hung. 2002. Generation and characterization of androgen receptor knockout (ARKO) mice: An in vivo model for the study of androgen functions in selective tissues. *Proc. Natl. Acad. Sci.* 99:13498–13503. doi:10.1073/pnas.212474399.

Zen, K., Y. Liu, I.C. McCall, T. Wu, W. Lee, B.A. Babbin, A. Nusrat, and C.A. Parkos. 2005. Neutrophil Migration across Tight Junctions Is Mediated by Adhesive Interactions between Epithelial Coxsackie and Adenovirus Receptor and a Junctional Adhesion Molecule-like Protein on Neutrophils. *Mol. Biol. Cell*. 16:2694–2703. doi:10.1091/mbc.E05-01-0036.

13. LIST OF PUBLICATIONS

- **Pelz, L.**, Purfürst, B., and F.G. Rathjen. 2017. The cell adhesion molecule BT-IgSF is essential for a functional blood–testis barrier and male fertility in mice. J. Biol. Chem. jbc.RA117.000113. doi:10.1074/jbc.RA117.000113.

- Matthäus, C., Langhorst, H., **Schütz, L.**, Jüttner, R., and F.G. Rathjen. 2016. Cell-cell communication mediated by the CAR subgroup of immunoglobulin cell adhesion molecules in health and disease. Mol. Cell. Neurosci. doi:10.1016/j.mcn.2016.11.009.

- Langhorst, H., Jüttner, R., Groneberg, D., Mohtashamdolatshahi, A., **Pelz, L.**, Purfürst, B., Schmidt-Ott, K., Friebe, A. and Rathjen, F.G. 2017. The IgCAM CLMP is required for intestinal and ureteral smooth muscle contraction by regulating Connexin43 and 45 expression in mice. In Revision.

- **Pelz, L.**, Wolf, L., Montag, D., Siemonsmeier, A.- G., Meyer,N. 2017 The function of BT-IgSF on astrocytes. In preparation.

14. CURRICULUM VITAE

Der Lebenslauf ist in der Online-Version aus Gründen des Datenschutzes nicht enthalten.

DANKSAGUNG

An erster Stelle möchte ich natürlich meinem Doktorvater **Professor Fritz G. Rathjen** für die Möglichkeit danken, meine Doktorarbeit in seiner Arbeitsgruppe anfertigen zu dürfen. Er gab mir die Freiheit meine Ideen zu verfolgen und neue Techniken und Themen in der Gruppe zu etablieren.

Danke auch an meinen Zweitgutachter, Professor **Oliver Daumke**, der sich dazu bereit erklärt hat, meine Dissertation zu begutachten.

Vielen Dank auch an **Karin Müller** vom IZW Berlin für die Expertise in der Andrologie und an **Corinna Göppner** für die vielen Wissensaustausche während der Doktorarbeit.

Danke an alle (jetzt) ehemaligen **Mitglieder der AG Rathjen**, durch eure Unterhaltung und Unterstützung wurden Inkubationspausen verkürzt, PCR Probleme gelöst und die Mittagspausen umso schmackhafter.

Ein besonderer Dank geht auch an **Anne**, die mir nicht nur im Labor und in den Mittagspausen zur Seite stand, sondern darüber hinaus auch zu meiner besten Freundin wurde.

Natürlich dürfen an dieser Stelle auch **meine Eltern** und **mein Bruder** nicht unerwähnt bleiben, die mich in all meinen Plänen immer unterstütz haben und die mich zu dem Menschen gemacht haben, der ich heute bin. Danke dafür!

Der wohl wichtigste Mensch in meinem Leben ist mein Mann **Andreas**, der mich während meiner Doktorarbeit immer unterstützt hat, der auch spät abends noch meinen theoretischen Überlegungen folgen musste und mir auch bei dem ein oder anderen Experiment weiterhelfen konnte. Danke, dass du vor über 11 Jahren in mein Leben getreten bist und mich so liebst wie ich bin.